DOI:10.14753/SE.2022.2667

SEMMELWEIS EGYETEM

DOKTORI ISKOLA

Ph.D. értekezések

2667.

ORESTIS STYLIANOU

A vérkeringési rendszer normális és kóros működésének mechanizmusai
című program

Programvezető: Dr. Benyó Zoltán, egyetemi tanár

Témavezető: Dr. Mukli Péter, egyetemi tanársegéd

DOI:10.14753/SE.2022.2667

SCALE-FREE FUNCTIONAL CONNECTIVITY OF BRAIN NETWORKS REVEALED BY ELECTROENCEPHALOGRAPHY

PhD thesis

Orestis Stylianou, MD

Doctoral School of Theoretical and Translational Medicine

Semmelweis University

Supervisor: Peter Mukli, MD, PhD

Official reviewers: Karoly Liliom, PhD

Laszlo Negyessy, PhD

Head of the Complex Examination Committee:

György Losonczy, PhD

Members of the Complex Examination Committee:

Andrea Székely, MD, PhD

Ákos Jobbágy, PhD

Budapest

2022

DOI:10.14753/SE.2022.2667

TABLE OF CONTENTS

DOI:10.14753/SE.2022.2667

DOI:10.14753/SE.2022.2667

LIST OF ABBREVIATIONS

- BFMF: bivariate focus-based multifractal
- BH: Benjamini-Hochberg
- DA: dorsal attention network
- DMN: default mode network
- EC: eyes-closed
- EEG: electroencephalogram
- EO: eyes-open
- FC: functional connectivity
- fMRI: functional magnetic resonance imaging
- fNIRS: functional near-infrared spectroscopy
- FP: frontoparietal network
- HAPPE: Harvard automated preprocessing pipeline for electroencephalography
- ICA: independent component analysis
- MARA: multiple artifact rejection algorithm
- MEG: magnetoencephalogram
- RSNs: resting-state networks
- RT: reaction time
- SM: somatomotor network
- SOC: self-organized criticality
- SR: success rate
- VAL: combined ventral attention and limbic networks
- VN: visual network
- VPR: visual pattern recognition
- wICA: wavelet-enhanced independent component analysis

DOI:10.14753/SE.2022.2667

SYMBOL LIST

- D^W: weighted node degree
- $\overline{D^W}$: average weighted node degree
- f: frequency
- L: length of time series
- P: power density
- q: statistical moment
- s: time scale – size of window in fractal analysis
- S_{XY}: scaling function of time series X and Y
- W: Kendall's coefficient of concordance
- β: spectral index – power-law exponent describing scale-free relationship in the frequency domain (inverse of the "slope")
- ΔH_{15}: strength of multifractality
- Ω: time-scale specific statistical measure of a process

DOI:10.14753/SE.2022.2667

1. INTRODUCTION

For several centuries, the study of brain activity was limited. The main reason for the slow progress has been the difficult access to alive and healthy human brains available for non-invasive investigation. Until the early 20th century, scientists had to rely on the study of cadaver or animal brains. Occasionally, they would have access to neuropsychiatric patients with distinct phenotypes that could offer a glance of the brain function. While the anatomy of the brain was well understood from morphological studies, most of the knowledge on brain function came from psychological research. Such approach was limited for several reasons, one of them being the inability to establish a link between neurophysiological processes and behavior. This changed drastically in the 20th century after the introduction of electroencephalogram (EEG), followed by imaging modalities like magnetoencephalogram (MEG), functional near-infrared spectroscopy (fNIRS) and functional magnetic resonance imaging (fMRI). In his seminal work introducing EEG (1), Berger showed that electrodes attached to the scalp could capture the electric potential difference between brain regions. This was the first time that human brain activity was recorded non-invasively in real-time. As a result, we expanded the repertoire of available experimental paradigms, allowing us to explore brain function in more detail.

Even from the early stages of this new era, it was apparent that EEG could capture the fluctuations of brain activity caused by mental strain. The most well-known example of such fluctuations is the desynchronization observed during the transition from eyes closed to eyes open. The increased sensory input caused by the opening of the eyes is accompanied by a shift of the EEG from alpha to beta oscillations (2), which Berger himself shown first in 1929 (1). Since then, EEG has been used to study healthy populations in laboratories and patients with neuropsychiatric diseases. Most of these studies focus on the narrowband (oscillatory) component of electrical activity, usually classified in 5 bands (delta: 0.5-4 Hz, theta: 4-7 Hz, alpha: 7-14 Hz, beta: 14-30 Hz and gamma: 30-60 Hz). Later, however, more attention has been paid to the broadband (scale-free) aspect of the EEG, as its fundamental physiological role has been recognized (3–5).

DOI:10.14753/SE.2022.2667

Along with the study of single time series (univariate analysis) of brain activity, the investigation of the relationship between pairs of time series (bivariate analysis) (6) began. The human brain is a vastly interconnected network [about 10^{11} neurons and 10^{15} synapses (7)], whose dense axonal grid acts as anatomical connections between distant brain areas. This anatomical connectivity is facilitated by the plethora of synapses found between neurons. On top of these structural connections, the brain's functional connectivity (FC) flourishes (8, 9). The main difference between FC and anatomical connectivity is that FC goes beyond the constraints of physical synapses since functional connections can exist either between: *i*) directly linked regions or *ii*) indirectly linked regions, connected by interneurons; meaning that anatomical connectivity is a subset of functional connectivity. The functional connection between two time series can be estimated by their statistical interdependence (10). Three main approaches of FC studies have emerged: *i*) seed-based analysis *ii*) graph theoretical analysis and *iii*) independent component analysis (ICA) (11). Only the interaction between a specific area and the rest of the brain is investigated in the seed-based analysis, based on the statistical coupling of the corresponding neural activities (12). The graph theoretical analysis extends the seed-based analysis by using all possible regions as seeds (13). The applied neuroimaging modality defines the potential regions; in EEG, MEG and fNIRS studies the regions are usually the recording channels, while fMRI usually uses anatomically (or functionally) cohesive units. On the other hand, ICA groups time series to statistically dependent components, assuming that a particular brain source is responsible for each component (12). Subsequently, the interdependence between each pair of components is estimated. From the three methodologies, we applied graph theoretical analysis that provides a straightforward framework for estimating functional connectivity and characterizing brain networks.

The functional connectome of a brain network can be constructed as a constellation of nodes interconnected by edges. The network nodes represent the different brain regions, while the edges are the functional links between them (FC). The direct study of FC is possible and straightforward for a small number of nodes and edges, but it becomes increasingly complicated for larger networks. For example, a (moderately dense) 64-channel EEG system has 2016 (64x63/2) possible connections. It is clear then that FC data needs to be reduced by appropriate mathematical techniques to distill

information about the network's architecture, at the cost of less circumscribed localization. Such a solution can be found in graph theory (13–15), which allows the estimation of several network properties by deriving measures of the connectome. Using graph theory, scientists could draw significant conclusions about the architecture of brain networks, both in healthy and diseased populations. For example, it has been found that the healthy brain follows a small-world network organization (16). According to this, most cortical areas are sparsely interconnected, while a small number of hub regions are responsible for the linkage between these functionally distant areas. These hub regions seem fundamental for normal brain function since disruption of hub regions and small-world architecture have been linked with clinical conditions like coma, Alzheimer's disease, and schizophrenia (17–22). The density of these small-world networks seems to be governed by scale-free dynamics (23).

While the study of FC started with cognitive and motor stimuli (8, 9), understanding resting-state FC is vital to precisely study the effect of task on brain network architecture. Resting-state is defined as the awake stake during which the subject is not performing any task and is requested to empty his/her mind. Despite its name, resting-state is associated with considerable neural activity accompanied by high energy consumption (due to cellular metabolism), which increases only by 5% during task (24). This shows that brain activation during a mental process is not as simple as the additional recruitment of brain regions; on the contrary, it is a balanced activation (deactivation) of relevant (irrelevant) areas (25). Due to their simultaneous activity in the resting-state, functionally coupled groups of brain regions give rise to resting-state networks (RSNs), with the default mode network (DMN) being the most prominent example (24, 26, 27). DMN is a constellation of brain regions, including precuneus, medial prefrontal cortex, and posterior cingulate gyrus, active during resting-state. Upon mental task, the activity of DMN decreases. These findings suggest that brain activity does not fluctuate randomly during rest. On the contrary, there is a universal baseline of brain activity, which is thus organized even without external stimulus (28). Recently, this resting-state neural architecture has been found to fluctuate in a scale-free manner (29).

The scale-free (or fractal) brain dynamics are ubiquitous (30–32). Fractals were initially introduced as geometrical constructs with a fractional dimension that can be

scaled-up or scaled-down yet maintain similar morphology (self-similarity) (33). One such example is the Koch curve in **Figure 1A**. Physiological processes also scale according to a self-affine manner (temporal fractals), meaning direction-wise self-similarity (34). **Figure 1B** shows how an EEG recording maintains similar morphology when scaled up. Since the rescaling of the EEG time series occurs only in time (and not in amplitude), the EEG signals show self-affinity (rescaling in one specific direction) rather than self-similarity (rescaling in all directions). Of course, for natural fractals, self-similarity is only in statistical distribution instead of that of geometrical fractals; we can thus infer that the self-affine models do not perfectly fit empirical data, such as neurophysiological processes recorded from the brain (34). This deviation from perfect fractal forms of the natural systems is due to the physical world's inherent randomness and finite nature. Mathematically, a scale-free property emerges in the power-law relationship between a measure (Ω) of the process and its scale (s): $\Omega \propto s^{\lambda}$ (34). It is then easily understood that Ω's ratio in two different scales is influenced only by the relative scale and not their explicit values: $\frac{\Omega 1}{\Omega 2} = \left(\frac{s1}{s2}\right)^{\lambda}$, hence the term "scale-free" is coined for the process. In the time domain, this relationship is illustrated by the scaling function, which describes the dependence of scale on the signals' covariance (see section **3.1.1**). Another example of scale-free brain dynamics is the $1/f$ noise of the EEG's power spectrum (35), where the power density (P) is related to the frequency (f) in a power-law manner ($P = f^{\lambda}$). This is best illustrated in the linear relationship observed in the log[1]-log power spectrum (**Figure 2A**). The superposition of oscillatory neural activity appears as narrow range peaks representing the traditional EEG bands (e.g. 10 Hz activity giving rise to the alpha peak). Earlier, researchers have focused on the oscillatory components of brain activity, while the broadband fractal component was believed to be noise, hence "$1/f$ noise". In the last decades, the importance of the scale-free component has been recognized as it bears fundamental physiological significance (30), which can be modulated by pharmacological agents (36, 37). As a result, several studies have investigated the fractal properties of EEG in healthy (38–40) and diseased populations (41–43). It was also shown that the EEG changes observed in schizophrenia (44) and during object recognition (45) are entirely caused by changes in the fractal profile of the

[1] In the entirety of this dissertation log corresponds to the natural logarithm.

signal, suggesting that a great wealth of information can be found in the scale-free analysis of EEG records. Moreover, fractal formalism has been extended to multifractality, where more complex interactions of this time-persisting FC can be studied (46). Such properties can be represented in the spectrogram, which is a time-resolved representation of the power spectrum of a signal. Monofractal signals have a generally homogeneous spectrogram, meaning that the frequency components remain constant throughout the signal (**Figure 3**). On the other hand, the relative ratio of frequency components changes in multifractal signals as function of time (**Figure 3**). So far, only the scale-free properties of the univariate EEG signals have been studied extensively; on the other hand, the scale-free coupled dynamics of EEG tracings have remained hidden.

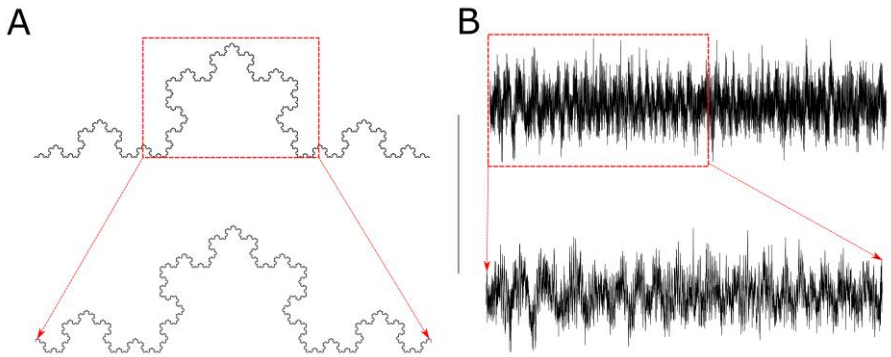

Figure 1: *Geometrical and statistical fractals.* Panel A: Self-similarity in Koch curve[2]. Geometrical fractals consist of smaller pieces identical to the whole structure. Note that the small piece of curve magnified in the lower part looks morphologically similar to the curve in the upper part. Panel B: Self-affinity in EEG signal. The lower part is the 20 seconds-long scaled-up version of the original 40 second time series. The two signals might not be identical, yet their values have the same distribution.

To this day, only a few studies have investigated the temporal fractal nature of FC (47–50). The aforementioned power-law relationship can be found in the coupled dynamics as well, both in the frequency (51) (power-law of cross-power spectrum shown in **Figure 2B**) and time domain (52) (scaling function shown in **Figure 4**). The fractal nature of FC indicates the existence of coupling that persists through time, in contrast to the FC of characteristic time scales captured by traditional methods [e.g. Pearson's correlation and mutual information (53), a non-parametric entropy-based bivariate measure].

[2] Janaka Wansapura (2021). KOCH CURVE (https://www.mathworks.com/matlabcentral/fileexchange/55796-koch-curve), MATLAB Central File Exchange. Retrieved May 28, 2021.

DOI:10.14753/SE.2022.2667

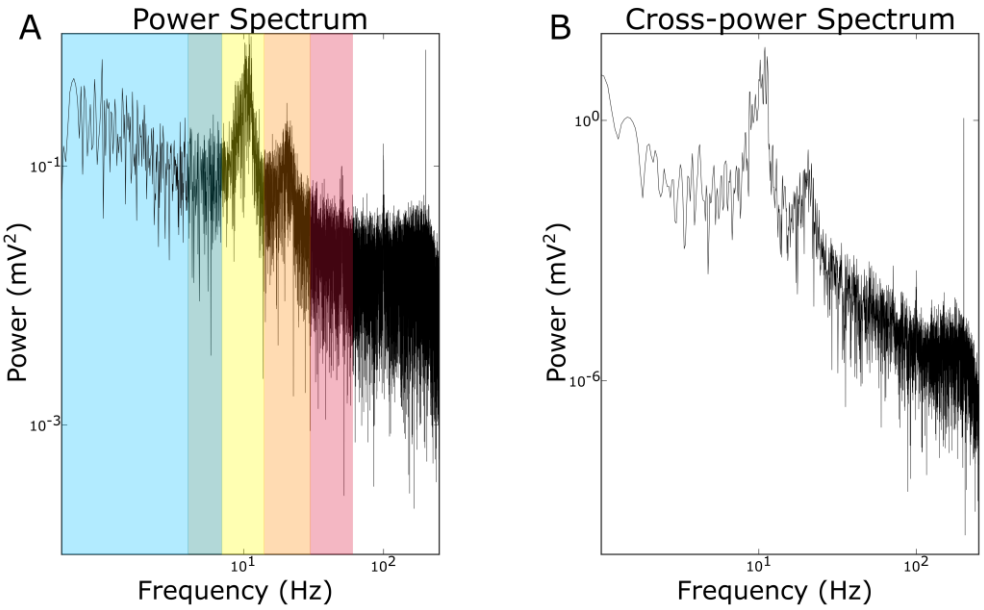

Figure 2: *Power-law relationship in the EEG spectra.* Panel A: The power-law relationship of the power spectrum of the EEG signal is best demonstrated in a log-log axis. Blue: delta band (0.5-4 Hz), Green: theta band (4-7 Hz), Yellow: alpha band (7-14 Hz), Orange: beta band (14-30 Hz), Pink: gamma band (30-60 Hz). Panel B: The power-law relationship of the cross-power spectrum of a pair of EEG signals is best demonstrated in a log-log axis.

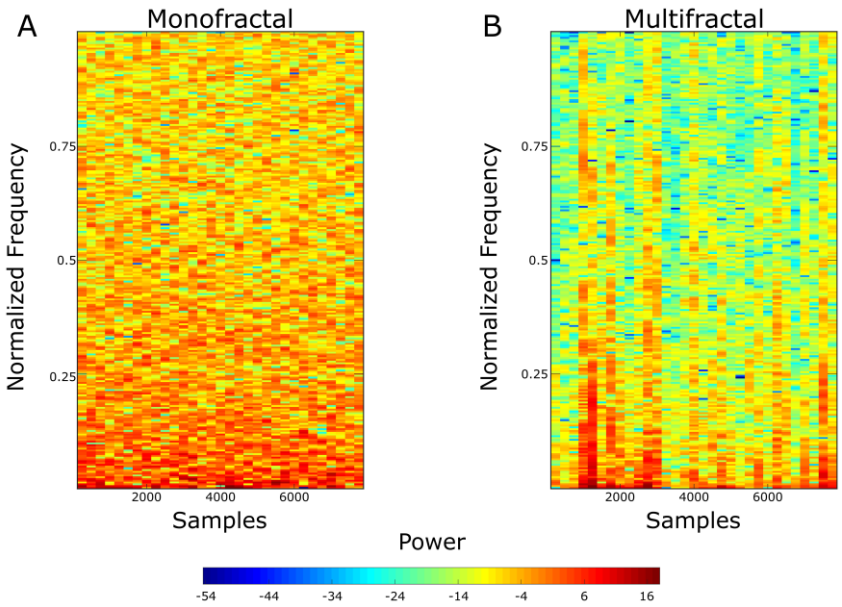

Figure 3: *Spectrograms of monofractal and multifractal signals*. Panel A: The distribution of frequency components remains fairly consistent during time in monofractal signals. Normalized frequency is the frequency divided by the sampling frequency of the signal. Panel B: The distribution of frequency components greatly varies during time in multifractal signals. Signals used for the demonstration originally appeared at Ihlen 2012 (54).

DOI:10.14753/SE.2022.2667

Even though the resting-state studies have dominated the field, more and more scientists have begun exploring the change of FC during mental strain. During a complex cognitive activity, distant brain regions have to cooperate, making task conditions great experimental paradigms for FC studies (55–58). For example, during visual pattern recognition (VPR), the information is relayed to the visual cortex found in the occipital lobe. From there, functional connections convey the signal to the high-level association areas located in the frontal and parietal cortices (59, 60). Such FC was studied earlier by our research group, which showed that the interconnectivity of the prefrontal cortex increases during VPR (61). This study used only Pearson's correlation as FC estimator, which can capture only linear relationships between the network nodes at a specific time scale (62).

DOI:10.14753/SE.2022.2667

2. OBJECTIVES

Previous studies showed that the coupling of the brain regions is scale-free. These findings have been so far constrained only to the monofractal case, even though brain dynamics have multifractal features. In the research underlying this dissertation, I investigated the multifractal aspect of functional connectivity using the already-introduced bivariate focus-based multifractal (BFMF) analysis. To evaluate the presence of scale-free coupled dynamics, we devised a new battery of bivariate multifractality assessment tests. These qualitative procedures were adapted from similar modifications of univariate tests or explicitly designed bivariate tests. BFMF analysis and subsequent scale-free assessment of FC were performed in two different sample populations and experimental protocols. An online dataset of resting-state eyes-closed EEG recordings was analyzed in the first study. Our goal was to validate BFMF as a viable FC estimator by studying the percentage of genuinely multifractal connections and the regional and subject variability of the examined coupled dynamics. I also attempted to elucidate the neurophysiological significance of scale-free coupled dynamics related to coordinated activities within and between resting-RSNs.

The second study targeted the task-related reorganization of multifractal functional connectivity during cognitive workload preceded by an eye-closed and eyes-open period. The utilized cognitive paradigm was a VPR task of stratified difficulty due to its ability to elicit network changes. The same battery of multifractality assessment tests was recruited to validate the multifractal nature of the connections during the task. The regional variability in task conditions was investigated. Finally, we studied the shift of brain's multifractal functional connectivity reconstructed from EEG recorded from 14 cortical regions during task and how it correlates with the performance metrics (success rate and reaction time).

3. METHODS

The methods section is divided into three parts. Our new algorithm for multifractal FC estimation is introduced in the first part, followed by its accompanying multifractality assessment tests. Then (second part), the construction of brain networks is described. Finally, the third part gives a detailed description of the measurement protocols and experimental paradigms.

3.1. Scale-free functional connectivity estimation

3.1.1. Bivariate focus-based multifractal analysis

In the last decades, different bivariate (i.e., concerning two time series) fractal analytical methods were developed (46, 52, 63). One of them is the bivariate focus-based multifractal analysis (64) which is the focus of this dissertation. The main goal of BFMF is to capture the scaling exponents with which the covariance of two signals depends on the used scale. These exponents can give insights about the multifractal coupled dynamics of the brain.

The BFMF analysis between two time series X and Y of length L progresses as follows. Initially, the mean is subtracted from every time series (centering), followed by bridge-detrending. Detrending is a common step in fractal time series analysis (65). In bridge-detrending, a line is drawn connecting the first and last datapoints of the v^{th} window. This line is then subtracted from the corresponding points of the window (66, 67). Subsequently, the scaling function S_{XY} can be calculated:

$$S_{XY}(q,s) = \left(\frac{1}{N_s}\sum_{v=1}^{N_s} |cov_{XY}(v,s)|^q\right)^{1/q}, \quad (1)$$

DOI:10.14753/SE.2022.2667

where N_s is the number of non-overlapping windows[3] of size[4] s (s=2^n) indexed by v. The statistical moment order, q, takes the integer values between -15 and +15, adequate[5] minimal and maximal values, respectively (68). The covariance of the two signals in the v^{th} window is denoted by $cov_{XY}(v, s)$. In the special case of q=0, the scaling function should be defined alternatively (due to the division of 0 in the exponent, 1/q), resulting in a modified formula:

$$S_{XY}(0,s) = e^{\frac{1}{2N_s}\sum_{v=1}^{N_S} log(|cov_{XY}(v,s)|)}, \quad (2)$$

in line with the univariate multifractal analysis (69). When the entire time series are used (s=L), the scaling function becomes independent of q:

$$S_{XY}(q,L) = |cov_{XY}|. \quad (3)$$

The scaling function is used for the estimation of the bivariate generalized Hurst exponent [$H(q)$], which is proportional to S_{XY} [$S_{XY}(q,s) \propto s^{H(q)}$]. This relationship is best visualized in a log-log axis (**Figure 4**). The simultaneous fit for every statistical moment (q), with regression lines intersecting at the same point [termed *Focus*, an estimated value of scaling function at s=L which is not equal to $S_{XY}(q,L)$], provides more robust estimates of bivariate $H(q)$ (70), compared to individual fit for every q (46, 63). The coefficients of these models define bivariate $H(q)$. As explained below, $H(2)$ signifies the degree of linear long-term cross-correlation between X and Y, while bivariate ΔH_{15} reflects the multifractality between X and Y.

[3]BFMF is a bivariate variation of focus-based multifractal formalism (FMF) (70) using signal summation conversion (SSC)(67). Preliminary analysis of FMF and SSC have shown that a sliding window approach does not provide additional benefits than non-overlapping windows. In order to avoid redundancy and for the sake of computational efficiency, we decided to use non-overlapping windows as in our previous publications (67, 70, 102, 103, 129)

[4] Dyadic scales are chosen because in logarithmic scales the points on the graph are equidistant, resulting in the best combination of small standard error and small leverage of points during the linear regression (137).

[5] More positive or negative values of q would have contributed minimally due to the redundancy of the multifractal spectrum, as illustrated in Figure 10C of Nagy et al. (103).

The meaning of the bivariate generalized Hurst exponent is a direct extension of its univariate counterpart (51) described below. The autocorrelation function (ρ_k) of a signal with a univariate $H(2$ is given by:

$$\rho_k = \frac{1}{2}\left(|k+1|^{2H(2)} - 2k^{2H(2)} + |k-1|^{2H(2)}\right), \quad (4)$$

where k is the lag (expressed in time or datapoints). Substituting univariate $H(2)$ with 0.5, the autocorrelation decays to 0 instantly. When univariate $H(2)<0.5$ the autocorrelation function will take longer to reach zero, yet its memory is still finite. This can be best understood by estimating $\int_0^\infty \rho_k$ for such signals; in these cases the univariate. integral is a finite real number (71). On the contrary, when univariate $H(2)>0.5$, the decay of ρ_k is much slower; $\int_0^\infty \rho_k$ is infinite, i.e. the memory of the signal would asymptomatically approximate zero but would never reach it. Based on these, the signal's memory is divided into 3 categories: *i*) short-term memory for univariate $H(2)<0.5$, *ii*) no memory for univariate $H(2)=0.5$ and *iii*) long-term memory for univariate $H(2)>0.5$. For bridge-detrended and centered signals with long-term memory signals positive (negative) values are more likely to be followed by positive (negative) values. For signals with the same preconditioning and lacking memory positive (negative) values are equally likely to be followed by positive or negative values. Finally, in case of signals with short-term memory positive (negative) values are more likely to be followed by negative (positive) values after centering and detrending. Even if Eq. 4 shows a power-law relationship for both $H(2)>0.5$ and $H(2)<0.5$, it is accustomed to say that processes with $H(2)<0.5$ decay in an exponential manner (72). This framework can be straightforwardly extended to the bivariate cases. In bivariate scale-free analysis: *i*) bivariate $H(2)>0.5$ corresponds to long-term cross-correlation *ii*) bivariate $H(2)=0.5$ indicates no-memory cross-correlation and *iii*) bivariate $H(2)<0.5$ represents short-term cross-correlation.

In the case of coupled monofractal dynamics, all bivariate $H(q)$ equal to bivariate $H(2)$; on the other hand, multifractal relationships display greater complexity. As seen in Eq. 1, the scaling function values for negative q are mainly determined by small covariances, while positive q are mainly influenced by large covariances. This deviation

DOI:10.14753/SE.2022.2667

from bivariate monofractality can be estimated with a parameter that measures the strength of multifractality (68):

$$\Delta H_{15} = H(-15) - H(15). \quad (5)$$

The higher the values of ΔH_{15}, the stronger the bivariate multifractality, which captures the *q*-dependent effect of small and large covariances on the long-term cross-correlation of the *X*-*Y* connection. In summary, bivariate $H(2)$ and ΔH_{15} are indicators of linear and non-linear coupling (73), respectively.

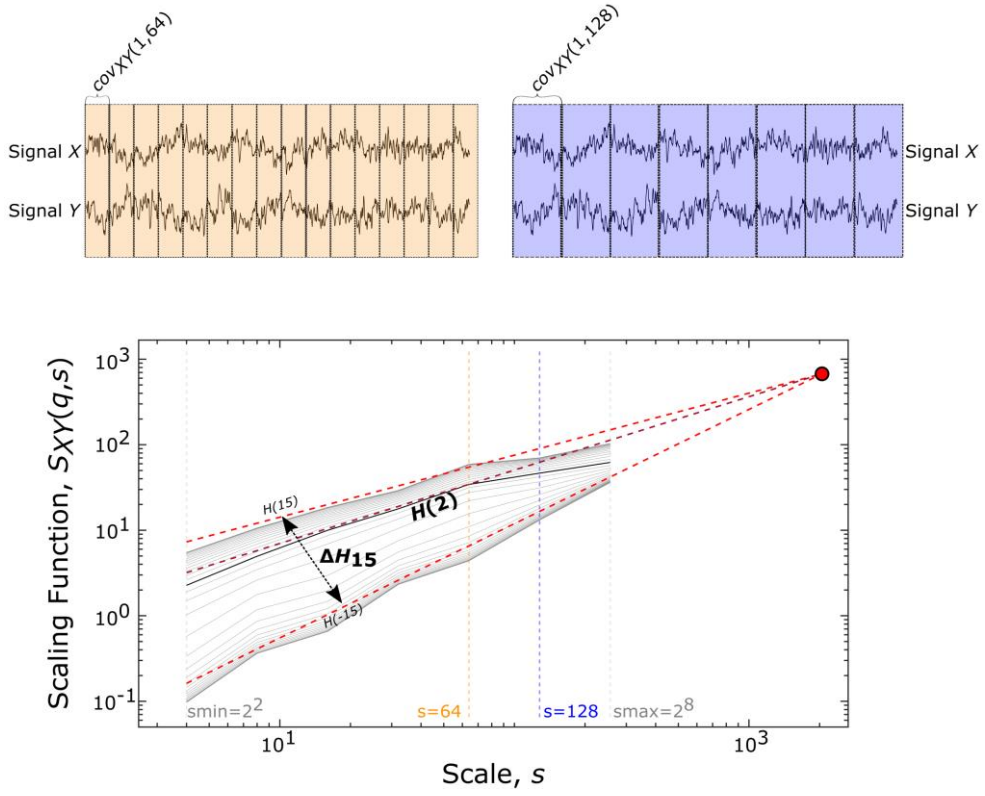

Figure 4: *Multifractal time series analysis and its endpoint parameters.* On the upper panels, a representative pair of 2048 datapoint-long EEG segments is displayed along with the windowing scheme for a smaller (*s*=64, shown in yellow) and larger (*s*=128, shown in blue) scale, which illustrates the calculation of covariance scaling function [$S_{XY}(q,s)$ displayed in the lower panel] according to Eq. 1. The *Focus* (red disk) is used as a reference point when simultaneously fitting linear models in the log-log transform of the $S_{XY}(q,s)$ vs *s*, the essential step of BFMF. The slope of each linear regression line represents the generalized bivariate Hurst exponent [$H(q)$] (shown for *q*=-15, +2, +15). Bivariate $H(2)$ describes the long-term cross-correlation between the signals *X* and *Y*, while the degree of multifractality (bivariate ΔH_{15}) is captured in the difference between $H(q)$ values at the extreme [i.e. minimal (-15) and maximal (15)] statistical moments. The figure originally appeared in Stylianou et al. (74).

3.1.2. Multifractality assessment tests

BFMF analysis can be applied to any pair of time series, even when no scale-free interactions occur; possible causes of spurious multifractality are presented in the next pages. Therefore, it is indispensable to assess true bivariate multifractality for every connection with an array of qualitative tests, each targeting a different multifractal property of the connection.

Figure 2A shows the power spectrum of a univariate EEG time series in the frequency domain. The slope of the log(spectral power) vs log(frequency) represents the spectral index (β) and is proportional to the univariate $H(2)$ [$\beta=2H(2)-1$] (34)[6]. A similar power-law relationship (**Figure 2B**) can also be derived in the bivariate setting where the slope of log(cross-spectral power) vs log(frequency) is proportional to the bivariate $H(2)$ [$\beta=2H(2)-1$] (51). We can investigate this relationship by modifying the power-law presented in Clauset et al. (75). To generate a sufficient population size for a two-tailed comparison with $\alpha=0.05$, 40 surrogate fractal time series are created using the spectral synthesis method (73) to investigate every pair of signals. The univariate $H(2)$ of these surrogates is equal to the estimated bivariate $H(2)$. A linear regression model is then fitted on the log-log transformed power spectrum. The Kolmogorov distance (KD)[7] between the actual and fitted values is estimated. Calculating KD for each surrogate results in a distribution of maximal distances ($\boldsymbol{D}_{\mathbf{univ}}$[8]). Similarly, a single D_{biv} for the cross-power spectrum of the original connection is computed. If the following inequality holds, the coupled dynamics show power-law characteristics in the frequency domain,

$$D_{biv} < \mu(\boldsymbol{D}_{\boldsymbol{univ}}) + 2\sigma(\boldsymbol{D}_{\boldsymbol{univ}}), \quad (6)$$

[6] According to the review of Eke and colleagues (34) $\beta=2H(2)-1$ or $\beta=2H(2)+1$ depending on the type of time series (fractional Gaussian noise or fractional Brownian motion). BFMF and its univariate equivalent (70) are based on the signal summation conversion method (67) which is type-agnostic, i.e. $\beta=2H(2)-1$ holds for both types of time series.

[7] If $A(i)$ and $B(i)$ are the power and linear regression estimate for $i=1,2,...n$, respectively. $KD = \max(\sqrt{[A(i)-B(i)]^2})$.

[8] Bold symbols indicate a vector.

with μ($\boldsymbol{D}_{\mathbf{univ}}$) and σ($\boldsymbol{D}_{\mathbf{univ}}$) indicating the mean and population standard deviation of $\boldsymbol{D}_{\mathbf{univ}}$, respectively. Any future μ() and σ() correspond to the mean and standard deviation of the sampled distribution in question, respectively.

In 2011, the detrended cross-correlation coefficient[9] (ρ) was introduced (76):

$$\rho(s) = \frac{S_{XY}^2(2,s)}{S_X(2,s)S_Y(2,s)}, \quad (7)$$

where $S_X(2,s)$, $S_Y(2,s)$ and $S_{XY}(2,s)$ are the scaling function values for scales s and the second order statistical moment of time series X, Y and their connection, respectively. Initially, univariate $H(2)$ and univariate ΔH_{15} of the signals creating the connection are calculated, using the univariate equivalent of BFMF (70). We continue by generating 100 pairs[10] of surrogate time series (77) of equal L, univariate $H(2)$ and univariate ΔH_{15}. Then ρ of every surrogate pair is calculated, resulting in a 100-value distribution which is compared with the original ρ (ρ_{orig}). ρ_{orig} is considered significantly different (successful test) if it is outside the 1-α confidence interval of the surrogate distribution. Since ρ is scale-specific, the same process is repeated for every scale. A coupled dynamics is multifractal only when all scales pass the test. To have an overall significance level of 0.05, α should be set to $0.05^{1/n}$, where n is the number of scales, as adapted from Blythe et al. (78).

The tests mentioned so far evaluated only bivariate $H(2)$, but a monofractal and a multifractal connection can have the same bivariate $H(2)$. For this reason, we had to investigate the multifractal nature of the coupling explicitly. The following test explores the non-linear dynamics of the functional coupling, which are closely related to multifractality (73, 79)[11]. Initially, for each original (measured) pair of time series, 40 surrogate pairs are synthesized. For every iteration, the original pair is Fourier

[9] The name detrended cross-correlation coefficient is due to the fact it was first used in detrended cross-correlation analysis (52). In our analytical pipeline ρ is estimated by focus-based multifractal analysis of signals (70) and connections (64).

[10] While usually we use a surrogate population of 40 synthesized signals for a two-tailed test with a significance level of 0.05, here we created 10-10 signals and tested all their combination. Notably this surrogate test was the least time consuming, compared to others.

[11] The cited papers show a relationship between multifractality and nonlinearity in the univariate setting, we extend this concept in the bivariate case.

transformed into the frequency domain. The phase of every frequency is randomized, followed by inverse Fourier transform. The same permutation order is used for the phase randomization of the two signals, ensuring the destruction of non-linear interdependencies while the linear relationships are maintained (80). This means that the bivariate $H(2)$ of the original and surrogate pairs will be the same, but the bivariate ΔH_{15} of the surrogates will be diminished. The test is considered successful (i.e., multifractality due to non-linear dynamics) when:

$$\Delta H_{15} > \mu(\boldsymbol{\Delta H_{15,sur}}) + 2\sigma(\boldsymbol{\Delta H_{15,sur}}), \quad (8)$$

with ΔH_{15} being the single value of the original connection and $\boldsymbol{\Delta H_{15,sur}}$ being the distribution of the surrogates.

So far, we have focused only on one type of bivariate multifractality, the long-term memory multifractality. Bivariate multifractality can also stem from other sources, one of them being the joint distribution of the signals (81). A shuffling test allows for distinguishing between these two types of multifractality, since shuffling – permutation according to a random sequence – the order of datapoints in a pair of signals destroys their interdependence without affecting their joint distribution (82). Let us suppose the multifractal profile [captured in the bivariate $H(2)$ and ΔH_{15}] of a shuffled pair of time series is diminished. In that case, the observed multifractality is due to long-term memory. In this test, 40 shuffled pairs of time series are generated for each pair of original signals by shuffling and the following inequalities are investigated:

$$\begin{aligned} H_{orig}(2) &> \mu[\boldsymbol{H_{shfl}(2)}] + 2\sigma[\boldsymbol{H_{shfl}(2)}] \\ H_{orig}(2) &< \mu[\boldsymbol{H_{shfl}(2)}] - 2\sigma[\boldsymbol{H_{shfl}(2)}] \end{aligned} \quad (9a)$$

$$\Delta H_{15,orig} > \mu(\boldsymbol{\Delta H_{15,shfl}}) + 2\sigma(\boldsymbol{\Delta H_{15,shfl}}), \quad (9b)$$

where subscripts *orig* and *shfl* refer to estimated BFMF parameters of the original and shuffled signal pairs, respectively. A pair of time series underlying FC expresses bivariate

multifractality of long-term memory type only if the two inequalities hold and long-term monofractality if only 9a holds.

The last test examines whether the bivariate multifractality originates from the genuine coupling of the concerned processes or not. Assume two time series *X* and *Y* with scale-free coupling. The bivariate Hurst exponent [$H_{XY}(2)$] is lower than the average of the univariate $H_X(2)$ and $H_Y(2)$ (83). If $H_{XY}(2)$ is equal or higher than the mean of univariate Hurst exponents, then the observed bivariate coupling is due to autocorrelation, finite length or non-normal distribution (83–86). Firstly, 40 surrogate pairs of independent time series are created using the spectral synthesis method (87). Every (*X*, *Y*) couple has the same univariate $H_X(2)$ and $H_Y(2)$ as the original *X* and *Y* time series. Subsequently, the average of the $\boldsymbol{H_X(2)}$ and $\boldsymbol{H_Y(2)}$ is calculated for every pair of surrogates, resulting in a distribution [$\boldsymbol{H_{XY,gen}(2)}$]. Finally, we evaluate the following inequality:

$$H_{XY}(2) < \mu[\boldsymbol{H_{XY,gen}(2)}] - 2\sigma[\boldsymbol{H_{XY,gen}(2)}]. \quad (10)$$

If it holds, then the observed bivariate multifractality between signals *X* and *Y* is true, reflecting genuine scale-free coupling. On the other hand, if the original $H_{XY}(2)$ is not significantly smaller than $\boldsymbol{H_{XY,gen}(2)}$, the connection's multifractality is spurious.

3.2. Brain network analysis

BFMF yields the strength of scale-free coupling for every connection in terms of bivariate $H(2)$ and ΔH_{15}, from such values either weighted or binary networks can be reconstructed (13). In binary networks, a threshold value of FC is determined. Values higher or lower than this threshold are converted to 1 or 0, respectively. On the other hand, the weighted networks maintain their original FC values. Weighted networks tend to favor the stronger (and possibly not spurious) functional connections, making thresholding less essential. After constructing the functional connectome, we can proceed with the calculation of network measures. A commonly used metric is the weighted node degree (D^W), the sum of weighted edges of a node. D^W shows the importance of a specific node; while the

average weighted node degree ($\overline{D^W}$) shows the general interconnectivity, or wiring cost of the network (13). D^W and $\overline{D^W}$ can be calculated as follows:

$$D^W = \sum_{i=1}^{n} c_{i'} \quad (11)$$

n represents the number of all possible edges of a node, while c_i is the strength of the i^{th} connection.

$$\overline{D^W} = \frac{\sum_{j=1}^{N} D_j^W}{N}, \quad (12)$$

N represents the number all nodes of the network, while D_j^W is the weighted degree of the j^{th} node. Other commonly used network metrics are clustering coefficient and efficiency, indicators of segregation and integration of the network, respectively. In our previous study (88), these two measures were highly correlated with node degree; hence they were not included in the current analysis.

3.3. Validation of BFMF in the resting-state brain

3.3.1. Data acquisition and participants

The analyzed dataset was made publicly available by Sockeel et al. (89). 12 right-handed, healthy subjects (26.6±2.1 years old, 6 females) took part in the recordings, which consisted of 5 minutes of eyes-closed resting state. The participants were lying supine during the experiment and listening to audio recordings similar to MRI sounds. The EEG system was a 62-channel BrainAmp amplifier (electrodes arranged according to 10-10 system) with a sampling rate of 5 kHz. Oz and Cz were used as ground and reference electrodes[12], respectively. Electrode impedance was kept under 10 kΩ. The experiment was approved by Comité de Protection des Personnes–Ile-de-France (CPP DGS2007-0555). Every participant provided written and signed informed consent before the measurement.

[12] Electrodes positioned along the midsagittal line, O: occipital, C: central

3.3.2. EEG preprocessing

I selected 55 seconds of artifact-free EEG segments through visual inspection. We first applied a 0.5-250 Hz band-pass filter followed by notch filters at 50, 100 and 200 Hz and then downsampled to 500 Hz. Next, artifacts not directly related to brain activity (e.g., muscle contractions, eye movements, cardiac cycle, noise) were removed using the Harvard automated processing pipeline for electroencephalography (HAPPE) (90). HAPPE performs a series of automated artifact-removal steps, including wavelet-enhanced independent component analysis (wICA) and independent component analysis with multiple artifact rejection Algorithm (MARA) (91, 92). The purpose of ICA is to decompose the signal into independent components based on their statistical properties (minimized mutual information and maximized non-Gaussianity), which might reflect separate physiological sources. Finally, the cleaned EEG signals were re-referenced to the common average reference.

3.3.3. Functional connectivity estimation

Only the first 2^{14} datapoints (approximately 33s) of preprocessed signals were analyzed using BFMF; scales ranged from 2^4 (16 data points) to 2^9 (512 data points). Upon estimation of bivariate $H(2)$ and ΔH_{15}, the multifractality assessment tests of **section 3.1.2** were used to validate the true scale-free nature of the brain's FC. The bivariate-univariate Hurst comparison was considered successful in the case of the bivariate Hurst exponent being smaller or larger than the mean of the univariate Hurst exponents[13].

3.3.4. Brain parcellation

Every channel was assigned to one of seven RSNs specified at Yeo et al. (93) according to the probabilistic map of Giacometti et al. (94). The limbic system and ventral attention networks were combined to a ventral attention-limbic network due to their high overlap (**Figure 5**). The goal of this parcellation was to minimize the effect of multiple comparisons while obtaining physiologically meaningful conclusions. As the last step,

[13] The description of the bivariate-univariate Hurst comparison in section **3.1.2** describes the final version of the test, which was modified after our validation study. The VPR study considers the test successful only if it is smaller than the mean of the univariate exponents, as stated in section **3.1.2**.

the BFMF-derived values of the connections were averaged, resulting in 6 within-RSNs and 15 between-RSNs values for each of the bivariate $H(2)$ and ΔH_{15} networks.

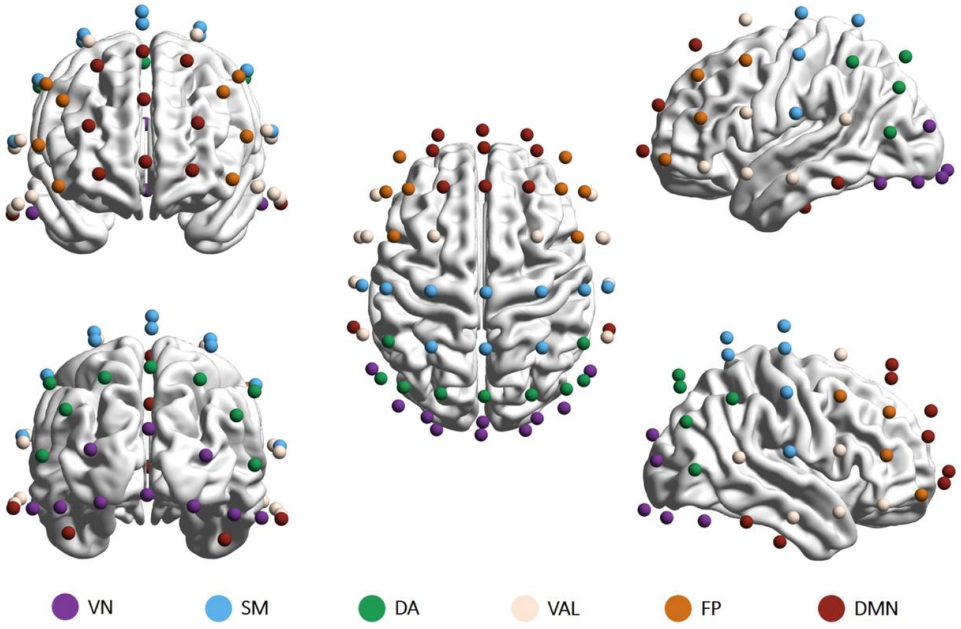

Figure 5*: Parcellation of EEG channels to resting-state networks (RSNs).* Electrodes were grouped to represent six RSNs: the visual network (VN, 10 channels), the somatomotor network (SM, 10 channels), the dorsal attention network (DA, 9 channels), the combined ventral attention and limbic networks (VAL, 12 channels), the frontoparietal network (FP, 8 channels) and the default mode network (DMN, 13 channels). Brain maps were created using the BrainNet Viewer software (95) after electrode positions were transformed to match a template head using SPM 12b (96). VN = visual network; SM = somatomotor; DA = dorsal attention; VAL = ventral attention and limbic; FP = frontoparietal; DMN = default mode network. The figure originally appeared in Racz et al. (97).

3.3.5. Statistical evaluation

Initially, the agreement between participants was evaluated using Kendall's coefficient of concordance (W). Then, we studied the effect of localization using the Friedman test (the level of significance was set to 0.05 for all tests, unless stated otherwise) – since the assumptions of ANOVA were not satisfied – followed by a series of paired comparisons (paired sample t-test if distributions were normal, Wilcoxon signed-rank test if at least one distribution was non-normal, normality was evaluated by Lilliefors test). The significance of every individual comparison was assessed by Benjamini-Hochberg (BH) correction (98).

We also investigated the validity of our parcellation scheme with the aid of 100 surrogate datasets. The original labels were shuffled in every surrogate, corresponding to a random grouping of channels to RSNs. For every iteration, we performed Friedman tests and Kendall's *W* calculations. For our parcellation to be physiologically meaningful, the following two conditions should be met: *i*) the Friedman's tests *p*-values do not show significance in at least 95 of the 100 iterations and *ii*) the original *W* is greater than the 95th percentile of the surrogate *W*s. The entire analytical pipeline was carried out in MATLAB 2012 (MA, Natick, USA).

3.4. Reorganization of multifractal FC during visual pattern recognition

3.4.1. Data acquisition and participants

We recruited 58 young colleagues and university students with no history of neuropsychiatric illness (24.2±3.4 years old, 28 females, 9 left-handed). The study was designed according to the Declaration of Helsinki and was approved by the Regional and Institutional Committee of Science and Research Ethics of Semmelweis University (approval number: 2020/6). The participants were requested to have a good night's sleep the day before the experiments.

The measurement consisted of two resting-states and 30 trials of a computer-based pattern recognition task (**Figure 6**). Initially, the subjects were instructed to stay relaxed for 3 minutes of eyes-closed (EC) resting-state, followed by 3 minutes of eyes-open (EO) resting-state. After completing the two resting-states, the participants solved 30 pattern recognition trials, modified after Racz and colleagues (61). Every trial consisted of an active period, followed by an interstimulus (passive) interval. In the active period, the volunteer had 10 seconds to recognize and click a subregion of a grayscale image presented on a computer screen. After clicking on the grayscale picture, the passive interstimulus interval started. A gray background was projected on the computer's monitor for 10 seconds during this section. The subject had maximum 10 seconds to click on the image during the active section; if he/she did not, the passive section started. 6 different images were projected during the task period. Every image was shown 5 times, every time with a different subsection to be identified, resulting in 30 (6x5) trials. The 6 images were divided into 3 categories (2 Easy, 2 Medium and 2 Hard) based on their

compressed/uncompressed image ratio (99). The order of the trials was randomized with a different permutation before every experiment to prevent fatigue-related bias. The following performance metrics were recorded during the pattern recognition task: *i*) success, defined as 1 when the volunteer correctly identified the image during the active section and 0 otherwise and *ii*) reaction time, the time between the beginning of image projection and response (mouse click) in the active section. If the volunteer did not complete the active section on time (10 seconds or less), the trial was considered a failure (success=0) and the reaction time was set to 10 seconds. All measurements took place in the facilities of the Department of Physiology of Semmelweis University. The measurements were carried out in a quiet and dimly lit room, while the participants were comfortably seated in a chair approximately 80 cm from a computer monitor, from where they saw the images sharply. I implemented the experimental paradigm in MATLAB 2012 (MA, Natick, USA).

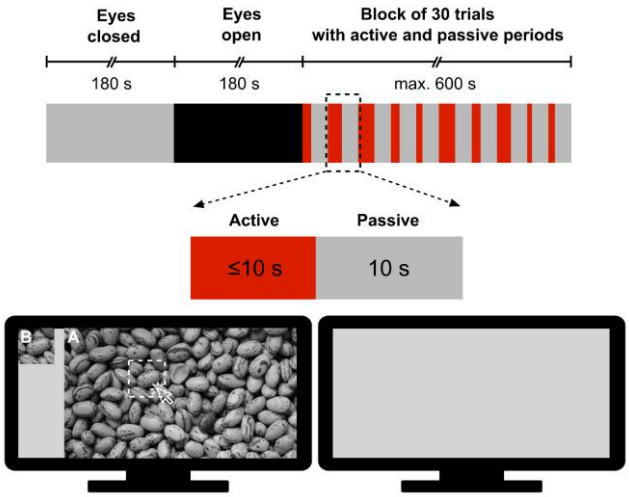

Figure 6: *Measurement protocol for obtaining electroencephalography records during resting states and subsequent cognitive stimulations.* First, two resting-state recordings were made in 90 seconds periods with eyes closed and eyes open, respectively. Then, the participant performed a computer-based visual pattern recognition task in a block of 30 trials, each consisting of a 10 second or less active and a 10 second passive period. In the active period, participants were presented a large-size image (A) and its cropped sub-region (B) and were required to click on A at the position of B if found. The figure originally appeared in Stylianou et al. (74).

To record EEG signals, we utilized an Emotiv Epoc+ system (Emotiv Systems Inc., San Francisco, CA, USA). The electrical impedance between the scalp and the device was kept below 20 kΩ, indicated by Emotiv's software (Emotiv Pro). Brain activities from 14 different cortical regions were recorded according to the 10-20

international system (**Figure 7**) at a sampling rate of 128 Hz[14]. Electrodes at the left and right mastoid processes were used as CMS and DRL reference, respectively. Participants were instructed to stay still as much as possible and refrain from facial expressions.

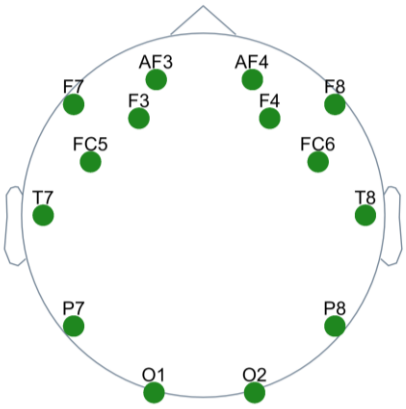

Figure 7: *Channel layout of Emotiv Epoc+*. The layout follows the 10-20 nomenclature: AF3, AF4, F3, F4, F7, F8, FC5, FC6, T7, T8, P7, P8, O1 and O2.

3.4.2. EEG preprocessing

Due to the device's built-in notch (50 and 60 Hz) and band-pass (0.2-45 Hz, digital 5th order Sinc) filters, no further filtering of the dataset was applied. Artifacts were removed from every trial separately. As in the previous study, we first cleaned spikes of electrical activity using wICA. Because of the short length of the trials (20 seconds or less), we could not utilize ICA-MARA; instead, we performed manual independent component analysis using built-in functions of EEGLAB (100), our selection criteria were based on the morphology of the component time series, localization and power spectrum (tutorial found at: https://labeling.ucsd.edu/tutorial/labels).

[14] 18 recordings were carried out with an Emotiv Epoc+ of 256 Hz sampling rate which was downsampled to 128 Hz prior to further preprocessing.

3.4.3. Functional connectivity estimation

Each trial (active session + 10 seconds of passive session) was analyzed individually. From the 3 min of EC and EO 9 non-overlapping 20 seconds-long segments were analyzed with BFMF to match the trial segments' length. For the BFMF analysis, we use dyadic scales ranging from 2^2 to 2^8. Upon estimation of bivariate $H(2)$ and ΔH_{15} the multifractality assessment tests of **section 3.1.2** were used to validate the true scale-free nature of the brain's FC.

3.4.4. Assessment of functional brain networks

In total, 48 segments per subject were analyzed (9 EC, 9 EO, 10 Easy, 10 Medium and 10 Hard). The bivariate $H(2)$ and ΔH_{15} values for the same state were averaged, yielding 5 segments (EC, EO, Easy, Medium, Hard) for every BFMF-derived network [bivariate $H(2)$ and ΔH_{15}]. To characterize the obtained networks, we calculated D^W and $\overline{D^W}$ of all brain graphs, using either bivariate $H(2)$ or ΔH_{15} as weights of edges.

3.4.5. Statistical evaluation

The first step of our analysis was to capture the between-states (e.g., Medium vs Hard) and within-states differences (e.g., AF4 vs AF3 in Easy). In the between-states comparisons, we contrasted both global and local node degrees. Due to the non-normal nature of the distributions in question (evaluated by Lilliefors test), we used a Friedman test followed by a series of paired comparisons. If both distributions were normal, we performed a paired sample t-test; in any other case, a Wilcoxon signed-rank test was used. To control the false discovery rate for multiple comparisons we used BH correction. In the within-state comparisons, we compared the local node degrees of each network by using the aforementioned Friedman test followed by paired t-test or Wilcoxon signed-rank test (depending on Lilliefors test results) followed by BH correction. An extra analytical step in our within-state analysis was calculating Kendall's coefficient of concordance of D^W.

As to the cognitive assessments we evaluated task performance and its correlation with the networks' architecture. Firstly, we compared the average reaction time (RT) and average success rate (SR) in the 3 difficulty levels, using the same statistical methods as

in the between-states comparisons. Then, to evaluate how network characteristics and performance relate, we calculated Spearman's correlation (r) between SR-$\overline{D^W}$ and RT-$\overline{D^W}$ for every difficulty level, followed by BH correction. The entire analysis was carried out in MATLAB 2012 (MA, Natick, USA).

4. RESULTS

4.1. Multifractal neural networks in the resting state

4.1.1. Presence of true bivariate multifractality during task

Table 1 summarizes the results of the multifractal tests of BFMF-derived FC in resting-state. Most of the connections passed the power-law, detrended cross-correlation, phase randomization and shuffling tests. On the other hand, the scale-free nature of almost half of the connections emerged simply due to the autocorrelation effects (bivariate-univariate Hurst comparison).

Table 1*: Success rate of multifractality tests at the subject level (mean±standard deviation).* PL: power-law test, PR: phase randomization test, S-ΔH_{15}: ΔH_{15} part of the shuffling test, S-$H(2)$: $H(2)$ part of the shuffling test, DCCC: detrended cross-correlation coefficient test, Biv-Univ: bivariate-univariate Hurst comparison

Tests					
PL	**PR**	**S-ΔH_{15}**	**S-$H(2)$**	**DCCC**	**Biv-Univ**
86.5±5%	100%	100%	99.7±0.3%	100%	52.4±6.8%

4.1.2. Topological differences in scale-free neural networks

To compare the networks reconstructed from $H(2)$ and ΔH_{15} values, we calculated each connection's Z score (deviation from the population average). Plotting these networks (**Figure 8**), we saw opposite patterns emerging in each, which was confirmed by Pearson's correlation (r=-0.6609, p<0.01). The higher bivariate $H(2)$ values were found mainly in the within-RSNs connections. On the other hand, the bivariate ΔH_{15} values of the between-RSNs connections were much higher than those found within the resting-state networks.

DOI:10.14753/SE.2022.2667

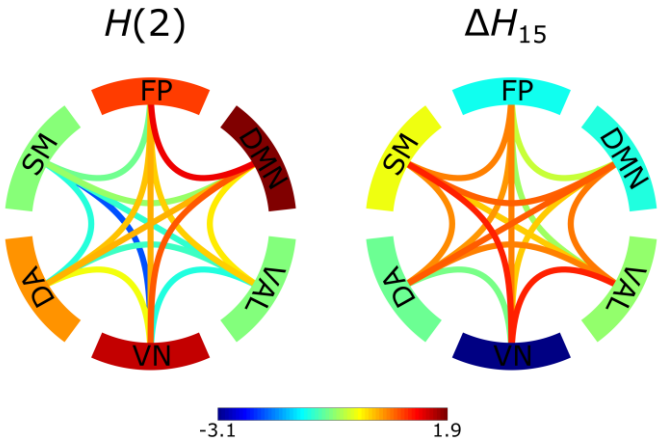

Figure 8: *Z-scores of constructed networks using bivariate H(2) and ΔH_{15} as functional connectivity estimators.* Z-scores represent deviation from the population average and their values are indicated by the color bar. The edges serve as the between-RSNs (inner edges) and within-RSNs (outer ring) connections with color representing the strength of the connection. The figure originally appeared in Stylianou et al. (101).

There is also a dichotomous model between bivariate $H(2)$ and ΔH_{15} in the regional and subject variability. Kendall's W revealed strong between-subject agreement in the case of bivariate $H(2)$ networks but only moderate agreement when the ΔH_{15} networks were investigated (**Table 2**). As for the topological differences, only 40% of the within-RSNs and between-RSNs paired comparisons of the ΔH_{15} networks were significant, while the $H(2)$ networks showed greater variability (73.3% and 68.6%, respectively) (**Table 2**). As seen in **Figure 9**, most regional variations were observed exclusively in one of the BFMF-derived networks.

Table 2*: Results of Kendall's W, success rate for individual paired difference tests after correction and Friedman test for bivariate H(2) and ΔH_{15} for between- and within- RSNs.*

		Kendall's *W*	**Paired difference test success rate**	**Friedman Test *p***
***H*(2)**	between-RSNs	0.72	68.6%	< 0.0001
	within-RSNs	0.65	73.3%	
ΔH_{15}	ΔH_{15} between-RSNs	0.44	40%	
	ΔH_{15} within-RSNs	0.47	40%	

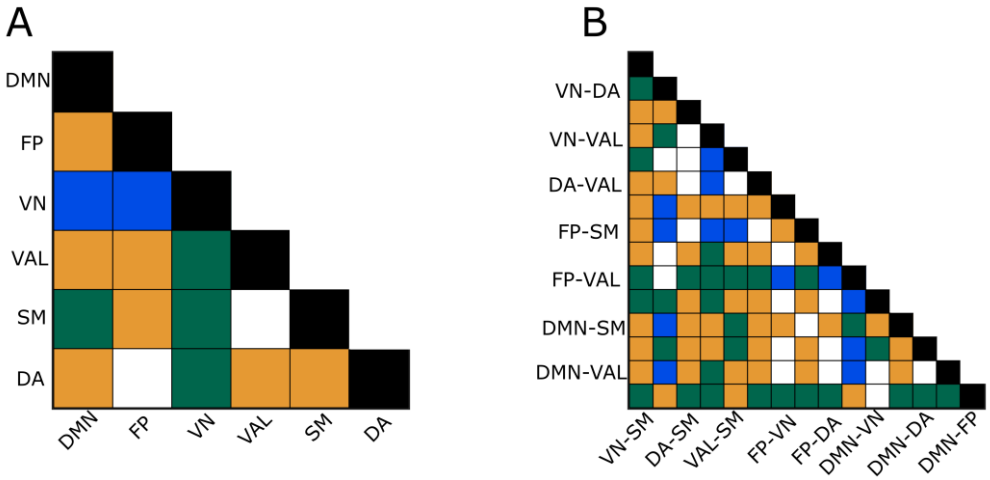

Figure 9: *Effect of regional variability. Significance of connection-to-connection comparisons of within- (Panel A) and between- (Panel B) RSNs after the appropriate correction for bivariate H(2) and ΔH_{15}.* Blue: Only ΔH_{15} comparison test was significant. Orange: Only $H(2)$ comparison test was significant. Green: Both $H(2)$ and ΔH_{15} comparison tests were significant. The figure originally appeared in Stylianou et al. (101).

Finally, we also investigated the physiological relevance of our parcellation scheme, using 100 spatially shuffled surrogates. W of the original within-RSNs and between-RSNs connections were significantly higher than those of the shuffled data, for both bivariate $H(2)$ and ΔH_{15} networks. Additionally, only 1% of the surrogate datasets showed topological differences ($p<0.05$).

4.2. Multifractal connectivity during pattern recognition

4.2.1. Presence of true bivariate multifractality during task

Once again, most connections showed true multifractal dynamics (**Table 3**), while a distinction between the rest (EC and EO) and task (Easy, Medium and Hard) states was observed. The resting states had lower success rates in the bivariate $H(2)$ part of the shuffling test, but a higher percentage of their connections passed the detrended cross-correlation coefficient test and bivariate-univariate Hurst comparison. These differences resulted in more functional connections showing true bivariate multifractality in the bivariate $H(2)$ and ΔH_{15} networks during rest (**Table 4**).

Table 3: *Success rate of multifractality tests at the subject level (mean±standard deviation).* PL: power-law test, PR: phase randomization test, S-ΔH_{15}: ΔH_{15} part of the shuffling test, S-$H(2)$: $H(2)$ part of the shuffling test, DCCC: detrended cross-correlation coefficient test, Biv-Univ: bivariate-univariate Hurst comparison

State	Tests					
	PL	**PR**	**S-ΔH_{15}**	**S-$H(2)$**	**DCCC**	**Biv-Univ**
EC	92±7%	96±4%	99±2%	70±18%	93±4%	85±18%
EO	94±3%	96±6%	98±4%	76±16%	93±4%	86±15%
Easy	93±2%	97±4%	99±2%	90±8%	64±19%	65±17%
Medium	94±2%	97±4%	99±2%	90±9%	65±16%	68±18%
Hard	94±2%	97±3%	99±2%	89±9%	62±17%	73±16%

Table 4: *Percentage of connections, at the subject level (mean±standard deviation), that passed all multifractality assessment tests*.

Network	State				
	EC	**EO**	**Easy**	**Medium**	**Hard**
***H*(2)**	48±13%	55±12%	31±10%	34±10%	35±9%
ΔH_{15}	46±13%	53±12%	30±10 %	33±10%	34±9%

4.2.2. Reorganization of scale-free neural networks during task

A similar rest vs task distinction was also observed in the node degree comparisons since the FC of the task states was higher for both bivariate $H(2)$ and ΔH_{15} networks. **Figure 10** suggests a negative correlation between the two created networks. The Spearman's correlations validated this by comparing the average of the local node degrees of the bivariate $H(2)$ and ΔH_{15} networks for every state (**Table 5**). Significant negative correlations were found in all states, except Easy. After BH correction only the correlation in the EC state remained significant. Additionally, the $\overline{D^W}$ of the task states was significantly higher compared to rest. Also, the $\overline{D^W}$ was higher in the EO compared to EC[15] (**Figure 11**). A similar pattern can be seen in the local D^W, where most differences are observed between rest and task states for both BFMF-derived networks (**Figure 12**). Statistically significant within-state comparisons were found for all 5 states. As it can be seen by the color-coding of **Figure 13**, most pairs of nodes that showed significant differences are in the ΔH_{15} networks (i.e., several blue and green edges but only a few

[15] The statistical power of the $\overline{D^W}$ tests was: *i*) 1 for rest vs task comparisons for both BFMF variables *ii*) 0.43 and 0.63 for the EC vs EO comparison of bivariate $H(2)$ and ΔH_{15}, respectively and *iii*) <0.12 for task vs task (e.g. Easy vs Medium) comparisons for both BFMF variables.

orange). Finally, small subject concordance was observed in the D^W of the ΔH_{15} networks (**Table 6**).

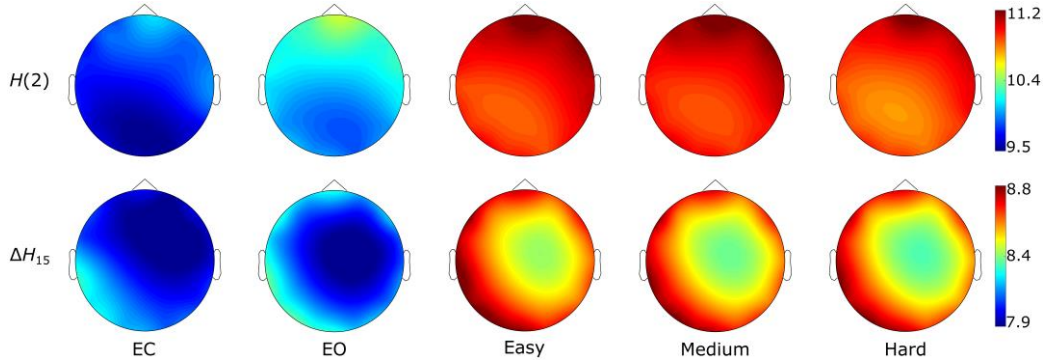

Figure 10 *State-dependent weighted node degree topology of H(2) and ΔH_{15} brain networks.* The color bars represent the values of the local node degrees. The figure originally appeared in Stylianou et al. (74).

Table 5: *Spearman's correlation (r) between the node degrees of the H(2) and ΔH_{15} brain networks and their significance levels (p).* The correlations that remained significant after Benjamini-Hochberg correction are in bold. The figure originally appeared in Stylianou et al. (74).

Spearman's Correlation	**State**				
	EC	**EO**	**Easy**	**Medium**	**Hard**
p	**<0.01**	0.05	0.08	0.02	0.04
r	**-0.85**	-0.54	-0.48	-0.62	-0.57

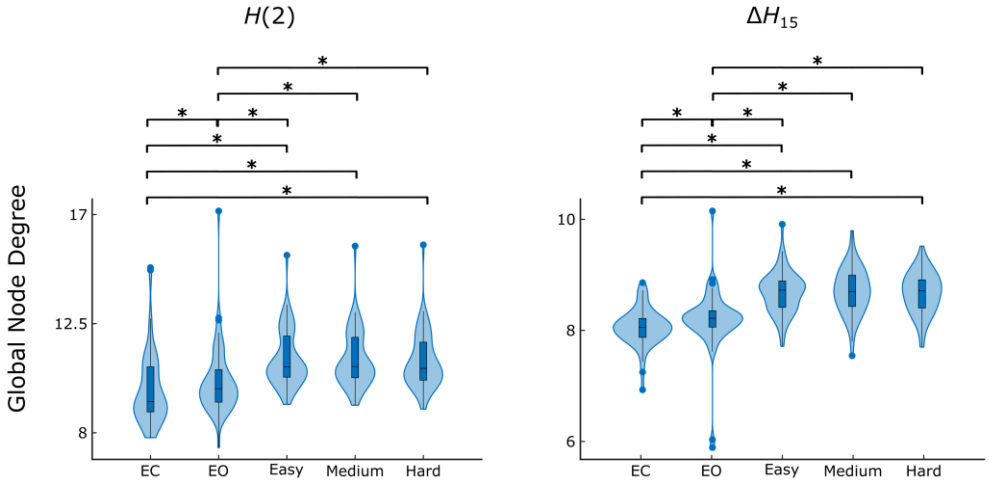

Figure 11*: State-dependent weighted global node degree distribution of H(2) and ΔH_{15} brain networks.* Significance marked by *. The figure originally appeared in Stylianou et al. (74).

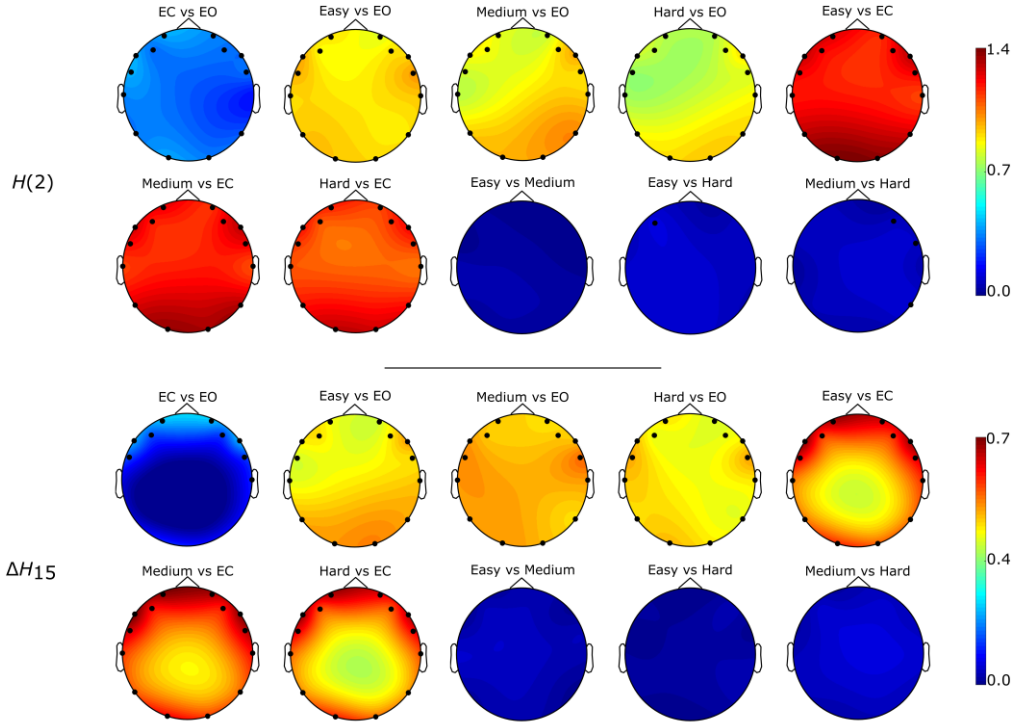

***Figure 12**: Localization of significantly different weighted node degrees for every between state comparison of the H(2) and ΔH_{15} brain networks*. The colormap is based on the absolute difference of the node degrees of the states under investigation (e.g.$|D^{W}_{O2,EC} - D^{W}_{O2,EO}|$). Only the significantly different nodes are shown. The figure originally appeared in Stylianou et al. (74).

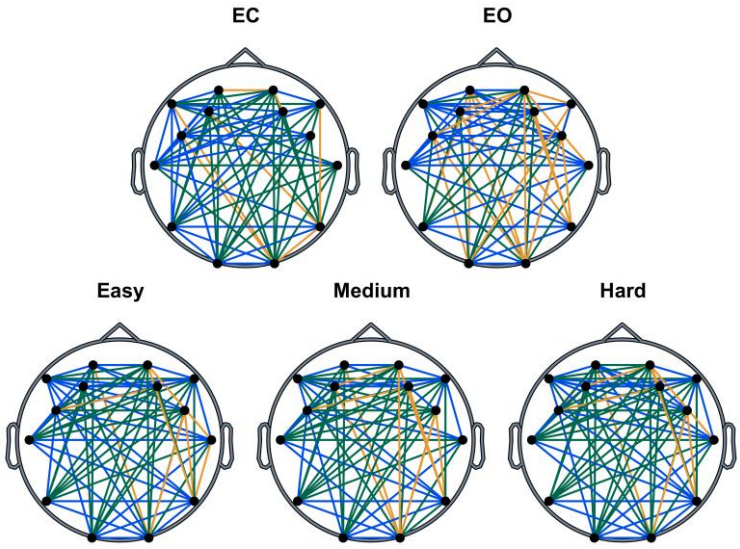

***Figure 13**: State-dependent paired comparisons of the node degrees of different brain regions*. The color of the edge corresponds to the significance of the comparison between the two nodes of the edge. Orange: only $H(2)$ network comparison was significant, Blue: only ΔH_{15} network comparison was significant, Green: both $H(2)$ and ΔH_{15} networks comparisons were significant after BH correction.

Table 6: *State-dependent subject concordance, as captured by Kendall's W.*

BFMF Output	State				
	EC	**EO**	**Easy**	**Medium**	**Hard**
$H(2)$	0.10	0.09	0.09	0.12	0.11
ΔH_{15}	0.24	0.15	0.25	0.24	0.26

4.2.3. Cognitive performance and its correlation with scale-free functional connectivity

The comparisons of the SR of every level revealed significant differences (p<0.05), with the Hard task being the least successful (**Figure 14**). For the other cognitive performance metric, we found that the lowest RT was recorded in the Easy, followed by the Medium and finally the Hard trials, which took the longest to solve (p<0.05 in every case) (**Figure 14**). Additionally, significant positive correlations (p<0.05) were observed between the $\overline{D^W}$ and RT of the Easy and Hard states of ΔH_{15} networks (**Figure 15**). These correlations were rendered non-significant after BH correction.

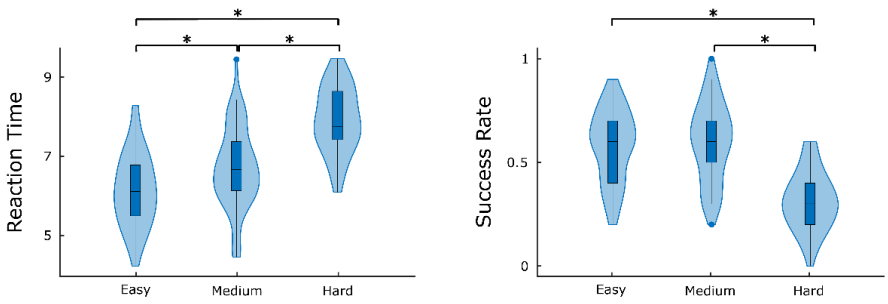

Figure 14: *Average success rate and reaction time (seconds) for different difficulty levels.* Significant differences are marked by *. The figure originally appeared in Stylianou et al. (74).

DOI:10.14753/SE.2022.2667

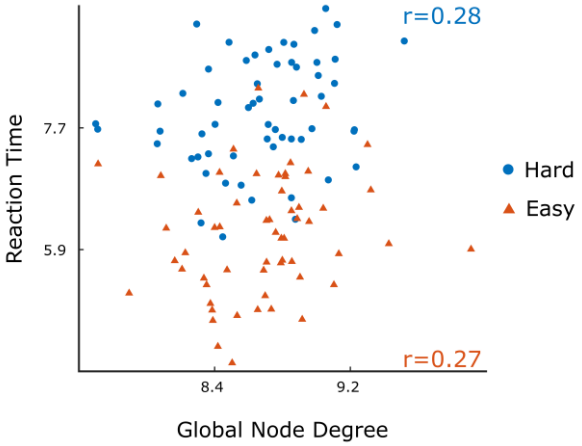

Figure 15: *Scatter plots of the reaction time (seconds) vs global node degree for Easy (orange) and Hard (blue) task in ΔH_{15} networks and their Spearman's correlation (r)*. The figure originally appeared in Stylianou et al. (74).

5. DISCUSSION

This dissertation describes a new method of investigating the brain's scale-free coupled dynamics, which builds on the methodological contributions to fractal physiology by Eke and colleagues (29, 64, 67, 70, 97, 102–104). The research underlying my dissertation started with validating a novel estimator of functional connectivity by the bivariate implementation of focus-based multifractal analysis, whose univariate version had been used by our research team in numerous studies (29, 64, 70, 97, 103, 104). Having characterized the resting-state FC, we aimed to examine the effect of task and evaluate the association between scale-free coupled dynamics and cognitive function measures. Our first study extended BFMF analysis by implementing a battery of multifractality assessment tests. I demonstrated the efficacy of our methodology in resting-state eyes-closed EEG recordings for the first time in the literature. As to the results of this work, a substantial percentage of connections showed true bivariate multifractality, which suggests genuine scale-free coupled dynamics. Subsequently, brain networks were constructed using bivariate $H(2)$ or ΔH_{15} – as estimators of FC. The spatiotemporal organization of coupled multifractal dynamics remained consistent across participants with substantial topological variability. In the second study, we applied the same analytical pipeline to all pairs of simultaneously recorded EEG signals during resting-state and a visual pattern recognition task. Once again, the bivariate multifractal character of a fraction of examined coupled dynamics was validated. Moreover, the scale-free FC increased during the task and showed regional variability, an original and novel contribution to the human functional neuroimaging field. Finally, the multifractal strength of the connections correlated with the participant's reaction time, which could be a signature of the link between large-scale neurophysiological processes and certain domains of cognition.

5.1. Significance of BFMF in Statistical Physics

In the last few years, statistical physics has infiltrated medical research, allowing scientists to recruit statistical tools to reveal complex interactions in biological systems (105). One such tool is the scale-free analysis of physiological time series (65, 106, 107). The first bivariate fractal methods were initially developed for monofractal (52, 108) and then multifractal (81, 109) cases. The novelty of BFMF is twofold. Firstly, by enforcing

a Focus point, computational errors can be avoided. This is a direct extension from Mukli et al. (70), who showed that univariate focus-based methods are more accurate and robust to inconsistencies of the multifractal formalism. Secondly, the introduction of bivariate ΔH_{15} makes the quantification of multifractality easy and straightforward. The current studies focused on neuroscience-related questions; nevertheless, BFMF can be applied to different kinds of time series [e.g. financial time series (110, 111)].

While scale-free dynamics are ubiquitous in nature, (multi)fractal time series analysis of non-fractal physiological processes can lead to false interpretation on the underlying dynamics (e.g. the blood pressure changes follow a periodic pattern with characteristic oscillations due to cardiac, respiratory and other physiological influences). Such pitfalls warrant the extensive use of surrogate testing (80, 112). This is especially true in the bivariate multifractality of the brain dynamics due to the limited number of published studies. It was then crucial that before extrapolating about the origin of these scale-free properties, we validated the existence of multifractal FC through a statistical framework we devised for this purpose (i.e. a battery of surrogate tests). As seen in **Tables 1** and **3**, a significant percentage of the brain's functional connections displayed true multifractal dynamics in rest and task states. We also divided the observed multifractality into intrinsic and extrinsic in the resting-state study based on the bivariate-univariate comparison test (**section 3.1.2**). Extrinsic connections were considered those whose multifractal profile was a direct consequence of autocorrelation effects; on the contrary, intrinsic multifractal connections were not (at least exclusively) influenced by autocorrelations. More than 50% of the connections were intrinsically multifractal. As explained in **footnote 13**, since the publication of the study, we revised our bivariate-univariate Hurst comparison. The updated version of the test was successful [bivariate $H(2)$ smaller than the average of univariate $H(2)$] for only 7% of the connections. This suggests that a large portion of the observed "intrinsic multifractality" (about 45%) was caused by the finite-length and non-normal joint distribution of the time series. Even if the resting-state study used a much larger number of datapoints than the VPR study (16384 vs 2560), the bivariate-univariate Hurst comparison of the VPR was successful in at least 65% of the cases. We can then conclude that the non-normal joint distribution of the time series is the main reason for the high failure rate of the updated bivariate-univariate Hurst comparison in the resting-state study.

The novelty of BFMF was also validated in the resting-state study when we constructed brain networks based on Pearson's correlation and mutual information. Since these estimators are scale-specific, we used the same scales as in BFMF for the window length of the analysis. The architecture of the created networks differed substantially from the BFMF networks. This is proof that BFMF can reveal novel aspects of FC that could have remained hidden if scale-specific estimators were used. Of course, this does not mean that scale-free is superior to scale-specific analysis of FC. Both methodologies are valid and complementary to each other. Details of this analysis can be found in the supplementary material of Stylianou et al. (101).

5.2. Neurophysiological Significance of Scale-free Coupled Dynamics

5.2.1. Origins of Multifractal Functional Connectivity

Even though no theories exclusively target bivariate scale-free dynamics, we can extrapolate from the explanations of univariate scale-free dynamics. The most influential and plausible theory comes from studying critical systems and statistical physics. According to the concept of self-organized criticality (SOC) (113–115), scale-free systems are at the edge of order and chaos, where small perturbations can have major repercussions. It is called self-organized because this balance is achieved by intrinsic control parameters (116, 117). The true origin of these control parameters in the brain remains a question; nevertheless, the circuitry of excitatory and inhibitory feedback loops is a good candidate. In the last few years, different research groups have shown that disturbance of the balance between excitatory and inhibitory stimuli can lead to deviations from criticality (i.e. power-law dynamics) (36, 37, 118). A similar observation has been made in the cardiovascular system, where blockage of the autonomic nervous system causes disturbance in the multifractal profile of the heart rate variability time series (119, 120).

Our work does not provide compelling evidence for the origin of the bivariate multifractality in the activities of brain. However, considering the presented results, we could establish a hypothesis for future studies. Even proponents of SOC urge us to avoid extravagant claims and pitfalls resulting from a superficial understanding of SOC (121, 122). Nevertheless, the scope of this dissertation is not to provide a thorough explanation

of the observed dynamics but instead to introduce them to the neuroscientific community and demonstrate the practical applications of the underlying method, BFMF, for characterizing complex brain network dynamics.

5.2.2. Multifractal Coupled Dynamics in Rest and Task

We observed an increase in the node degrees of the constructed networks during the VPR task compared to EC or EO, due to an increase of bivariate $H(2)$ and ΔH_{15} (**Figures 10-12**). The higher values of bivariate $H(2)$ indicate a shift towards higher long-term cross-correlation between the distant cortical regions during the task. This can result from pruning temporally-long connections in rest to conserve energy. Such connections might be reestablished in complex mental tasks as the one administered in the current experiment. We also noticed higher bivariate $H(2)$ during EO than EC. The transition from EC to EO caused increased mental strain since new visual stimuli arrived in the occipital cortex when subjects opened their eyes. The mental effort observed during EO was not as substantial as the task states (Easy, Medium, Hard); hence differences were observed between EO and task as well. Racz and colleagues used a similar experimental paradigm and found that the global node degree in the prefrontal cortex increased during the task using Pearson's correlation as FC estimator (61). This could suggest that both scale-free [captured by bivariate $H(2)$ and ΔH_{15}] and scale-specific (captured by Pearson's correlation) FC increases during visual pattern recognition. These results indicate that the strength of both short-term and long-term connections increases during the task. Still, this is only a hypothesis since the two investigations used different imaging modalities (EEG vs fNIRS) and different brain regions were studied (whole brain vs prefrontal cortex). Concrete conclusions could only be made using the same imaging modalities and preprocessing pipelines for both scale-free and scale-specific investigations. The observed increase of multifractal FC was not influenced by the difficulty level of the task (**Figures 10-12**), even if significant differences in the success rate and reaction time between the three levels (Easy, Medium, Hard) were observed (**Figure 14**). This is reminiscent of our previous n-back study that found no significant differences between the global node degree of the 2-back and 3-back tasks (88). Nevertheless, in the paper of Káposzta et al., the task was accompanied by decreased interconnectivity instead of the increased FC in the current study. Such inconsistencies

can emerge because different mental tasks induce unique changes to the architecture of functional brain networks (123).

Higher bivariate $H(2)$ corresponds to a greater slope of cross-spectral index (see **Methods**), i.e. relative shift to lower frequencies. At first glance, this might seem counter-intuitive since a shift to higher frequencies is expected during eyes opening and mental tasks (see **Introduction**). Nevertheless, this is just another proof that band-specific analysis of EEG should not overshadow its broadband counterpart since the two methodologies capture different aspects of brain dynamics. Due to the novelty of scale-free FC studies, the comparison with the literature is limited. Only one more study investigated the scale-free FC during task (48), so far. Ciuciu and colleagues used fMRI recordings to capture the scale-free dynamics of the brain. They found that the scale-free dynamics shift towards faster frequencies during a motor task, i.e. change to the opposite directions. Considering that EEG systems have a much higher sampling rate, I can postulate that the two studies show convergence of the scale-free coupled dynamics to the same frequencies (fast frequencies for fMRI and slow frequencies for EEG recordings). A similar increase during task was observed for the ΔH_{15} networks as well (**lower panels of Figure 10**). Bivariate ΔH_{15} is an estimator of multifractality, i.e. the unequal dependence of covariance on small and large fluctuations. As opposed to the linear monofractality [bivariate $H(2)$], multifractal analysis reveals non-linear dynamics (73, 79); hence an increase of bivariate ΔH_{15} suggests an expansion of non-linear coupling during task. Most of our electrodes were positioned over the frontal cortex, a region dominated by higher-level association areas. These cortical regions are responsible for information integration and are activated during mental tasks (60). Based on our hypothesis **in section 5.2.1**, it is reasonable to assume that the increased excitatory/inhibitory feedback loops – caused by the activation of the prefrontal cortex during task – resulted in greater long-term cross-correlation and multifractality.

In the resting-state study, the regional variability of the constructed networks was more apparent in the $H(2)$ network (**Table 2** and **Figure 9**). On the other hand, the VPR-study showed that the local node degrees varied the most within the ΔH_{15} networks (**Figure 13**). The difference in the channel number of the EEG devices (62 vs 14) could explain this inconsistency. From the two outcomes, the higher variability in the ΔH_{15}

networks seems to agree with the fact that multifractality is a more complex property (124); hence more significant topological differences are expected. Nevertheless, both studies have found great heterogeneity in the localization of the multifractal FC, suggesting that we should study these dynamics at high spatial resolution. Another difference between the two investigations was the subject concordance. In the resting-state study, Kendall's *W* values indicated strong subject agreement in the bivariate $H(2)$ and moderate agreement in the bivariate ΔH_{15} values (**Table 2**). In contrast, we see the opposite pattern in the fractal properties of FC corresponding to our VPR-protocol. We found only small concordance in the ΔH_{15} networks, while the subject agreement in the $H(2)$ networks was non-existent. A high subject concordance suggests that our methodology is consistent across participants and can draw conclusions and help in the clinical setting. The low Kendall's *W* values in the VPR study can be attributed to the fact that most channels were located above the frontal and parietal cortices, regions whose FC has been shown to vary the most from subject to subject in fMRI recordings (125). Another reason for this low subject agreement could be that the exact position of the EEG channels in the VPR study varied from subject to subject due to the nature of the EEG device.

An interesting byproduct of our recent studies has been the anticorrelated relationship between $H(2)$ or ΔH_{15}, as shown in **Figure 8** and **Table 5.** Similar negative correlations were observed between univariate $H(2)$ and ΔH_{15} in resting-state conditions but only in the delta band (29). In both of our current studies, 50% of the used scales were within the delta band (resting-state study: 128, 256 and 512; VPR-study: 32, 64, 128 and 256). We can then conclude that both univariate and bivariate $H(2)$ and ΔH_{15} are anticorrelated in the low-frequency range. The physiological relevance of this relationship remains unknown. A possible explanation could be that an increase (decrease) of non-linear dynamics is followed by a decrease (increase) of linear dynamics in an attempt to balance the energy expenditure of the brain.

5.3. Performance Metrics and its Associations with Multifractal FC

In the VPR study, we modified an already existing paradigm. In Racz et al. (61), the participant was presented with a series of images and was asked to identify subsections of them, but his/her response was not recorded. This did not allow for the investigation

of possible correlations between the FC and success rate of the task. In the previous study, the reaction time could not be estimated either since the active part of the trial was fixed and did not depend on the subject's response. Another major advantage of our current version is the inclusion of difficulty levels based on image compression principles. This gave us an objective way to classify the images in different levels of difficulty and compare how the brain networks organize in each one of them. We decided to include only grayscale images so colorblind individuals can participate and because the projection of colored images elicits different EEG patterns compared to grayscale images (126, 127). Our experiment investigated only the short-term non-verbal memory. Although if our participants were well educated (university students or graduates), we intend to expand our pool of subjects to other demographics where the inclusion of text and/or numbers could impair our findings. For example, the applied paradigm can be easily implemented in attention deficit hyperactivity disorder studies, where the onset of the disease starts at an age where children might not be able to read or count (around 4 years of age) (128).

The reaction time within the three difficulty levels was significantly different, with Easy having the fastest reaction time and Hard the slowest. Similar patterns were observed from the success rate, where Hard trials were the most difficult to solve (**Figure 14**). We can then conclude that our image classification process – based on image compression ratios (see **Methods**) – was successful.

We also calculated Spearman's correlation between the global node degree and performance metrics. No significant correlations were found between $\overline{D^W}$ and success rate. This agrees with the independence of node degree on the difficulty level. If the success rate (and by extension, difficulty) had any association with $\overline{D^W}$ we would have seen a difference between the node degrees of the Easy, Medium and Hard networks. We also found that the higher multifractal coupled dynamics of the network correspond to slower solving of the task (**Figure 15**), or in other words the $\overline{D^W}$ of the ΔH_{15} networks is positively correlated with the reaction time. Considering that feedback loops might cause/amplify multifractality, this could mean that excessive feedback can be detrimental to the fast solving of a task. Nevertheless, direct conclusions cannot be drawn since these correlations were rendered non-significant after BH correction. In future studies, this association should be investigated further.

5.4. Bivariate vs Univariate Scale-free Dynamics During Task

While the bivariate scale-free alterations during different states are not well studied, similar investigations have been performed using various univariate approaches. Racz et al. (129) calculated the global node degree of a 14-node brain network in a sliding window manner – using a non-linear FC estimator [synchronization likelihood (130)]. As a result, we captured the temporal evolution of FC, obtaining time series during EC and EO. Subsequently, the univariate equivalent of BFMF was implemented in those time series. The results showed that the univariate $H(2)$ of the global node degrees time series increased when the subjects transitioned from EO to EC. Even though the methodologies of Racz et al. and the current one might seem similar, there is a fundamental difference. In that paper, the FC is defined by a scale-specific (synchronization likelihood) estimator, which is then used to construct a time series and calculate the univariate multifractal profile of this time series. In this dissertation, I used BFMF to capture the scale-free profile of FC, thus revealing the topology of scale-free coupled dynamics. In the same fMRI study mentioned earlier by Ciuciu and colleagues (48), the univariate $H(2)$ decreased during the task. Similar results were found in an EEG study by He at al. (131), where the power-law exponent [hence univariate $H(2)$] was lower when the subjects performed a motor task. These three studies showed that the univariate $H(2)$ decreases during increased stimuli, opposing our current findings. This suggests that the brain's bivariate and univariate scale-free dynamics do not change in the same direction during increased mental workload. Of course, definite conclusions cannot be drawn since each study used different methodologies, which could have influenced the results. In future projects, it would be worth calculating both univariate and bivariate multifractal measures to reveal the actual relationship between them.

5.5. Limitations

The 62 EEG channels were grouped in 6 RSNs based on a probabilistic map in the resting-state study. A more accurate mapping to RSNs could have been achieved using source reconstruction (132), where the brain activity recorded from EEG is assigned to a specific brain region using magnetic resonance imaging. The study's main objective was to demonstrate the applicability of BFMF in EEG datasets; our grouping was only used as a

dimensionality reduction tool. Moreover, as stated in section **4.1.2.** our parcellation scheme was successful as opposed ato random assignments of channels to RSNs.

In the VPR study, the sample did not represent the general population; all participants were university students or graduates. Despite the difficulties of recruiting off-campus participants, population-wide conclusions can be made only by including more diverse samples. Secondly, only 14 EEG channels were used, which is insufficient for RSN-based investigations.

5.6. Future Perspectives

In the resting-state study, we used a bimodal version of BFMF in our preliminary analysis. In the bimodal BFMF two scaling functions are being fitted, one for small and one for large scales. The breaking point between the two scaling ranges was around 0.5 Hz, probably due to a filtering artifact. Nevertheless, the univariate version of BFMF can capture the bimodal nature of neural dynamics (64, 103). Future investigations could include high-pass filters with lower cut-off frequency allowing us to study the possible existence of bimodality in the multifractal FC.

Five of the participants repeated the VPR study about a year later. The success rate and reaction time were not significantly different between the two visits. Kendall's W showed moderate agreement for the bivariate $H(2)$ and ΔH_{15} values obtained from the first and second measurements. These findings indicate that our experimental design can be used reliably in reproducibility studies and that the multifractal coupled dynamics remain consistent.

To demonstrate the effect of task on the multifractal FC, we used only a visual pattern recognition task. Previous investigations have suggested that the architecture of brain networks varies depending on the nature of the administered task (123). Although certain publications indicate that learning a task can influence the brain's interconnectivity (133, 134), the effect of learning is not widely investigated in FC studies. Future investigations of multifractal FC should focus on diverse mental tasks that are repeated, so both effects mentioned above can be examined.

Finally, our current experiments targeted only the young, healthy population. EEG of diseased populations has been studied only in a univariate multifractal manner (41–44). Recently we showed that the observed EEG changes in schizophrenic subjects are solely caused by a shift of the scale-free component of the signal (135). Additionally, schizophrenia is widely considered as a disconnection syndrome (21, 22), meaning that there is a great disruption in the structure of the functional networks. It is then logical to extend our multifractal FC studies by including schizophrenic patients. Epilepsy research can also be benefitted from the investigation of bivariate scale-free dynamics. The scale-free profile of the EEG signals is altered during epileptic attacks (136), while antiepileptic (36) and central nervous system suppressants (37) can also affect the fractal character of the EEG tracing. Alterations in the fractal coupled dynamics of the EEG have already been demonstrated during aging (50), but only in the monofractal setting. In an ongoing study, we repeat our VPR task using two different age groups (young and elderly). Such comparison could give us information for the multifractal FC changes as we age and how our short-term memory is affected by getting older. So far, we have focused on population inference to increase our understanding of the underlying coupled dynamics. The increase in computational power allows us to construct predictive models, capable of classifying participants in different groups. For example, we could extend the analytical pipeline presented in Racz et al. (104), in order to identify schizophrenic subjects based on their multifractal FC. Such machine learning algorithms could be implemented in the day-to-day clinical diagnosis of neuropsychiatric patients, where there is dire need of objective measurement protocols and easily interpretable, straightforward analytical frameworks.

DOI:10.14753/SE.2022.2667

6. CONCLUSION

The dissertation elaborated the application of bivariate focus-based multifractal analysis, which turned out to be a robust estimator of multifractal functional connectivity in EEG recordings. The novel multifractality assessment tests could validate the true scale-free nature of several connections both during rest and task. The multifractal coupled dynamics were found to vary across the brain cortex, suggesting that the scale-free coupling of the brain is region-specific. Additionally, the long-term memory and multifractality of the brain networks increased during a complex visual pattern recognition task. Finally, the high degree of multifractality was associated with slow task solving. In conclusion, our analytical pipeline is a viable and accurate candidate for bivariate multifractal analysis of neurophysiological time series, which could facilitate future research on complex brain dynamics in healthy and diseased populations.

DOI:10.14753/SE.2022.2667

7. SUMMARY

Imaging of complex brain function became possible with the advent of neuroimaging modalities and statistical physical methods that revealed the spatiotemporal organization of neural activity. Bivariate methods allowed us to construct networks that represent the brain's functional connectivity (FC). The assessment of FC can be achieved by estimating of the statistical relationship between the different brain regions. A plethora of estimators has been recruited for such a task, with most of them focusing on the scale-specific neural coupling. The scale-wise coupling assumes that FC is concentrated in distinct peaks of the connection's cross-power spectrum. On the contrary, scale-free (or fractal) approaches study the whole range of cross-power spectrum for the construction of brain networks. The presented work leverages fractal analytical methods to investigate the bivariate multifractal patterns of electroencephalogram (EEG), which have been investigated inadequately so far. My dissertation elaborates a complete pipeline for estimating and validating bivariate scale-free FC. It begins with the bivariate focus-based multifractal (BFMF) analysis, whose outputs indicate the long-term cross-correlation [bivariate $H(2)$] and multifractality (bivariate ΔH_{15}) of the connection. The real nature of these properties is further investigated by a battery of newly developed multifractality assessment tests. The first study introduced this analytical pipeline by estimating the multifractal FC in resting-state EEG. The results suggest that a substantial percentage of the resting-state coupled dynamics are scale-free. Additionally, the distribution of multifractal FC varied across the cortex, indicating that BFMF can capture functionally relevant information. In the second study, we analyzed the EEG tracings of participants during a visual pattern recognition task preceded by a resting-state. The findings indicate that the multifractal character of FC found in the resting-state coupled dynamics is maintained even during cognitive stimuli. We also observed that the multifractal profile was more pronounced in the task states, yet differences between the three difficulty levels were not registered. These two studies pave the way for the introduction of BFMF to clinical research, where the scale-free coupled dynamics have not been investigated yet.

DOI:10.14753/SE.2022.2667

8. ÖSSZEFOGLALÁS

A komplex humán agyműködés tér- és időbeli szerveződésének megértéséhez döntő mértékben járul hozzá a funkcionális képalkotó módszerek és a statisztikai fizikai módszerek fejlődése. A szimultán idősorpárokat elemző algoritmusok – melyek a statisztikai kapcsolatot mérik – segítségével rekonstruált funkcionális konnektivitás (FC) jellemzi az agyi funkcionális hálózatok topológiáját és dinamikáját és ezáltal az agyi régiók együttműködését. E célból számos paramétert vezettek be, melyek túlnyomó többsége az idegi működés időskála-specifikus kooperációját számszerűsítik. A disszertációban a skálafüggetlen együttműködést karakterizáló idősorelemző módszer alkalmazását mutatom be. Ezt a kétváltozós fókusz-alapú multifraktális analízist (BFMF), a skálafüggetlen FC rekonstruálására alkalmaztam, melyhez elektroencefalogram (EEG) adatokat használtam. A BFMF kimeneti paraméterei jellemzik a funkcionális kapcsolat memóriáját hosszú távú keresztkorreláció, mérőszáma: kétváltozós $H(2)$] és a multifraktalitást (nem-lineáris csatolás, kétváltozós ΔH_{15}). Ezen tulajdonságok valódi természetét az újonnan kifejlesztett multifraktalitási tesztek sora vizsgálja tovább, mely a BFMF módszerrel együtt a munka egyik új aspektusa. További újdonság, hogy a nyugalmi állapotban gyűjtött adatokon történt validálást követően (első tanulmány), a kognitív terhelés agyi hálózati tevékenységre gyakorolt hatását igazoltuk (második tanulmány). Az első vizsgálatban ezt az analitikai protokollt alkalmaztuk a multifraktális FC nyugalmi állapotú EEG-ben történő becsléséhez. Eredményeink alapján a nyugalmi állapothoz tartozó funkcionális kapcsolatok dinamikája jelentős részben skálafüggetlen. Ezenkívül a multifraktális FC eloszlása a kéregben jellegzetes, a nyugalmi agyi hálózatokat megközelítő topológia szerint oszlik el, mely bizonyítja, hogy a BFMF képes funkcionálisan releváns hálózati szerveződést kimutatni. A második vizsgálatban a résztvevők EEG adatait regisztráltuk egy vizuális mintafelismerési feladat és nyugalmi állapot során, amelyet követően BFMF analízist végeztünk. Az eredmények azt mutatják, hogy az FC nyugalmi állapotban kapcsolt dinamikában talált multifraktális jellege a kognitív stimulus során is megmarad és annak jellege kifejezettebb.

9. BIBLIOGRAPHY

1. Berger H. 1929. Uber das Elektrenkephalogramm des Menschen (On the human elec- troencephalogram). Arch f Psychiatr u Nervenkrankheiten 87:527–570.

2. Ivanitsky AM, Ivanitsky GA, Nikolaev AR, Sysoeva O V. Electroencephalography, p. 1067–1072. *In* Encyclopedia of Neuroscience. Springer Berlin Heidelberg, Berlin, Heidelberg.

3. Accardo A, Affinito M, Carrozzi M, Bouquet F. 1997. Use of the fractal dimension for the analysis of electroencephalographic time series. Biol Cybern 77:339–350.

4. Nan X, Jinghua X. 1988. The fractal dimension of EEG as a physical measure of conscious human brain activities. Bull Math Biol 50:559–565.

5. Preißl H, Lutzenberger W, Pulvermüller F, Birbaumer N. 1997. Fractal dimensions of short EEG time series in humans. Neurosci Lett 225:77–80.

6. Lang EW, Tomé AM, Keck IR, Górriz-Sáez JM, Puntonet CG. 2012. Brain Connectivity Analysis: A Short Survey. Comput Intell Neurosci 2012:1–21.

7. Ihlen EAF, Vereijken B. 2010. Interaction-dominant dynamics in human cognition: Beyond $1/f\alpha$ fluctuation. J Exp Psychol Gen 139:436–463.

8. Biswal B, Zerrin Yetkin F, Haughton VM, Hyde JS. 1995. Functional connectivity in the motor cortex of resting human brain using echo-planar mri. Magn Reson Med 34:537–541.

9. Friston KJ, Frith CD, Liddle PF, Frackowiak RSJ. 1993. Functional Connectivity: The Principal-Component Analysis of Large (PET) Data Sets. J Cereb Blood Flow Metab 13:5–14.

10. Friston KJ. 2011. Functional and effective connectivity: a review. Brain Connect 1:13–36.

11. Lowe MJ, Sakaie KE, Beall EB, Calhoun VD, Bridwell DA, Rubinov M, Rao SM. 2016. Modern Methods for Interrogating the Human Connectome. J Int Neuropsychol Soc 22:105–119.

12. Lv H, Wang Z, Tong E, Williams LM, Zaharchuk G, Zeineh M, Goldstein-Piekarski AN, Ball TM, Liao C, Wintermark M. 2018. Resting-State Functional MRI: Everything That Nonexperts Have Always Wanted to Know. Am J Neuroradiol https://doi.org/10.3174/ajnr.A5527.

13. Rubinov M, Sporns O. 2010. Complex network measures of brain connectivity: Uses and interpretations. Neuroimage 52:1059–1069.

14. Sporns O. 2011. The human connectome: a complex network. Ann N Y Acad Sci 1224:109–125.

15. Sporns O. 2013. Structure and function of complex brain networks. Dialogues Clin Neurosci 15:247–62.

16. Sporns O, Honey CJ. 2006. Small worlds inside big brains. Proc Natl Acad Sci U S A 103:19219–19220.

17. Engels MMA, Stam CJ, van der Flier WM, Scheltens P, de Waal H, van Straaten ECW. 2015. Declining functional connectivity and changing hub locations in Alzheimer's disease: an EEG study. BMC Neurol 15:145.

18. Achard S, Delon-Martin C, Vertes PE, Renard F, Schenck M, Schneider F, Heinrich C, Kremer S, Bullmore ET. 2012. Hubs of brain functional networks are radically reorganized in comatose patients. Proc Natl Acad Sci 109:20608–20613.

19. Krukow P, Jonak K, Karpiński R, Karakuła-Juchnowicz H. 2019. Abnormalities in hubs location and nodes centrality predict cognitive slowing and increased performance variability in first-episode schizophrenia patients. Sci Rep 9:1–13.

20. Micheloyannis S, Pachou E, Stam CJ, Breakspear M, Bitsios P, Vourkas M, Erimaki S, Zervakis M. 2006. Small-world networks and disturbed functional connectivity in schizophrenia. Schizophr Res 87:60–66.

21. Friston KJ. 1998. The disconnection hypothesis. Schizophr Res 30:115–125.

22. Friston K, Brown HR, Siemerkus J, Stephan KE. 2016. The dysconnection hypothesis (2016). Schizophr Res 176:83–94.

23. Barabási A-L, Albert R. 1999. Emergence of Scaling in Random Networks. Science (80-) 286:509–512.

24. Raichle ME. 2010. Two views of brain function. Trends Cogn Sci 14:180–190.

25. Fox MD, Snyder AZ, Vincent JL, Corbetta M, Van Essen DC, Raichle ME. 2005. The human brain is intrinsically organized into dynamic, anticorrelated functional networks. Proc Natl Acad Sci U S A 102:9673–8.

26. Rosazza C, Minati L. 2011. Resting-state brain networks: literature review and clinical applications. Neurol Sci 32:773–85.

27. Raichle ME, MacLeod AM, Snyder AZ, Powers WJ, Gusnard DA, Shulman GL. 2001. A default mode of brain function. Proc Natl Acad Sci 98:676–682.

28. Gusnard DA, Raichle ME. 2001. Searching for a baseline: Functional imaging and the resting human brain. Nat Rev Neurosci 2:685–694.

29. Racz FS, Stylianou O, Mukli P, Eke A. 2018. Multifractal Dynamic Functional Connectivity in the Resting-State Brain. Front Physiol 9.

30. He BJ. 2014. Scale-free brain activity: past, present, and future. Trends Cogn Sci 18:480–487.

31. Fraiman D, Chialvo DR. 2012. What kind of noise is brain noise: anomalous scaling behavior of the resting brain activity fluctuations. Front Physiol 3:1–11.

32. Werner G. 2010. Fractals in the nervous system: conceptual implications for theoretical neuroscience. Front Physiol 1 JUL:1–28.

33. Mandelbrot B. 1967. How Long Is the Coast of Britain? Statistical Self-Similarity and Fractional Dimension. Science (80-) 156:636–638.

34. Eke A, Herman P, Kocsis L, Kozak LR. 2002. Fractal characterization of complexity in temporal physiological signals. Physiol Meas 23:R1–R38.

35. Buzsáki G, Draguhn A. 2004. Neuronal Oscillations in Cortical Networks. Science (80-) 304:1926–1929.

36. Meisel C. 2020. Antiepileptic drugs induce subcritical dynamics in human cortical networks. Proc Natl Acad Sci 117:11118–11125.

37. Mazzoni A, Broccard FD, Garcia-Perez E, Bonifazi P, Ruaro ME, Torre V. 2007. On the Dynamics of the Spontaneous Activity in Neuronal Networks. PLoS One 2:e439.

38. Stam CJ, de Bruin EA. 2004. Scale-free dynamics of global functional connectivity in the human brain. Hum Brain Mapp 22:97–109.

39. Georgiev S, Minchev Z. 2009. EEG Fractal Dimension Measurement before and after Human Auditory Stimulation 70–81.

40. Ahmadi K, Ahmadlou M, Rezazade M, Azad-Marzabadi E, Sajedi F. 2013. Brain activity of women is more fractal than men. Neurosci Lett 535:7–11.

41. Zappasodi F, Olejarczyk E, Marzetti L, Assenza G, Pizzella V, Tecchio F. 2014. Fractal Dimension of EEG Activity Senses Neuronal Impairment in Acute Stroke. PLoS One 9:e100199.

42. França LGS, Miranda JGV, Leite M, Sharma NK, Walker MC, Lemieux L, Wang Y. 2018. Fractal and Multifractal Properties of Electrographic Recordings of Human Brain Activity: Toward Its Use as a Signal Feature for Machine Learning in Clinical Applications. Front Physiol 9.

43. Polychronaki GE, Ktonas PY, Gatzonis S, Siatouni A, Asvestas PA, Tsekou H, Sakas D, Nikita KS. 2010. Comparison of fractal dimension estimation algorithms for epileptic seizure onset detection. J Neural Eng 7:046007.

44. Racz FS, Farkas K, Stylianou O, Kaposzta Z, Czoch A, Mukli P, Csukly G, Eke A. 2021. Separating scale-free and oscillatory components of neural activity in schizophrenia. Brain Behav 11:1–15.

45. Ouyang G, Hildebrandt A, Schmitz F, Herrmann CS. 2020. Decomposing alpha and 1/f brain activities reveals their differential associations with cognitive processing speed. Neuroimage 205:116304.

46. Zhou W-X. 2008. Multifractal detrended cross-correlation analysis for two nonstationary signals. Phys Rev E 77:066211.

47. Achard S, Bassett DS, Meyer-lindenberg A, Bullmore E. 2008. Fractal connectivity of long-memory networks. Phys Rev E Stat Nonlin Soft Matter Phys 77:036104.

48. Ciuciu P, Abry P, He BJ. 2014. Interplay between functional connectivity and scale-free dynamics in intrinsic fMRI networks. Neuroimage 95:248–263.

49. La Rocca D, Wendt H, Wassenhove V van, Ciuciu P, Abry P. 2020. Fractal Connectivity: Revisiting Functional Connectivity for Infraslow Scale-Free Brain Dynamics using Complex Wavelet. Front Physiol https://doi.org/10.3389/fphys.2020.578537.

50. Wang J, Zhao D-Q. 2012. Detrended cross-correlation analysis of electroencephalogram. Chinese Phys B 21:028703.

51. Kristoufek L. 2014. Spectrum-based estimators of the bivariate Hurst exponent. Phys Rev E 90:062802.

52. Podobnik B, Stanley HE. 2008. Detrended Cross-Correlation Analysis: A New Method for Analyzing Two Nonstationary Time Series. Phys Rev Lett 100:084102.

53. Jiang A-H, Huang X-C, Zhang Z-H, Li J, Zhang Z-Y, Hua H-X. 2010. Mutual information algorithms. Mech Syst Signal Process 24:2947–2960.

54. Ihlen EAF. 2012. Introduction to Multifractal Detrended Fluctuation Analysis in Matlab. Front Physiol 3:1–18.

55. Kaufmann T, Alnæs D, Brandt CL, Doan NT, Kauppi K, Bettella F, Lagerberg T V., Berg AO, Djurovic S, Agartz I, Melle IS, Ueland T, Andreassen OA, Westlye LT. 2017. Task modulations and clinical manifestations in the brain functional connectome in 1615 fMRI datasets. Neuroimage 147:243–252.

56. Gonzalez-Castillo J, Bandettini PA. 2018. Task-based dynamic functional connectivity: Recent findings and open questions. Neuroimage 180:526–533.

57. Gonzalez-Castillo J, Hoy CW, Handwerker DA, Roopchansingh V, Inati SJ, Saad ZS, Cox RW, Bandettini PA. 2015. Task dependence, tissue specificity, and spatial distribution of widespread activations in large single-subject functional MRI datasets at 7T. Cereb Cortex 25:4667–4677.

58. Di X, Gohel S, Kim EH, Biswal BB. 2013. Task vs. rest-different network configurations between the coactivation and the resting-state brain networks. Front Hum Neurosci 7:1–9.

59. Van Hoesen GW. 1993. The modern concept of association cortex. Curr Opin Neurobiol 3:150–154.

60. Kandel ER, Schwartz JH, Jessell TM. 2012. Principles of Neural Science. McGraw-Hill Professional Pub.

61. Racz FS, Mukli P, Nagy Z, Eke A. 2017. Increased prefrontal cortex connectivity during cognitive challenge assessed by fNIRS imaging. Biomed Opt Express 8:3842.

62. Liuzzi L, Quinn AJ, O'Neill GC, Woolrich MW, Brookes MJ, Hillebrand A, Tewarie P. 2019. How Sensitive Are Conventional MEG Functional Connectivity Metrics With Sliding Windows to Detect Genuine Fluctuations in Dynamic Functional Connectivity? Front Neurosci 13.

63. Kwapień J, Oświęcimka P, Drożdż S. 2015. Detrended fluctuation analysis made flexible to detect range of cross-correlated fluctuations. Phys Rev E 92:052815.

64. Mukli P, Nagy Z, Racz FS, Herman P, Eke A. 2018. Impact of Healthy Aging on Multifractal Hemodynamic Fluctuations in the Human Prefrontal Cortex. Front Physiol 9:1–21.

65. Peng C -K., Havlin S, Stanley HE, Goldberger AL. 1995. Quantification of scaling exponents and crossover phenomena in nonstationary heartbeat time series. Chaos An Interdiscip J Nonlinear Sci 5:82–87.

66. Cannon MJ, Percival DB, Caccia DC, Raymond GM, Bassingthwaighte JB. 1997. Evaluating scaled windowed variance methods for estimating the Hurst coefficient of time series. Phys A Stat Mech its Appl 241:606–626.

67. Eke A, Hermán P, Bassingthwaighte J, Raymond G, Percival D, Cannon M, Balla I, Ikrényi C. 2000. Physiological time series: distinguishing fractal noises from motions. Pflügers Arch - Eur J Physiol 439:403–415.

68. Grech D, Pamuła G. 2012. Multifractal Background Noise of Monofractal Signals. Acta Phys Pol A 121:B-34-B-39.

69. Kantelhardt JW, Zschiegner SA, Koscielny-Bunde E, Havlin S, Bunde A, Stanley HE. 2002. Multifractal detrended fluctuation analysis of nonstationary time series. Phys A Stat Mech its Appl 316:87–114.

70. Mukli P, Nagy Z, Eke A. 2015. Multifractal formalism by enforcing the universal behavior of scaling functions. Phys A Stat Mech its Appl 417:150–167.

71. Li M. 2010. Fractal time series-a tutorial review. Math Probl Eng 2010.

72. Beran J. 1994. Statistics for Long-Memory Processes.

73. Ashkenazy Y, Havlin S, Ivanov PC, Peng C-K, Schulte-Frohlinde V, Stanley HE. 2003. Magnitude and sign scaling in power-law correlated time series. Phys A Stat Mech its Appl 323:19–41.

74. Stylianou O, Racz FS, Kim K, Kaposzta Z, Czoch A, Yabluchanskiy A, Eke A, Mukli P. 2021. Multifractal Functional Connectivity Analysis of Electroencephalogram Reveals Reorganization of Brain Networks in a Visual Pattern Recognition Paradigm. Front Hum Neurosci 15.

75. Clauset A, Shalizi CR, Newman MEJ. 2009. Power-Law Distributions in Empirical Data. SIAM Rev 51:661–703.

76. Podobnik B, Jiang Z-Q, Zhou W-X, Stanley HE. 2011. Statistical tests for power-law cross-correlated processes. Phys Rev E 84:066118.

77. Schumann AY, Kantelhardt JW. 2011. Multifractal moving average analysis and test of multifractal model with tuned correlations. Phys A Stat Mech its Appl 390:2637–2654.

78. Blythe DAJ, Nikulin V V., Müller K-R. 2016. Robust Statistical Detection of Power-Law Cross-Correlation. Sci Rep 6:27089.

79. Ivanov PC, Amaral LAN, Goldberger AL, Havlin S, Rosenblum MG, Struzik ZR, Stanley HE. 1999. Multifractality in human heartbeat dynamics. Nature 399:461–465.

80. Prichard, Theiler, Prichard D, Theiler J, Prichard, Theiler. 1994. Generating surrogate data for time series with several simultaneously measured variables. Phys Rev Lett 73:951–954.

81. Wang J, Shang P, Ge W. 2012. Multifractal cross-correlation analysis based on statistical moments. Fractals 20:271–279.

82. Louis S, Borgelt C, Grün S. 2010. Generation and Selection of Surrogate Methods for Correlation Analysis, p. 359–382. *In* Analysis of Parallel Spike Trains. Springer US, Boston, MA.

83. Kristoufek L. 2015. Can the bivariate Hurst exponent be higher than an average of the separate Hurst exponents? Phys A Stat Mech its Appl 431:124–127.

84. Kristoufek L. 2011. Multifractal height cross-correlation analysis: A new method for analyzing long-range cross-correlations. EPL (Europhysics Lett 95:68001.

85. Arbabshirani MR, Damaraju E, Phlypo R, Plis S, Allen E, Ma S, Mathalon D, Preda A, Vaidya JG, Adali T, Calhoun VD. 2014. Impact of autocorrelation on functional connectivity. Neuroimage 102:294–308.

86. Kristoufek L. 2016. Power-law cross-correlations estimation under heavy tails. Commun Nonlinear Sci Numer Simul 40:163–172.

87. Saupe D. 1988. Algorithms for random fractals, p. 71–136. *In* The Science of Fractal Images. Springer New York, New York, NY.

88. Kaposzta Z, Stylianou O, Mukli P, Eke A, Racz FS. 2021. Decreased connection density and modularity of functional brain networks during n-back working memory paradigm. Brain Behav 11:1–16.

89. Sockeel S, Schwartz D, Pélégrini-Issac M, Benali H. 2016. Large-Scale Functional Networks Identified from Resting-State EEG Using Spatial ICA. PLoS One 11:e0146845.

90. Gabard-Durnam LJ, Mendez Leal AS, Wilkinson CL, Levin AR. 2018. The Harvard Automated Processing Pipeline for Electroencephalography (HAPPE): Standardized Processing Software for Developmental and High-Artifact Data. Front Neurosci 12:97.

91. Winkler I, Haufe S, Tangermann M. 2011. Automatic Classification of Artifactual ICA-Components for Artifact Removal in EEG Signals. Behav Brain Funct 7:30.

92. Winkler I, Brandl S, Horn F, Waldburger E, Allefeld C, Tangermann M. 2014. Robust artifactual independent component classification for BCI practitioners. J Neural Eng 11:035013.

93. Thomas Yeo BT, Krienen FM, Sepulcre J, Sabuncu MR, Lashkari D, Hollinshead M, Roffman JL, Smoller JW, Zöllei L, Polimeni JR, Fischl B, Liu H, Buckner RL. 2011. The organization of the human cerebral cortex estimated by intrinsic functional connectivity. J Neurophysiol 106:1125–1165.

94. Giacometti P, Perdue KL, Diamond SG. 2014. Algorithm to find high density EEG scalp coordinates and analysis of their correspondence to structural and functional regions of the brain. J Neurosci Methods 229:84–96.

95. Xia M, Wang J, He Y. 2013. BrainNet Viewer: A Network Visualization Tool for Human Brain Connectomics. PLoS One 8:e68910.

96. Penny W, Friston K, Ashburner J, Kiebel S, Nichols T. 2007. Statistical Parametric Mapping, 1st ed. Elsevier. https://linkinghub.elsevier.com/retrieve/pii/B9780123725608X50001.

97. Racz FS, Stylianou O, Mukli P, Eke A. 2019. Multifractal and entropy analysis of resting-state electroencephalography reveals spatial organization in local dynamic functional connectivity. Sci Rep 9:13474.

98. Benjamini Y, Hochberg Y. 1995. Controlling the False Discovery Rate: A Practical and Powerful Approach to Multiple Testing. J R Stat Soc Ser B 57:289–300.

99. Yu H, Winkler S. 2013. Image complexity and spatial information, p. 12–17. *In* 2013 Fifth International Workshop on Quality of Multimedia Experience (QoMEX). IEEE.

100. Delorme A, Makeig S. 2004. EEGLAB: an open source toolbox for analysis of single-trial EEG dynamics including independent component analysis. J Neurosci Methods 134:9–21.

101. Stylianou O, Racz FS, Eke A, Mukli P. 2021. Scale-Free Coupled Dynamics in Brain Networks Captured by Bivariate Focus-Based Multifractal Analysis. Front Physiol 11:1–14.

102. Hartmann A, Mukli P, Nagy Z, Kocsis L, Hermán P, Eke A. 2013. Real-time fractal signal processing in the time domain. Phys A Stat Mech its Appl 392:89–102.

103. Nagy Z, Mukli P, Herman P, Eke A. 2017. Decomposing Multifractal Crossovers. Front Physiol 8:533.

104. Racz FS, Stylianou O, Mukli P, Eke A. 2020. Multifractal and Entropy-Based Analysis of Delta Band Neural Activity Reveals Altered Functional Connectivity Dynamics in Schizophrenia. Front Syst Neurosci 14:1–22.

105. Kwapień J, Drozdz S. 2012. Physical approach to complex systems. Phys Rep. Elsevier B.V. https://doi.org/10.1016/j.physrep.2012.01.007.

106. Stanley HE, Amaral LAN, Goldberger AL, Havlin S, Ivanov PC, Peng C-K. 1999. Statistical physics and physiology: Monofractal and multifractal approaches. Phys A Stat Mech its Appl 270:309–324.

107. Peng CK, Buldyrev S V, Havlin S, Simons M, Stanley HE, Goldberger AL. 1994. Mosaic organization of DNA nucleotides. Phys Rev E Stat Phys Plasmas Fluids Relat Interdiscip Topics 49:1685–9.

108. Horvatic D, Stanley HE, Podobnik B. 2011. Detrended cross-correlation analysis for non-stationary time series with periodic trends. EPL (Europhysics Lett 94:18007.

109. Oświęcimka P, Drożdż S, Forczek M, Jadach S, Kwapień J. 2014. Detrended cross-correlation analysis consistently extended to multifractality. Phys Rev E 89:023305.

110. Pal M, Madhusudana Rao P, Manimaran P. 2014. Multifractal detrended cross-correlation analysis on gold, crude oil and foreign exchange rate time series. Phys A Stat Mech its Appl 416:452–460.

111. Arianos S, Carbone A. 2009. Cross-correlation of long-range correlated series. J Stat Mech Theory Exp 2009:P03037.

112. Theiler J, Eubank S, Longtin A, Galdrikian B, Farmer JD. 1992. Testing for nonlinarity in time series: the method of surrogate data. Phys D 58:77–94.

113. Bak P, Paczuski M. 1995. Complexity, contingency, and criticality. Proc Natl Acad Sci 92:6689–6696.

114. Bak P, Tang C, Wiesenfeld K. 1987. Self-organized criticality: An explanation of the 1/ f noise. Phys Rev Lett 59:381–384.

115. Bak P, Tang C, Wiesenfeld K. 1988. Self-organized criticality. Phys Rev A 38:364–374.

116. Bonachela JA, de Franciscis S, Torres JJ, Muñoz MA. 2010. Self-organization without conservation: are neuronal avalanches generically critical? J Stat Mech Theory Exp 2010:P02015.

117. Hesse J, Gross T. 2014. Self-organized criticality as a fundamental property of neural systems. Front Syst Neurosci 8:1–14.

118. Poil S-S, Hardstone R, Mansvelder HD, Linkenkaer-Hansen K. 2012. Critical-State Dynamics of Avalanches and Oscillations Jointly Emerge from Balanced Excitation/Inhibition in Neuronal Networks. J Neurosci 32:9817–9823.

119. Ivanov PC, Amaral LAN, Goldberger AL, Stanley HE. 1998. Stochastic feedback and the regulation of biological rhythms. Europhys Lett 43:363–368.

120. Nunes Amaral L, Ivanov P, Aoyagi N, Hidaka I, Tomono S, Goldberger A, Stanley H, Yamamoto Y. 2001. Behavioral-Independent Features of Complex Heartbeat Dynamics. Phys Rev Lett 86:6026–6029.

121. Stanley HE. 1999. Scaling, universality, and renormalization: Three pillars of modern critical phenomena. Rev Mod Phys 71:S358–S366.

122. Frigg R. 2003. Self-organised criticality—what it is and what it isn't. Stud Hist Philos Sci Part A 34:613–632.

123. Krienen FM, Thomas Yeo BT, Buckner RL. 2014. Reconfigurable task-dependent functional coupling modes cluster around a core functional architecture. Philos Trans R Soc B Biol Sci 369.

124. Tel T. 1988. Fractals, Multifractals, and Thermodynamics. Zeitschrift für Naturforsch A 1174:1154–1174.

125. Mueller S, Wang D, Fox MD, Yeo BTT, Sepulcre J, Sabuncu MR, Shafee R, Lu J, Liu H. 2013. Individual Variability in Functional Connectivity Architecture of the Human Brain. Neuron 77:586–595.

126. 2020. Decoding Brain Patterns for Colored and Grayscale Images using Multivariate Pattern Analysis. KSII Trans Internet Inf Syst 14.

127. Bekhtereva V, Müller MM. 2017. Bringing color to emotion: The influence of color on attentional bias to briefly presented emotional images. Cogn Affect Behav Neurosci 17:1028–1047.

128. Krull KR. 2019. Attention deficit hyperactivity disorder in children and adolescents: Clinical features and diagnosisUpToDate.

129. Racz FS, Stylianou O, Mukli P, Eke A. 2018. Multifractal Dynamic Functional Connectivity in the Resting-State Brain. Front Physiol 9:1–18.

130. Stam CJ, Van Dijk BW. 2002. Synchronization likelihood: An unbiased measure of generalized synchronization in multivariate data sets. Phys D Nonlinear Phenom 163:236–251.

131. He BJ, Zempel JM, Snyder AZ, Raichle ME, Biyu J. He, John M. Zempel, Abraham Z. Snyder and MER. 2010. The temporal structures and functional significance of scale-free brain activity. Neuron 66:353–369.

132. Michel CM, Brunet D. 2019. EEG Source Imaging: A Practical Review of the Analysis Steps. Front Neurol 10.

133. Bassett DS, Wymbs NF, Porter MA, Mucha PJ, Carlson JM, Grafton ST. 2011. Dynamic reconfiguration of human brain networks during learning. Proc Natl Acad Sci 108:7641–7646.

134. Lewis CM, Baldassarre A, Committeri G, Romani GL, Corbetta M. 2009. Learning sculpts the spontaneous activity of the resting human brain. Proc Natl Acad Sci 106:17558–17563.

135. Racz FS, Farkas K, Stylianou O, Kaposzta Z, Czoch A, Mukli P, Csukly G, Eke A. 2021. Separating scale-free and oscillatory components of neural activity in schizophrenia. Brain Behav https://doi.org/10.1002/brb3.2047.

136. Meisel C, Storch A, Hallmeyer-Elgner S, Bullmore E, Gross T. 2012. Failure of adaptive self-organized criticality during epileptic seizure attacks. PLoS Comput Biol 8.

137. James G, Witten D, Hastie T, Tibshirani R. 2013. An Introduction to Statistical Learning. Springer New York, New York, NY. http://link.springer.com/10.1007/978-1-4614-7138-7.

10. CANDIDATE'S PUBLICATIONS

Dissertation-related Publications

1. **Stylianou O**, Racz FS, Eke A, Mukli P. 2021. Scale-Free Coupled Dynamics in Brain Networks Captured by Bivariate Focus-Based Multifractal Analysis. Front Physiol 11:1–14.

2. **Stylianou O**, Racz FS, Kim K, Kaposzta Z, Czoch A, Yabluchanskiy A, Eke A, Mukli P. 2021. Multifractal Functional Connectivity Analysis of Electroencephalogram Reveals Reorganization of Brain Networks in a Visual Pattern Recognition Paradigm. Front Hum Neurosci 15.

Other Publications

1. Racz FS, **Stylianou O**, Mukli P, Eke A. 2018. Multifractal Dynamic Functional Connectivity in the Resting-State Brain. Front Physiol 9:1–18.

2. Racz FS, **Stylianou O**, Mukli P, Eke A. 2019. Multifractal and entropy analysis of resting-state electroencephalography reveals spatial organization in local dynamic functional connectivity. Sci Rep 9:13474.

3. Racz FS, **Stylianou O**, Mukli P, Eke A. 2020. Multifractal and Entropy-Based Analysis of Delta Band Neural Activity Reveals Altered Functional Connectivity Dynamics in Schizophrenia. Front Syst Neurosci 14:1–22.

4. Kaposzta Z, **Stylianou O**, Mukli P, Eke A, Racz FS. 2021. Decreased connection density and modularity of functional brain networks during n-back working memory paradigm. Brain Behav 11:1–16.

5. Mukli P, Nagy Z, Racz FS, Portoro I, Hartmann A, **Stylianou O**, Debreczeni R, Bereczki D, Eke A. 2021. Two-Tiered Response of Cardiorespiratory-Cerebrovascular Network to Orthostatic Challenge. Front Physiol 12.

6. Racz FS, Farkas K, **Stylianou O**, Kaposzta Z, Czoch A, Mukli P, Csukly G, Eke A. 2021. Separating scale-free and oscillatory components of neural activity in schizophrenia. Brain Behav 11:1–15.

7. Mukli P, Csipo T, Lipecz A, **Stylianou O**, Racz FS, Owens CD, Perry JW, Tarantini S, Sorond FA, Kellawan JM, Purebl G, Yang Y, Sonntag WE, Csiszar A, Ungvari ZI, Yabluchanskiy A. 2021. Sleep deprivation alters task-related changes in functional connectivity of the frontal cortex: A near-infrared spectroscopy study. Brain Behav 11.

8. Kaposzta Z, Czoch A, **Stylianou O**, Kim K, Mukli P, Eke A, Racz FS. 2022. Real-Time Algorithm for Detrended Cross-Correlation Analysis of Long-Range Coupled Processes. Front Physiol 13.

9. Racz FS, Czoch A, Kaposzta Z, **Stylianou O**, Mukli P, Eke A. 2022. Multiple-Resampling Cross-Spectral Analysis: An Unbiased Tool for Estimating Fractal Connectivity With an Application to Neurophysiological Signals. Front Physiol 13.

DOI:10.14753/SE.2022.2667

11. ACKNOWLEDGMENTS

I would like to thank my PhD supervisor, Dr. Péter Mukli, for his constant help both during my TDK and PhD years. I would like to express my appreciation to Dr. András Eke, my TDK supervisor, who accepted me as an underground research student in his laboratory and has been providing feedback on my work. I am grateful to Dr. Frigyes Sámuel Rácz for being my TDK co-supervisor and guiding me through my PhD studies. I thank Keumbi Kim, Dr. Ákos Czoch and Zalán Káposzta, members of our research team, for helping me out with data collection and preprocessing. It has been an honor to work in the prestigious Department of Physiology. Especially, I would like to thank Prof. László Hunyady, who was the Head of Department, and Prof. Erzsébet Ligeti for supporting my application to the Doctorate School of Semmelweis University. I am also extremely grateful to Prof. Zoltán Benyó, who supported me in the last two years. I would also like to thank Prof. János Réthelyi for supporting my application to the Doctorate School of Semmelweis University. I acknowledge the volunteering subjects for their participation in our studies; this work could not be completed without their contribution. Lastly, a big “Thank you” to my parents and sister, who continue to support me throughout my life.

frontiers in Physiology

DOI:10.14753/SE.2022.2667

ORIGINAL RESEARCH
published: 03 February 2021
doi: 10.3389/fphys.2020.615961

Scale-Free Coupled Dynamics in Brain Networks Captured by Bivariate Focus-Based Multifractal Analysis

Orestis Stylianou[1,2], Frigyes Samuel Racz[1], Andras Eke[1,3] and Peter Mukli[1,4]**

[1] Department of Physiology, Semmelweis University, Budapest, Hungary, [2] Institute of Translational Medicine, Semmelweis University, Budapest, Hungary, [3] Department of Radiology and Biomedical Imaging, Yale University School of Medicine, New Haven, CT, United States, [4] Vascular Cognitive Impairment and Neurodegeneration Program, Oklahoma Center for Geroscience and Healthy Brain Aging, Department of Biochemistry and Molecular Biology, University of Oklahoma Health Sciences Center, Oklahoma City, OK, United States

OPEN ACCESS

Edited by:
Paul Bogdan, University of Southern California, Los Angeles, United States

Reviewed by:
Alexander Caicedo, Del Rosario University, Colombia
Philippe Ciuciu, Commissariat à l'Energie Atomique et aux Energies Alternatives (CEA), France
Duoji Ma, Anhui Normal University, China

***Correspondence:**
Peter Mukli
mukli.peter@med.semmelweis-univ.hu
Andras Eke
eke.andras@med.semmelweis-univ.hu

Specialty section:
This article was submitted to Fractal and Network Physiology, a section of the journal Frontiers in Physiology

Received: *10 October 2020*
Accepted: *29 December 2020*
Published: *03 February 2021*

Citation:
Stylianou O, Racz FS, Eke A and Mukli P (2021) Scale-Free Coupled Dynamics in Brain Networks Captured by Bivariate Focus-Based Multifractal Analysis. Front. Physiol. 11:615961. doi: 10.3389/fphys.2020.615961

While most connectivity studies investigate functional connectivity (FC) in a scale-dependent manner, coupled neural processes may also exhibit broadband dynamics, manifesting as power-law scaling of their measures of interdependence. Here we introduce the bivariate focus-based multifractal (BFMF) analysis as a robust tool for capturing such scale-free relations and use resting-state electroencephalography (EEG) recordings of 12 subjects to demonstrate its performance in reconstructing physiological networks. BFMF was employed to characterize broadband FC between 62 cortical regions in a pairwise manner, with all investigated connections being tested for true bivariate multifractality. EEG channels were also grouped to represent the activity of six resting-state networks (RSNs) in the brain, thus allowing for the analysis of within- and between- RSNs connectivity, separately. Most connections featured true bivariate multifractality, which could be attributed to the genuine scale-free coupling of neural dynamics. Bivariate multifractality showed a characteristic topology over the cortex that was highly concordant among subjects. Long-term autocorrelation was higher in within-RSNs, while the degree of multifractality was generally found stronger in between-RSNs connections. These results offer statistical evidence of the bivariate multifractal nature of functional coupling in the brain and validate BFMF as a robust method to capture such scale-independent coupled dynamics.

Keywords: scale-free, bivariate, multifractal, functional connectivity, network physiology, electroencephalography

INTRODUCTION

Physiological systems are integrated through a series of intricate connections giving rise to networks of dynamically interacting elements. These may emerge at various scales from molecular pathways (Covert, 2006; Prentki et al., 2020) to the brain connectome (Sporns, 2011) and even at the level of the entire organism (Bashan et al., 2012; Bartsch et al., 2015). The universality of this organizing principle gave birth to the field of network physiology (Bashan et al., 2012; Ivanov and Bartsch, 2014; Bartsch et al., 2015; Ivanov et al., 2016), aiming at unfolding the

DOI:10.14753/SE.2022.2667

mechanisms through which diverse physiological systems interact. This goal may be achieved through characterizing various aspects of the temporal coupling between such systems and processes. Novel bivariate analytical methods (Bashan et al., 2012; Schulz et al., 2013; Jalili, 2016) kept advancing the research in this field. Even though many of these methodologies have been proven invaluable for the investigation of scale-specific interactions, they largely neglect the plausible broadband nature of the functional coupling itself (i.e. coupling that spans across a wide range of frequencies). This may, however, become relevant, as many biological processes have been shown to express broadband, scale-free dynamics; examples include the variability of heart rate (Ivanov et al., 1999, 2004; Nunes Amaral et al., 2001; Bartsch et al., 2005), spontaneous brain activity (Ivanov et al., 2009; Lin et al., 2020) or gait variability (Bartsch et al., 2007), to name a few. While these biological functions may contain narrowband components that can also be of interest, their broadband dynamics indicate scale-free (or *fractal*) behavior (Eke et al., 2000). Scale-free features may reveal fundamental aspects of complex systems – such as the human organism – that otherwise remain hidden from traditional methods of analysis. The ubiquity of the univariate fractal dynamics in physiological processes warrants the application of bivariate scale-free time series analysis to study the complexity of coupling between such processes.

Among fields where the human organism (or subsystems thereof) is modeled as a network of functionally coupled elements, brain functional connectivity (FC) studies probably gained the most momentum in past decades (Friston et al., 1993; Biswal et al., 1995; Rubinov and Sporns, 2010; Sporns, 2011; Finn et al., 2015; Lowe et al., 2016; Preti et al., 2017). In that, the network theoretical approach has been shown by many studies to be a powerful tool for the analysis of neural activity patterns (Bullmore and Sporns, 2009; Stam, 2014). According to this framework, the investigated brain regions are considered as nodes of the reconstructed network, while its edges represent the statistically estimated functional coupling between these regions (Rubinov and Sporns, 2010). However, a 'static' assessment of FC poses a limitation since the strength of functional coupling between neuronal assemblies has been shown to change over time (Chang and Glover, 2010; Hutchison et al., 2013). Therefore, characterizing the temporal organization of brain network topology requires a model that can account for these time-dependent aspects of FC. This led to the introduction of various tools capable of capturing the dynamic characteristics of brain networks (Dimitriadis et al., 2010; Tagliazucchi et al., 2012; Yu et al., 2015; Preti et al., 2017). Additionally, the ubiquitous presence of scale-free dynamics in the resting-state brain (Werner, 2010; Fraiman and Chialvo, 2012), – especially in the electroencephalogram (EEG) (Lutzenberger et al., 1992; Preißl et al., 1997; Gong et al., 2003; Stam and de Bruin, 2004; Racz et al., 2018b) – encouraged the investigation of power-law scaling in time-varying network properties. Utilizing a combination of dynamic graph theoretical analysis and multifractal time series analysis, we recently revealed that both global (Racz et al., 2018a,b) and local (Racz et al., 2019) properties of functional brain networks fluctuate according to a multifractal pattern, which may also be affected in pathological conditions (Racz et al., 2020). However, a different aspect of connectivity dynamics, namely the scale-free nature of the inter-regional coupling itself, remained inaccessible to these approaches, which mainly utilized a sliding window technique. In contrast to the univariate approach, bivariate multifractal methods – such as detrended cross-correlation analysis (Podobnik and Stanley, 2008) or wavelet-based analysis (Abry et al., 2019; Jaffard et al., 2019a,b)– characterize fractal properties of the coupling between dynamic processes; therefore, they would be able to capture these aspects of functional connections. Furthermore, such approaches could be adapted to the graph-theoretical framework of FC analysis, where edge weights in the network would be assigned as the fractal characteristics of the functional coupling between the investigated brain regions. Networks reconstructed by this approach would inherently represent the fluctuating nature of the connections, in contrast to the traditional way of reconstructing dynamic connections by calculating static indices of interdependence in a sliding window approach. Despite this, to date only a handful of studies investigated the scale-free aspects of functional brain connectivity (Achard et al., 2008; Wang and Zhao, 2012; Ciuciu et al., 2014; La Rocca et al., 2021). In this present work, we set out to address this issue by applying multifractal covariance analysis – introduced earlier by Mukli et al. (2018) – for assessing resting-state functional connectivity reconstructed from EEG measurements.

Some precautions must be addressed, however, when assessing the scale-free properties of empirical signals. In the case of univariate multifractal analysis, it is critical to verify that the obtained indices indeed characterize an inherent property of the observed process, and they not only represent noise or numerical instabilities of the analysis itself (Kantelhardt et al., 2002; Kwapień et al., 2005; Grech and Pamuła, 2012; Rak and Grech, 2018). Similar considerations must be made in the case of bivariate multifractal analysis. Therefore, it is indispensable to verify the presence of true bivariate scale-free coupling by carrying out appropriate statistical tests of power-law cross-coherence (Kristoufek, 2014) and cross-correlation (Wendt et al., 2009; Podobnik et al., 2011; Blythe et al., 2016). Although true multifractality can be confirmed with statistical certainty by extending the testing framework applied for univariate analytical tools (Kantelhardt et al., 2002; Clauset et al., 2009; Roux et al., 2009; Racz et al., 2019, 2020), these methods do not provide much insight into the generating mechanism of bivariate multifractality. Depending on the mechanism, bivariate multifractality could be considered as a consequence of independent univariate dynamics (Wendt et al., 2009; Jaffard et al., 2019a). On the other hand, an appropriate testing framework may identify the genuine scale-free nature of the coupling. This type of bivariate multifractality corresponds to an inherent aspect of the relationship between the processes that otherwise remains undetectable to univariate fractal analysis. For this purpose – namely, to confirm the source of bivariate multifractality –, we devise a testing procedure building on previous studies (Wendt et al., 2009; Kristoufek, 2011) that compares the bivariate fractal measures with their univariate equivalents obtained from the investigated time series to reveal their origin.

DOI:10.14753/SE.2022.2667

So far, the majority of bivariate fractal studies has focused on the analysis of financial time series (Podobnik and Stanley, 2008; Oświęcimka et al., 2014; Pal et al., 2014; Kwapień et al., 2015), while only a few studies applied these tools on physiological datasets (Wang and Zhao, 2012; Ciuciu et al., 2014; La Rocca et al., 2021). Moreover, to the best of our knowledge there have been no studies statistically validating the existence of bivariate multifractality in coupled processes in the human brain or body. Here we apply a novel bivariate method – exploiting the focus-based regression scheme of Mukli et al. (2015) – to investigate if functional connectivity, as reconstructed from EEG recordings, may exhibit a coupled multifractal nature. First, we design and perform a series of statistical tests to confirm true scale invariance and multifractality of individual connections. Second, we assess between-subject and within-subject (i.e., regional) variability of bivariate multifractal indices in order to explore the consistency and discriminatory power of the presented method. Third, we explore whether scale-free coupling displays a topology at the level of large-scale functional networks in the brain. By confirming the plausible bivariate multifractal nature of neural interactions, the present study may not only enhance our understanding of how neural activity is organized in time and space but also provide an efficient analytical pipeline for capturing long-term interdependencies of physiological processes even outside the human brain, on the level of the entire organism.

MATERIALS AND METHODS

Data and Participants

The EEG database analyzed in this study was made publicly available by Sockeel et al. (2016) and consisted of recordings from 12 right-handed, healthy participants (aged 26.6 ± 2.1 years, six females). Each recording contained a 5-minute long segment of resting-state, eyes closed neural activity in which the subjects were lying supine and were listening to an audio recording equivalent to the sounds of an MRI system. EEG tracing was carried out using a 62-channel BrainAmp amplifier, in which the electrodes were arranged according to the international 10–10 system. The sampling rate was set to 5 kHz with the ground and reference electrodes placed at Oz and Cz positions, respectively. Electrode impedance was kept under 10 kΩ during the recordings. The original study was approved by the local ethics committee (Comité de Protection des Personnes–Ile-de-France under the number CPP DGS2007-0555), with measurements being carried out in accordance with the Declaration of Helsinki. All participants provided written informed consent before the measurement. For further details on participants and data collection the reader is referred to the original article of Sockeel et al. (2016).

Preprocessing

All preprocessing was carried out using Matlab (The Mathworks, Natick, MA, United States). The procedure followed steps of the Batch Electroencephalography Automated Preprocessing Platform (Levin et al., 2018), which uses functions of the EEGLAB toolbox (Delorme and Makeig, 2004) along with custom functions and scripts. First, the data was visually inspected; artifact-free segments of length approximately 55 s long were selected and band-pass filtered with lower and upper cut-off frequencies of 0.5 and 250 Hz, respectively. Additional notch filters at 50, 100, and 200 Hz were applied for line noise removal. Subsequently, the signals were downsampled from 5 kHz to 500 Hz. Further artifact removal was performed using the Harvard Automated Processing Pipeline for Electroencephalography (HAPPE) (Gabard-Durnam et al., 2018). HAPPE implements a series of steps, including wavelet-enhanced independent component analysis followed by independent component analysis with Multiple Artifact Rejection Algorithm (Winkler et al., 2011, 2014). Thus, signal components that likely originate from sources other than neural activity, such as eye movements or scalp muscle contractions, were excluded. Finally, the pruned data was re-referenced to the common average reference. Subsequently, the first 2^{14} datapoints (approximately 33 s) were selected from every preprocessed dataset for further analysis.

Bivariate Focus-Based Multifractal Analysis

The focus-based multifractal (FMF) analysis framework was introduced by Mukli et al. (2015) in order to provide a robust and efficient way of multifractal time series analysis. Originally, FMF was put forward as a univariate method, i.e., to analyze a single time series. The concept of FMF was then extended to the bivariate domain in a later study (Mukli et al., 2018), with the new method termed bivariate focus-based multifractal analysis (BFMF). Such modification (as detailed below) made the analysis of the multifractal aspect of coupled dynamics feasible and robust, and constitutes the main advantage of BFMF over other bivariate multifractal tools.

Specifically, BFMF is implemented in the time domain using statistical moments (of order q) of the scale-wise covariance of sampled time series X and Y (cov_{xy}) calculated at various window sizes. In that, the scaling function, S_{XY}, is defined according to

$$S_{XY}(q,s) = \left(\frac{1}{N_s} \sum_{v=1}^{N_s} |cov_{XY}|(v,s)^q \right)^{1/q} \quad (1)$$

with N_s being the number of non-overlapping windows of size s indexed by v and $L = 2^{14}$ the length of the time series in data points. The cumulatively summed signal is bridge-detrended in each temporal window prior to calculating the covariance. Values of q are set to range from −15 to 15 with increments of 1, as this selection of moment orders is sufficient to reliably capture multifractality (Grech and Pamuła, 2012). Scales are defined according to a dyadic scale, i.e., as 2^n with n ranging from 4 to 9; higher scales were excluded to avoid artifacts due to band-pass filtering. Setting the scale s equal to the total signal length L renders the sum in (1) independent of q. Consequently, in the limit of $s = L$, values of $S(q,s)$ converge to one point termed the *Focus* (**Figure 1**). The *Focus* serves as an iterated reference point in the regression model – based on the equations (18–21) of

DOI:10.14753/SE.2022.2667

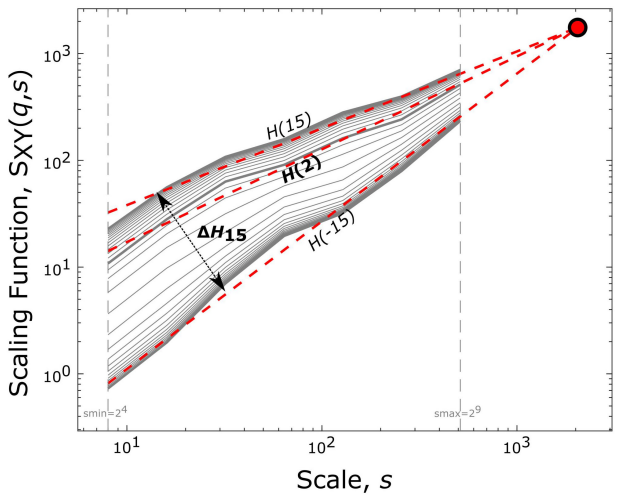

FIGURE 1 | End-point parameters of bivariate focus-based multifractal analysis. Log-log transform of the scaling function [$S_{XY}(q,s)$] vs. scale (s) relationship is plotted. The generalized Hurst exponent [$H(q)$], for several statistical moments (q), is acquired via linear regression with the *Focus* (solid red circle) used as a reference point. $H(2)$ expresses the long-term correlation between the two time series. At the same time, the degree of multifractality (ΔH_{15}) is captured by the difference between $H(q)$ at the minimal (–15) and maximal (15) statistical moments.

Mukli et al. (2015) – that simultaneously estimates the best-fitting linear function of $\log(s)$ to obtain $\log(S(q, s))$ for all values of q. The fitting procedure yields a set of power-law exponents (i.e., the slopes of the fitted linear functions), the generalized Hurst exponent function (Barunik and Kristoufek, 2010):

$$S_{XY}(q, s) \propto s^{H(q)} \tag{2}$$

From the estimated $H(q)$, the ones of particular interest in this study are $H(2)$, $H(-15)$, and $H(15)$. $H(2)$ is a measure of global long-term interdependence between X and Y with the particular case of $H(2) = 0.5$, indicating uncoupled dynamics. $H(2) < 0.5$ shows long-term anticorrelation while $H(2) > 0.5$ positive long-term correlation of the two processes. Since multifractality refers to the temporally altering nature of long-term (cross-) correlations, the degree (or strength) of multifractality can be considered as to what extent this property might change in the process. Since positive and negative moment orders emphasize the contributions of large and small covariance, respectively, a measure characterizing the degree of multifractality can be obtained by calculating the difference between the scaling exponent obtained at the minimal and maximal moments (Grech and Pamuła, 2012; Mukli et al., 2015). Therefore, in our study multifractal strength was captured in $\Delta H_{15} = H(-15) - H(15)$, which provides a good and robust approximation of the theoretical limit $\lim_{q\to\infty} H(-q) - H(q)$ (Grech and Pamuła, 2012; Mukli et al., 2015).

Assessing Multifractality

In order to verify the true multifractal nature[1] of the functional connections, an array of tests was utilized. The purpose of these tests was to differentiate the true, time-varying scale-free nature of these connections, emerging from the presence of long-term cross-correlations, from those appearing as spurious multifractality (Kantelhardt et al., 2002). First, we tested the power-law dependence of the cross-spectral power on the scale, based on the work of Clauset et al. (2009). In the case of a fractal process, the spectral index (β) of its power spectrum represents the slope of the fitted linear regression of the logarithmic amplitude vs. frequency plot and is proportional to its univariate Hurst exponent, $H_{univ}(2)$ [$\beta = 2H_{univ}(2)$-1] (Eke et al., 2002). This relationship also holds in the bivariate case, as the spectral index of the cross-power spectrum of two processes expressing fractal coupling is equivalent to $\beta = 2H_{biv}(2) - 1$ (Kristoufek, 2014), where $H_{biv}(2)$ is the bivariate Hurst exponent. Therefore, the cross-power spectrum of the two processes is suitable for identifying the plausible power-law dependence in their coupling. For each pair of time series, 40 surrogates were generated whose value of $H_{univ}(2)$ was equal to that of $H_{biv}(2)$, according to the spectral synthesis method (Saupe, 1988). Then, a linear regression model was fitted to the log-log transformed power-spectrum and a Kolmogorov distance was calculated for every generated time series denoting its maximal distance from its power-spectrum (D_{univ}). The distribution of D_{univ} was compared with the maximal distance of the linear function fitted to the log-log transformed cross-power spectrum of the original connection (D_{biv}). The original connection was considered scale-free (successful test), if

$$D_{biv} < \mu(D_{univ}) + 2\sigma(D_{univ}) \tag{3}$$

where $\mu(D_{univ})$ and $\sigma(D_{univ})$ are mean and standard deviation obtained from the D_{univ} distribution. Onward, $\mu()$ represents the mean and $\sigma()$ indicates the standard deviation of the distribution in question.

In addition, we examined the detrended cross-correlation coefficients (ρ) calculated for each scale by adopting a method proposed by Podobnik et al. (2011):

$$\rho(s) = \frac{S_{XY}^2(2, s)}{S_X(2, s)\, S_Y(2, s)} \tag{4}$$

where $S_X(2, s)$, $S_Y(2, s)$, and $S_{XY}(2, s)$ are the scaling function values for scales s and the 2nd order statistical moment of time series X, Y and their connection, respectively. We used a stochastic binomial cascade algorithm (Schumann and Kantelhardt, 2011) to generate a population (100 pairs) of multifractal signals with L, $H(2)$ and ΔH_{15} adjusted to the univariate time series concerned. In line with the refinement of Blythe et al. (2016), all coefficients were tested simultaneously for every scale. Thus, the null hypothesis was only rejected if statistical analysis confirmed that the original $\rho(s)$ exceeded

[1]The multifractal nature of the coupling was based on the dichotomus model of fractional Gaussian noise and fractional Brownian motion (Eke et al., 2000) extended to the multivariate setting (Lavancier et al., 2009).

DOI:10.14753/SE.2022.2667

that of the surrogate population of cross-correlation coefficients for each scale, yielding an overall $p < 0.05$. Accordingly, the individual significance levels were set to $(0.05)^{1/6}$. Connections that passed the test were considered to have genuine long-term interdependence.

To test if the observed multifractality was due to non-linearities, the following phase randomization scheme was applied. Forty surrogates for each time series were generated by: (*i*) Fourier transforming the data of all channels and (*ii*) randomly permutating the phases before inverse Fourier transformation of the spectrum (Prichard and Theiler, 1994). Since the same permutation was carried out to randomize the phases of data from all channels, this procedure destroyed the non-linear interdependencies between the signals while the linear dependencies remained intact. If the original ΔH_{15} ($\Delta H_{15,orig}$) did not satisfy the inequality

$$\Delta H_{15,orig} > \mu(\Delta H_{15,sur}) + 2\sigma(\Delta H_{15,sur}) \quad (5)$$

true multifractality due to non-linearity could not be confirmed.

Shuffling of time series is necessary to distinguish between correlation- and distribution-type bivariate multifractality (Wang et al., 2012). Since shuffling destroys all long-term correlations within (Kantelhardt et al., 2002) and between (Louis et al., 2010) the signals, the shuffled time series are expected to show diminished multifractal profile if their bivariate multifractality is due to long-term correlations. Forty shuffled surrogates were generated from every original signal that resulted in a distribution of $H(2)$ and ΔH_{15} values for every connection. Consequently, the following inequalities between the original and shuffled datasets were investigated:

$$H_{orig}(2) > \mu(H_{shfl}(2)) + 2\sigma(H_{shfl}(2)) \ldots$$
$$H_{orig}(2) < \mu(H_{shfl}(2)) - 2\sigma(H_{shfl}(2)) \quad (6a)$$

$$\Delta H_{15,orig} > \mu(\Delta H_{15,shfl}) + 2\sigma(\Delta H_{15,shfl}) \quad (6b)$$

If inequalities (6a) and (6b) hold, then the multifractal character of the connection can be attributed to long-term cross-correlations.

The final assessment was the bivariate-univariate Hurst exponent relationship test, which investigated if further information could be retrieved from bivariate multifractal analysis compared to univariate multifractal analysis. Assume two time series X and Y with $H_{XY}(2)$, $H_X(2)$, and $H_Y(2)$ being their bivariate and univariate Hurst exponents, respectively. If $H_{XY}(2)$ does not differ significantly from the arithmetic mean of $H_X(2)$ and $H_Y(2)$, then the bivariate exponent refers to a scale-free coupling whose Hurst exponent can be predicted from its univariate equivalents (Kristoufek, 2011). In this test, 40 datasets were generated for each time series with the same univariate $H(2)$ as that of the original signal, according to the spectral synthesis method (Saupe, 1988). Afterward, the true scale-free nature of the EEG signal was evaluated by performing a univariate power-law test [for details see Racz et al. (2018b)]. For every pair of time series that passed the univariate power-law test, the average of their Hurst exponents, $H_{XY,gen}(2)$, was calculated in each of the 40 generated datasets resulting in a distribution. The original $H_{XY}(2)$ was then compared in the following fashion:

$$H_{XY}(2) > \mu(H_{XY,\ gen}(2)) + 2\sigma(H_{XY,\ gen}(2)) \quad (7a)$$

$$H_{XY}(2) < \mu(H_{XY,gen}(2)) - 2\sigma(H_{XY,gen}(2)) \quad (7b)$$

If any of the two inequalities was met, then the pair of time series passed the test and their bivariate multifractality was considered intrinsic to the connection. Conversely, a connection failing the bivariate-univariate test was viewed as a case of extrinsic multifractality. This extrinsic multifractality possibly belongs to a functionally non-significant type of bivariate multifractality due to autocorrelation effects (Kristoufek, 2011; Arbabshirani et al., 2014).

Brain Parcelation and Graph Construction

To reduce the dimensionality of data while also providing a basis for physiological interpretation, a brain parcelation scheme proposed by Giacometti et al. (2014) was applied. The 62 EEG electrodes were grouped based on electrode proximity to seven – functional magnetic imaging (fMRI) labeled – resting-state networks (RSNs) as specified by Thomas Yeo et al. (2011)[2]. Due to the great degree of overlap in electrode locations between

[2]Note that the optimal method of matching EEG channels to RSNs (or more correctly to regions of interest) is by source-reconstruction (Michel and Brunet, 2019) and subsequent generation of time-series for each RSN. Our parcelation targeted mainly the dimensionality reduction and hence no strong conclusions about RSNs should be made based on this. For a source-reconstructed scale-free functional connectivity study we suggest reading (La Rocca et al., 2021).

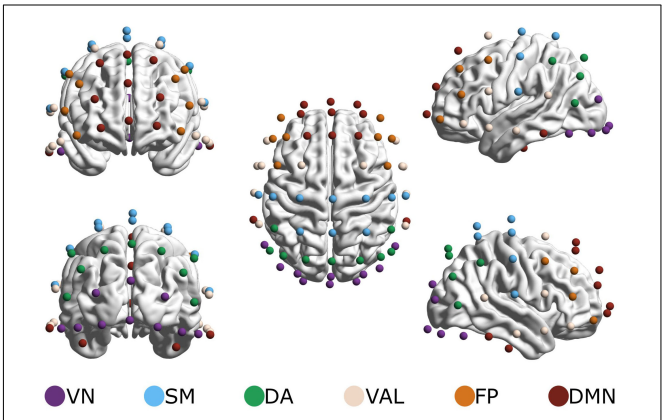

FIGURE 2 | Resting-state networks (RSNs). Electrodes were grouped to represent six RSNs: the visual network (VN, 10 channels), the somatomotor network (SM, 10 channels), the dorsal attention network (DA, 9 channels), the combined ventral attention and limbic networks (VAL, 12 channels), the frontoparietal network (FP, 8 channels) and the default mode network (DMN, 13 channels). Brain maps were created using the BrainNet Viewer software (Xia et al., 2013) after electrode positions were transformed to match a template head using SPM 12b (Penny et al., 2007). The figure originally appeared in Racz et al. (2019).

DOI:10.14753/SE.2022.2667

the ventral attention and limbic system networks, these were combined into a ventral attention-limbic network (**Figure 2**), as in Racz et al. (2019). This parcelation thus resulted in 6 RSNs and 15 RSN-to-RSN connections, whose indices were obtained by averaging the obtained values [$H(2)$ and ΔH_{15}] of corresponding connections. We examined connections within each RSN (within-RSNs) and connections between different RSNs (between-RSNs) separately.

Statistical Analyses

Following the previously described analytical pipeline and brain parcelation scheme, the obtained results were organized into a 12×6 within-RSNs matrix (12 subjects, 6 RSNs) and a 12×15 between-RSNs matrix (12 subjects, 15 RSN-to-RSN connections) for $H(2)$ and ΔH_{15}, separately. To evaluate the consistency of results among subjects, Kendall's coefficient of concordance (W) was calculated in every matrix. As to verify if cortical localization affected multifractal connection dynamics (i.e., to investigate if multifractal properties of functional connections vary according to various brain regions), we performed the Friedman test with level $\alpha_s = 0.05$ and pairwise comparisons (paired sample t-test if distributions were normal, Wilcoxon signed-rank if at least one distribution was non-normal, normality was evaluated by Lilliefors test) followed by Benjamini–Hochberg correction ($\alpha_s = 0.05$) (Yekutieli and Benjamini, 2001).

Finally, to further confirm the significant effect of spatial localization, 100 surrogate datasets were generated, where in every iteration the labels of the channels were randomly permuted before performing the brain parcelation. Subsequently, the Friedman tests were carried out and Kendall's coefficient of concordance was calculated. The effect of localization was considered statistically significant if the p-value obtained from the Friedman test failed to reach significance (i.e., $p > 0.05$) in at least 95 out of 100 cases. W values of the original dataset were validated as statistically significant only if they were above the 95th percentile of the W resulted from the distribution of the 100 generated datasets.

RESULTS

Verifying Bivariate Multifractality

The results of the bivariate multifractality assessment tests are summarized in **Table 1**. At the subject level, 86.5 ± 5% (mean ± standard deviation) of the total connections passed the power-law test, validating their scale-free nature. The detrended cross-correlation coefficients of all links were found to be significantly higher than those of the surrogate datasets, validating the existence of long-term cross-correlations. All connections passed the phase randomization test, which verified true multifractal coupling due to non-linear interactions. The shuffling test revealed that inequalities (6a) and (6b) held for 99.7 ± 0.3% and 100% of all connections, respectively. These results confirm that the observed multifractality was attributed to long-term cross-correlations.

TABLE 1 | Success rate of the different scale-free assessing tests at the subject level (mean ± standard deviation).

Performed Test	Success Rate
Power-Law Test	86.5 ± 5%
Detrended Cross-Correlation Coefficient Test	100%
Phase Randomization Test	100%
Shuffling Test – $H(2)$	99.7 ± 0.3%
Shuffling Test – ΔH_{15}	100%

Intrinsic vs. Extrinsic Multifractality of Connections

We considered bivariate multifractality as having extrinsic origin if it failed the bivariate-univariate Hurst exponent relation test (equations 7a and 7b) and intrinsic otherwise. The results revealed that a relevant proportion (52.4 ± 6.9%) of the observed functional connections had intrinsic scale-free characteristics. Group-averaged $H(2)$ networks separately reconstructed from intrinsic and extrinsic multifractal connections are shown in **Figure 3**. There is a clear distinction between the two networks [the correlation between the bivariate $H(2)$ values consisting of the two networks expressed in Pearson's $r = -0.98$, $p < 0.001$]. Specifically, within-RSNs connections tend to have stronger intrinsic multifractality, while the between-RSNs links show a higher degree of extrinsic multifractality.

To further illustrate these results, for every connection we calculated its averaged probability of expressing intrinsic multifractality when compared to the distribution of surrogates

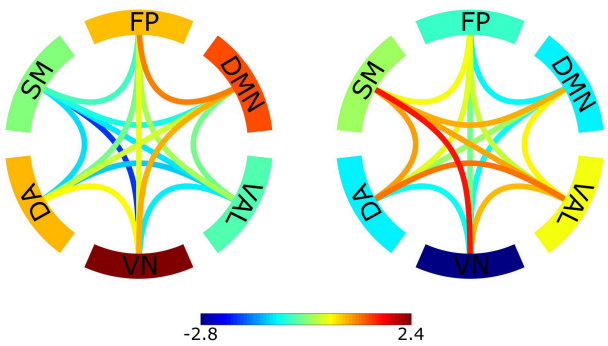

FIGURE 3 | Z-scores of intrinsic and extrinsic $H(2)$ network connections. The intrinsic network consisted of the $H(2)$ values of connections that passed the bivariate-univariate Hurst exponent relationship test, connections that failed were represented as 0. The extrinsic network consisted of the $H(2)$ values of connections that failed the bivariate-univariate Hurst exponent relationship test, connections that passed were represented as 0. Subsequently, the Z-scores of the connections were calculated. Z-scores represent deviation from the population average and their values are indicated by the color bar. The edges serve as the between-RSNs connections with color representing the strength of the connection. The outer ring comprises of the 6 RSNs with the color indicating the Z-score of within-RSN connections.

DOI:10.14753/SE.2022.2667

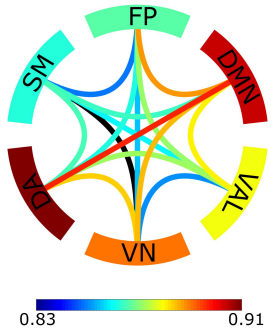

FIGURE 4 | Probabilistic network of intrinsic multifractality. The probability was obtained through the *Z*-score of the original bivariate Hurst exponent of the connection compared to the surrogate distribution created in the bivariate-univariate Hurst exponent relationship test. The edges serve as the between-RSNs connections with color representing the population average probability of the connection showing intrinsic multifractality. The outer ring comprises of the 6 RSNs with the color indicating the population average probability of within-RSNs connections being intrinsically multifractal.

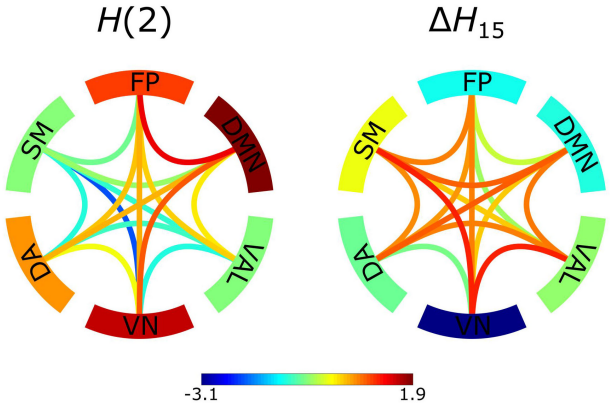

FIGURE 5 | *Z*-scores of constructed networks using $H(2)$ and ΔH_{15} as functional connectivity estimators. *Z*-scores represent deviation from the population average and their values are indicated by the color bar. The edges serve as the between-RSNs connections with color representing the strength of the connection. The outer ring comprises of the 6 RSNs with the color indicating the population average strength of the within-RSNs connections.

characterized only by extrinsic multifractality (**Figure 4**). Two RSNs stood out from the rest, namely the default mode network (DMN) and the dorsal attention network (DA). Not only connections within these RSNs showed a higher probability of intrinsic multifractality when compared to other RSNs, but also the same could be observed for connections linking these to RSNs in comparison to other between-RSNs connections.

Network Comparison

Two networks were constructed from the results obtained by BFMF analysis, one from $H(2)$ and one from ΔH_{15} values of functional connections (**Figure 5**). The two networks showed markedly different patterns (the correlation between the two networks expressed in Pearson's $r = -0.6609$, $p < 0.01$). Specifically, it appeared that $H(2)$ and ΔH_{15} of functional connections were inversely related, as within-RSNs connections expressing higher $H(2)$ values could be characterized with lower ΔH_{15}, and vice versa. The same inverse relationship could be observed for the multifractal properties of between-RSNs connections, although less prominently.

Effect of Subject and Regional Variability

The between- and within-subject variability of connections in both network types were analyzed using Kendall's *W*, Friedman tests and paired difference tests. For the $H(2)$ network, Kendall's *W* values of 0.72 and 0.65 were obtained for between- and within-RSNs connections, respectively, indicating strong concordance among subjects. Friedman tests revealed a significant main effect

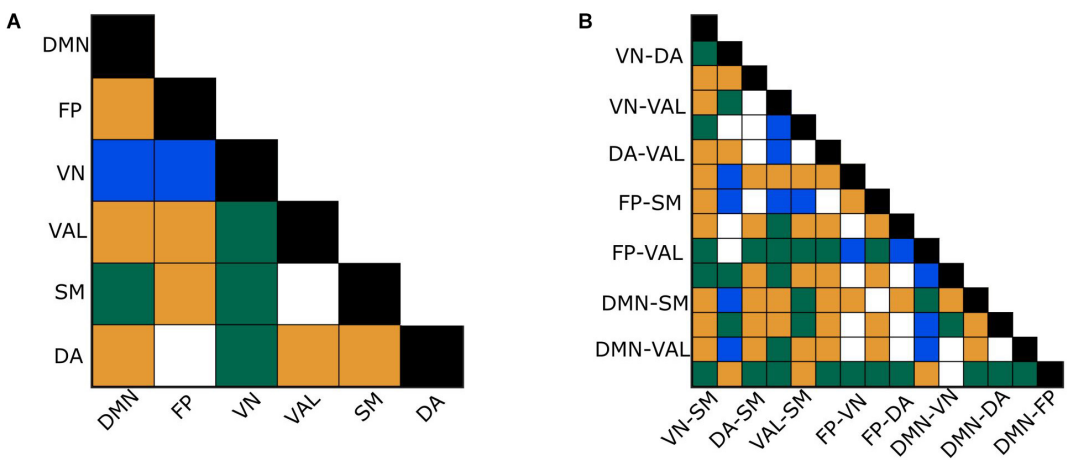

FIGURE 6 | Effect of regional variability. Significance of connection-to-connection comparisons of within- **(A)** and between- **(B)** RSNs after the appropriate correction for $H(2)$ and ΔH_{15}. Blue: Only ΔH_{15} comparison test was significant. Orange: Only $H(2)$ comparison test was significant. Green: Both $H(2)$ and ΔH_{15} comparison tests were significant.

DOI:10.14753/SE.2022.2667

TABLE 2 | Results of Kendall's *W*, success rate for individual paired difference tests after correction and Friedman test for $H(2)$ and ΔH_{15} for between- and within- RSNs.

	Kendall's *W*	Paired difference test success rate	Friedman Test *p*
$H(2)$ Between-RSNs	0.72	68.6%	<0.0001
$H(2)$ Within-RSNs	0.65	73.3%	<0.0001
ΔH_{15} Between-RSNs	0.44	40%	<0.0001
ΔH_{15} Within-RSNs	0.47	40%	<0.0001

of localization ($p < 0.0001$). 68.6% of the between-RSNs and 73.3% of the within-RSNs of the pairwise *post hoc* tests were found significant. The *W* values of the ΔH_{15} network were 0.44 and 0.47 for between- and within- RSNs connections, suggesting moderate subject agreement. Friedman test again indicated a significant main effect of localization for the ΔH_{15} values of functional connections ($p < 0.0001$), while 40% of the paired tests of between- and within-RSNs connections indicated a significant difference. Moreover, the two different networks displayed mostly different connections as statistically different (**Figure 6**). **Table 2** summarizes the results of the statistical tests performed on $H(2)$ and ΔH_{15} networks.

To further validate that cortical localization significantly impacted connection dynamics, the parcelation scheme was evaluated against $n = 100$ spatially shuffled surrogates (see section "Materials and Methods"). In that, only 1% of the generated datasets showed *p*-values smaller than 0.05 after shuffling the channel labels. Moreover, Kendall's *W* values for between-RSNs and within-RSNs for both $H(2)$ and ΔH_{15} were found significantly higher than those obtained from randomized data. These results further confirm that functional connections linking various regions of the brain express different scale-free characteristics.

DISCUSSION

In this study, we present a novel bivariate adaptation of focus-based multifractal time series analysis and show its applicability for studying the spatiotemporal organization of functional brain networks. The main contribution of this work, therefore, lies with the utilization of the BFMF method and its associated statistical framework for the reconstruction of brain networks based on scale-free coupled dynamics. In that, using detrended covariance as a time-domain measure for BFMF, we examined the fractal connectivity by calculating bivariate $H(2)$ and ΔH_{15} for each pair of processes, thereby assessing linear and non-linear aspects of their scale-free dynamics, respectively. The applied tests were essential in validating our findings and confirming that most of the connections were indeed multifractal. Moreover, with a combined application of bivariate and univariate focus-based multifractal analysis, we revealed whether the observed cross-regional temporal dynamics emerged from genuine scale-free interactions intrinsic to the connection, or were simply a consequence of long-term autocorrelation present in both processes. The reconstructed networks and their topology were highly consistent among subjects, while significant regional variability over the cortex was also observed. Our findings demonstrate that BFMF is an analytical tool capable of capturing scale-free coupled dynamics of physiological networks, a feature that may otherwise remain undetected by univariate fractal analytical methods.

Bivariate Multifractality in the Brain

Despite the ubiquity of scale-free characteristics in neural dynamics (He et al., 2010), only a limited number of studies investigated the fractal nature of the functional coupling between these processes. Ciuciu et al. (2014) assessed scale-free coupling of neural dynamics from fMRI datasets using frequency- and wavelet-based measures, thereby having to resort to an inherently low temporal sampling rate limiting both the precision and possible interpretation of their results. Other functional connectivity studies verified the presence of scale-free coupling in magnetoencephalography recordings using wavelet coherence function (La Rocca et al., 2021). The only bivariate scale-free study of EEG datasets was an exploratory investigation reporting significant differences in the bivariate multifractal profiles between young and elderly populations (Wang and Zhao, 2012).

Although these works reported on relevant aspects of neural dynamics, they did not provide statistical tests for the validation of the true multifractal nature of the investigated connections. This study aimed to rectify this limitation by adapting univariate scale-free assessment tests in the bivariate setting, as well as improving already-existing bivariate equivalents. Most of the analyzed connections in our study showed genuine multifractal coupling due to long-range cross-correlations, as indicated by the high success rates in the power-law, detrended cross-correlation, phase randomization and shuffling tests. It was indispensable to examine the presence of power-law relationship since coupled oscillatory dynamics confined to a specific time scale/frequency range might be present in our dataset. Robust detection of this feature was ensured by a statistical framework implemented in the frequency domain (Clauset et al., 2009). Moreover, the detrended cross-correlation coefficients of the original connections were significantly different from those of surrogate data at every scale, directly indicating the presence of scale-free long-term cross-correlations in the time domain (Podobnik et al., 2011). The purpose of phase randomization was to yield a population of surrogate data with abolished non-linearity (Prichard and Theiler, 1994). Comparing the multifractal characteristics of the surrogate population with those of the original data revealed that multifractality was indeed a consequence of the non-linear nature of the coupling between processes. The shuffling test, which distinguished between correlation- and distribution-type multifractality (Kantelhardt et al., 2002), indicated that most of our connections were of the former type. However, the bivariate multifractality of EEG-signals observed in this study can be attributed only partly to long-term cross-correlations, since the finite size effect will always contribute to the observed multifractality (Grech and Pamuła, 2012). To the best of our knowledge, our study is the first to statistically validate the existence of multifractality between elements of a physiological network, in this case the

DOI:10.14753/SE.2022.2667

brain. However, our findings may also open the way for the investigation of other networks of the human organism, whose constituents also express scale-free dynamics [such as heart rate variability (Ivanov et al., 1999, 2004; Nunes Amaral et al., 2001; Bartsch et al., 2005), gait variability (Bartsch et al., 2007), muscle activity (Santuz and Akay, 2020), breathing (Fadel et al., 2004), or blood glucose level fluctuations (Weissman and Binah, 2014)]. By applying BFMF to assess the coupling in such systems, novel aspects of their interactions could be revealed that have not yet been accounted for.

An essential aspect of scale-free interactions is whether the observed multifractality is an intrinsic property of the relationship. Considering the fact that covariance estimation is influenced by the autocorrelation of the signals (Arbabshirani et al., 2014), we can safely assume that the intrinsic multifractality of a connection represents true statistical interdependence between the different brain regions while a large part of extrinsic multifractality could be ascribed to autocorrelation effects (Kristoufek, 2011). According to **Figures 3**, **4**, while the between-RSNs connections showed a *mostly* extrinsic type of multifractality, the within-RSNs connections *mainly* featured intrinsic multifractality. This finding to some extent can be evident since a higher number of intrinsic (i.e., true) multifractal connections could be expected to exist within functionally cohesive neural populations, such as RSNs (van den Heuvel et al., 2010), as opposed to the links between them. These results may further support the notion that cortical regions that are considered to form RSNs are: *(i)* indeed functionally coupled and *(ii)* segregated from the rest of the brain (to some extent). Another noteworthy finding illustrated by **Figure 4** is that the default mode network, dorsal attention network and the connections between them showed the highest probability of intrinsic multifractality. DMN comprises of brain regions with increased FC during idling (Chen et al., 2008), and considering that the analyzed datasets were obtained in the resting-state, we can expect strong within-DMN connectivity. On the other hand, DA has increased FC during tasks that require attention (Vossel et al., 2014), making the high probability of intrinsic multifractality of connections both within DA and between DA and DMN unexpected. A recent study (Murphy et al., 2020) indicated an indirect functional connection between DMN and DA mediated by the frontoparietal network, providing partial support for our findings of a high chance of intrinsic multifractality in the DMN-DA connections. Although our parcelation scheme prevents us from drawing stronger conclusions on the activities of RSNs, our findings still allow a clear demonstration of the regional variability of scale-free coupling in large-scale brain networks.

The origin of scale-free/multifractal nature in brain activity is still an active field of research, which yet remains to be fully resolved. One plausible explanation may be provided from the study of critical systems. Accordingly, the brain can be considered as a complex system that exists at the brink of order and chaos (Weil, 1994; Beggs and Timme, 2012; Hesse and Gross, 2014), with its fine-tuned equilibrium and $1/f$-dynamics indicating the presence of self-organized criticality (SOC) (Bak et al., 1987; Buzsáki, 2006). The concept of SOC emphasizes that the brain tends to operate in a critical state (Bonachela et al., 2010; Hesse and Gross, 2014), where even a local perturbation can elicit a global response. In SOC-based interpretations of neural dynamics, criticality is achieved by fine-tuning a control parameter inherent to the brain. Despite options emerging from electrophysiological experiments (Freeman, 2004; Buzsáki, 2006), the identity of this control parameter remains elusive, sustaining a dispute within the neuroscience community over the relevance of SOC in explaining the observed dynamics (Beggs and Timme, 2012; Hesse and Gross, 2014). A likely candidate is a balance between incoming excitatory and inhibitory signaling of the neuronal populations. It has already been demonstrated that power-law scaling at local field potentials and global electromagnetic brain signals (Beggs and Timme, 2012; Poil et al., 2012) can emerge through such equilibrium of incoming excitatory and inhibitory stimuli. A similar model, attributed to the balance between the two divisions of the autonomic nervous system, has been suggested as the source of the scale-free fluctuations of the heart rate variability (Ivanov et al., 1998; Nunes Amaral et al., 2001). In line with these considerations, the stochastic influx of excitatory/inhibitory signals may be a possible source of bivariate multifractality of the brain networks, however this hypothesis requires further research.

Aspects of Functional Coupling Captured by BFMF

In this study, BFMF was used as a functional connectivity estimator, from which two brain networks were reconstructed. A network was defined by assigning the bivariate $H(2)$ values as edge weights, reflecting the topology of long-term cross-correlation. Similarly, bivariate ΔH_{15} values were assigned to all connections forming a network that displays the topology of the multifractal strength. It should be emphasized that the obtained scale-free pattern of functional connections appeared highly consistent among subjects, in agreement with previous studies (Gong et al., 2003). Moreover, our results indicated significant regional variability for both within- and between- RSNs connections. This regional variation was notably different between the $H(2)$ and ΔH_{15} networks (**Figure 6**), emphasizing that these two measures of scale-free dynamics are complementary to each other also in the bivariate setting. The complementary nature of $H(2)$ and ΔH_{15} has already been demonstrated in the univariate fractal analysis (Mukli et al., 2015; Racz et al., 2018b). Furthermore, the two networks yielded opposite patterns regarding their topologies, i.e., those connections with high $H(2)$ values were found to express low ΔH_{15} values and vice versa (**Figure 5**). A similar relationship between univariate $H(2)$ and ΔH_{15} was found in an earlier study; however, only for delta band connections (Racz et al., 2018b). In that work, synchronization likelihood was used as a dynamic functional connectivity estimator and multifractal properties of time-varying synchronization levels (i.e., dynamic functional connections) were estimated using the univariate FMF method. Since three out of the six scales (128, 256, 512 data points) used in the current analysis fall within the delta band

DOI:10.14753/SE.2022.2667

(0.5–4 Hz), this may explain the observed similarities with the study discussed above.

A source of inconsistency among FC studies may emerge from the application of various thresholding schemes. In that, most studies use some form of pruning procedure to exclude connections from the reconstructed networks that may be spurious or originating from noise (Rubinov and Sporns, 2010; van den Heuvel et al., 2017). Given that the primary goal of the study was to demonstrate the existence of multifractal coupling in brain networks as well as the introduction of a new method for its assessment, our main analytical pipeline did not contain a thresholding step. Nevertheless, in order to explore the plausible effect of thresholding on scale-free network topology we applied a parallel pipeline, which included thresholding as follows. The ΔH_{15} networks only included connections that passed all four multifractality assessment tests. $H(2)$ networks consisted of links that successfully passed the power-law, detrended-cross correlation and shuffling tests. Further details about this parallel analysis are provided in the **Supplementary Material.** Notably, the localization of intrinsic multifractality and the $H(2)$ and ΔH_{15} networks architectures were highly similar to the unthresholded case, while the regional variability and subject concordance was found diminished (**Supplementary Figures S1–S3** and **Supplementary Table S1**). The inference of this comparison is that intrinsic multifractality only marginally depends on the thresholding procedures while between- and within-subject variability of $H(2)$ and ΔH_{15} networks is clearly influenced.

Comparison of BFMF With Scale-Dependent FC Estimators

Given the novelty of our method, it is important to compare our results to those obtained by other FC methods commonly used in the literature (van den Heuvel and Fornito, 2014). For this purpose, we also reconstructed brain networks with the aid of Pearson correlation (r) and Mutual Information (MI) (details found in **Supplementary Material**). The purpose of this testing was to investigate if BFMF could reveal network architectures different from those obtained with scale-dependent linear or non-linear methods, thus implying its utility in capturing novel aspects of spatio-temporal neural dynamics. Since r and MI are indeed scale-dependent, we analyzed our signals at the same six scales as in BFMF analysis (16, 32, 64, 128, 256, and 512 data points) in a non-overlapping windowed manner. While the r networks showed a similar distribution of FC as the $H(2)$ network (**Figure 5** and **Supplementary Figure S4**), the MI networks did not resemble any of the two BFMF networks (**Figure 5** and **Supplementary Figure S5**). Moreover, regional variability was more significant in the r and MI networks (**Supplementary Table S2**), suggesting the influence of oscillatory dynamics. These oscillatory dynamics, despite their physiological correlates, cannot capture the scale-independent network connectivity evaluated by BFMF. To conclude, these results call for the careful interpretation of observed functional connectivity patterns pertinent to the estimator used for their assessment, while also highlight the fact that BFMF captured patterns of neural dynamics that remained undetected by r or MI.

Limitations and Future Perspectives

Finally, the limitations of this study should also be addressed. The 5-minute eyes-closed resting-state EEG recordings did not allow for a comparison of networks under different mental states, which have been shown to influence the fractal properties of neural dynamics (Ciuciu, 2012; Ciuciu et al., 2014). Nevertheless, as the primary objective of this study was to demonstrate the applicability of BFMF as a novel tool for reconstructing physiological networks of functional significance. For that purpose, a homogenous resting-state EEG dataset was sufficient, while subsequent research should indeed consider more elaborate experimental paradigms. Even though more than half of the connections showed intrinsic multifractality in every subject, at the population level there was only a tendency (maximal probability was 0.91) of localization of intrinsically multifractal connections within the resting-state networks (**Figure 4**). A possible explanation of this could be the low sample size of the study. It is reasonable to assume that future studies with a larger subject cohort could further confirm enhances the significance of this dichotomous model. Due to limitations of the applied parcelation scheme in demonstrating RSN-dependent contrast of bivariate multifractal measures, more elaborate experimental paradigms are needed for a thorough investigation of the origin of the scale-free character between and within the different RSNs via source-reconstruction (La Rocca et al., 2021). Infra-slow neural activity (<0.5 Hz) was not considered in this study since our preliminary investigations showed that breakpoints of the scaling function appear around 0.5 Hz (for further details in bimodal multifractal analysis, see Nagy et al., 2017). In future investigations, low-frequency EEG could be examined by a scaling-range adaptive, bimodal extension of BFMF, which appears as a reasonable next step considering recent advances in the analysis of multimodal fractal time series (Nagy et al., 2017; Mukli et al., 2018). These investigations should include high-pass filtering with a much lower cut-off frequency, which however will also require appropriate measurement length and sampling rate. The relevance of this consideration is supported by findings from fMRI recordings indicating that frequencies closer to 0.01 Hz contribute to multifractal functional connections to a greater extent (Ciuciu et al., 2014). Our study investigated only one exemplary case of physiological networks, namely functional networks of the human brain. In general, investigation of any biological process observed for a sufficiently long period of time and sampled at adequate temporal resolution could benefit from this method, as the BFMF framework enriches the analytical repertoire suitable for investigating dynamic physiological networks. In fact, multifractal covariance analysis has revealed a genuine scale-free coupling between oxy- and deoxyhemoglobin fluctuations (Mukli et al., 2018) that could be ascribed to mechanisms of neurovascular coupling. A certainly important direction of further research should be to implement this methodology in clinical studies, especially in psychiatry, where new biomarkers with good performance and reliability in individualized treatment are much needed (Topol, 2019).

DOI:10.14753/SE.2022.2667

Finally, even though BFMF was developed for the study of physiological networks, it can still be applied in a variety of other disciplines, like in the field of economics on which the bivariate multifractal analysis has been focusing so far (Oświęcimka et al., 2014; Pal et al., 2014).

CONCLUSION

Here we introduced the bivariate focus-based multifractal analysis for the dynamic investigation of physiological networks and showed that it captures novel features of resting-state brain network dynamics. Namely, supported by statistical testing, BFMF could reveal true multifractality in most of the functional connections estimated from EEG signals. Moreover, topological patterns identified with BFMF appeared robust, as indicated by high subject concordance and strong regional variability. Our results could facilitate further research on brain networks under different experimental conditions using bivariate multifractal analysis, as well as on extended physiological networks at the level of the entire organism.

DATA AVAILABILITY STATEMENT

The original contributions presented in the study are included in the article/**Supplementary Material**, further inquiries can be directed to the corresponding author/s.

ETHICS STATEMENT

The studies involving human participants were reviewed and approved by Comité de Protection des Personnes–Ile-de-France. The patients/participants provided their written informed consent to participate in this study.

AUTHOR CONTRIBUTIONS

OS implemented the analytical framework, performed the data analysis and interpretation, and wrote the first draft of the manuscript. FR contributed to data visualization, data analysis and manuscript development. AE provided the conceptual guidance and supervision throughout the study. PM developed the code for BFMF and specified the concept and aims of the study. All the authors contributed to reviewing the manuscript and approved its final version.

FUNDING

FR and PM acknowledge financial support from the 'Development of scientific workshops for medical, health sciences and pharmaceutical training' Project (EFOP-3.6.3-VEKOP-16-2017-00009).

ACKNOWLEDGMENTS

The authors express their gratitude to Sockeel et al. (2016) for the EEG data analyzed in this study and Oleg Komorov for the SchemaBall MATLAB code https://www.mathworks.com/matlabcentral/fileexchange/42279-okomarov-schemaball Copyright (c) 2017, Oleg Komavorv. **Figure 2** of the manuscript was originally published in Racz et al. (2019) under Creative Commons Attribution 4.0 International License.

SUPPLEMENTARY MATERIAL

The Supplementary Material for this article can be found online at: https://www.frontiersin.org/articles/10.3389/fphys.2020.615961/full#supplementary-material

REFERENCES

Abry, P., Wendt, H., Jaffard, S., and Didier, G. (2019). Multivariate scale-free temporal dynamics: from spectral (Fourier) to fractal (wavelet) analysis. *Comptes Rendus Phys.* 20, 489–501. doi: 10.1016/j.crhy.2019.08.005

Achard, S., Bassett, D. S., Meyer-Lindenberg, A., and Bullmore, E. (2008). Fractal connectivity of long-memory networks. *Phys. Rev. E. Stat. Nonlin. Soft Matter Phys.* 77:036104. doi: 10.1103/PhysRevE.77.036104

Arbabshirani, M. R., Damaraju, E., Phlypo, R., Plis, S., Allen, E., Ma, S., et al. (2014). Impact of autocorrelation on functional connectivity. *Neuroimage* 102, 294–308. doi: 10.1016/j.neuroimage.2014.07.045

Bak, P., Tang, C., and Wiesenfeld, K. (1987). Self-organized criticality: an explanation of the 1/ f noise. *Phys. Rev. Lett.* 59, 381–384. doi: 10.1103/PhysRevLett.59.381

Bartsch, R., Hennig, T., Heinen, A., Heinrichs, S., and Maass, P. (2005). Statistical analysis of fluctuations in the ECG morphology. *Phys. A Stat. Mech. its Appl.* 354, 415–431. doi: 10.1016/j.physa.2005.03.019

Bartsch, R., Plotnik, M., Kantelhardt, J. W., Havlin, S., Giladi, N., and Hausdorff, J. M. (2007). Fluctuation and synchronization of gait intervals and gait force profiles distinguish stages of Parkinson's disease. *Phys. A Stat. Mech. its Appl.* 383, 455–465. doi: 10.1016/j.physa.2007.04.120

Bartsch, R. P., Liu, K. K. L., Bashan, A., and Ivanov, P. C. (2015). Network physiology: how organ systems dynamically interact. *PLoS One* 10:e0142143. doi: 10.1371/journal.pone.0142143

Barunik, J., and Kristoufek, L. (2010). On Hurst exponent estimation under heavy-tailed distributions. *Phys. A Stat. Mech. its Appl.* 389, 3844–3855. doi: 10.1016/j.physa.2010.05.025

Bashan, A., Bartsch, R. P., Kantelhardt, J. W., Havlin, S., and Ivanov, P. C. (2012). Network physiology reveals relations between network topology and physiological function. *Nat. Commun.* 3:702. doi: 10.1038/ncomms1705

Beggs, J. M., and Timme, N. (2012). Being critical of criticality in the brain. *Front. Physiol.* 3:163. doi: 10.3389/fphys.2012.00163

Biswal, B., Zerrin Yetkin, F., Haughton, V. M., and Hyde, J. S. (1995). Functional connectivity in the motor cortex of resting human brain using echo-planar mri. *Magn. Reson. Med.* 34, 537–541. doi: 10.1002/mrm.1910340409

Blythe, D. A. J., Nikulin, V. V., and Müller, K.-R. (2016). Robust statistical detection of power-law cross-correlation. *Sci. Rep.* 6:27089. doi: 10.1038/srep27089

Bonachela, J. A., de Franciscis, S., Torres, J. J., and Muñoz, M. A. (2010). Self-organization without conservation: are neuronal avalanches generically critical? *J. Stat. Mech. Theory Exp.* 2010:02015. doi: 10.1088/1742-5468/2010/02/P02015

Bullmore, E., and Sporns, O. (2009). Complex brain networks: graph theoretical analysis of structural and functional systems. *Nat. Publ. Gr.* 10, 186–198. doi: 10.1038/nrn2575

DOI:10.14753/SE.2022.2667

Buzsáki, G. (2006). *Rhythms of the Brain*. Oxford: Oxford University Press, doi: 10.1093/acprof:oso/9780195301069.001.0001

Chang, C., and Glover, G. H. (2010). Time–frequency dynamics of resting-state brain connectivity measured with fMRI. *Neuroimage* 50, 81–98. doi: 10.1016/j.neuroimage.2009.12.011

Chen, A. C. N., Feng, W., Zhao, H., Yin, Y., and Wang, P. (2008). EEG default mode network in the human brain: spectral regional field powers. *Neuroimage* 41, 561–574. doi: 10.1016/j.neuroimage.2007.12.064

Ciuciu, P. (2012). Scale-free and multifractal time dynamics of fMRI signals during rest and task. *Front. Physiol.* 3:186. doi: 10.3389/fphys.2012.00186

Ciuciu, P., Abry, P., and He, B. J. (2014). Interplay between functional connectivity and scale-free dynamics in intrinsic fMRI networks. *Neuroimage* 95, 248–263. doi: 10.1016/j.neuroimage.2014.03.047

Clauset, A., Shalizi, C. R., and Newman, M. E. J. (2009). Power-Law distributions in empirical data. *SIAM Rev.* 51, 661–703. doi: 10.1137/070710111

Covert, M. W. (2006). "Integrated regulatory and metabolic models," in *Computational Systems Biology*, eds A. Kriete and R. Eils (Amsterdam: Elsevier), 191–204. doi: 10.1016/B978-012088786-6/50029-50020

Delorme, A., and Makeig, S. (2004). EEGLAB: an open source toolbox for analysis of single-trial EEG dynamics including independent component analysis. *J. Neurosci. Methods* 134, 9–21. doi: 10.1016/j.jneumeth.2003.10.009

Dimitriadis, S. I., Laskaris, N. A., Tsirka, V., Vourkas, M., Micheloyannis, S., and Fotopoulos, S. (2010). Tracking brain dynamics via time-dependent network analysis. *J. Neurosci. Methods* 193, 145–155. doi: 10.1016/j.jneumeth.2010.08.027

Eke, A., Hermán, P., Bassingthwaighte, J., Raymond, G., Percival, D., Cannon, M., et al. (2000). Physiological time series: distinguishing fractal noises from motions. *Pflügers Arch. - Eur. J. Physiol.* 439, 403–415. doi: 10.1007/s004249900135

Eke, A., Herman, P., Kocsis, L., and Kozak, L. R. (2002). Fractal characterization of complexity in temporal physiological signals. *Physiol. Meas.* 23, R1–R38. doi: 10.1088/0967-3334/23/1/201

Fadel, P. J., Barman, S. M., Phillips, S. W., and Gebber, G. L. (2004). Fractal fluctuations in human respiration. *J. Appl. Physiol.* 97, 2056–2064. doi: 10.1152/japplphysiol.00657.2004

Finn, E. S., Shen, X., Scheinost, D., Rosenberg, M. D., Huang, J., Chun, M. M., et al. (2015). Functional connectome fingerprinting: identifying individuals using patterns of brain connectivity. *Nat. Neurosci.* 18, 1664–1671. doi: 10.1038/nn.4135

Fraiman, D., and Chialvo, D. R. (2012). What kind of noise is brain noise: anomalous scaling behavior of the resting brain activity fluctuations. *Front. Physiol.* 3:307. doi: 10.3389/fphys.2012.00307

Freeman, W. J. (2004). Origin, structure, and role of background EEG activity. part 2. analytic phase. *Clin. Neurophysiol.* 115, 2089–2107. doi: 10.1016/j.clinph.2004.02.028

Friston, K. J., Frith, C. D., Liddle, P. F., and Frackowiak, R. S. J. (1993). Functional connectivity: the Principal-Component Analysis of Large (PET) data sets. *J. Cereb. Blood Flow Metab.* 13, 5–14. doi: 10.1038/jcbfm.1993.4

Gabard-Durnam, L. J., Mendez Leal, A. S., Wilkinson, C. L., and Levin, A. R. (2018). The Harvard Automated Processing Pipeline for Electroencephalography (HAPPE): standardized processing software for developmental and high-artifact data. *Front. Neurosci.* 12:97. doi: 10.3389/fnins.2018.00097

Giacometti, P., Perdue, K. L., and Diamond, S. G. (2014). Algorithm to find high density EEG scalp coordinates and analysis of their correspondence to structural and functional regions of the brain. *J. Neurosci. Methods* 229, 84–96. doi: 10.1016/j.jneumeth.2014.04.020

Gong, P., Nikolaev, A. R., and van Leeuwen, C. (2003). Scale-invariant fluctuations of the dynamical synchronization in human brain electrical activity. *Neurosci. Lett.* 336, 33–36. doi: 10.1016/S0304-3940(02)01247-1248

Grech, D., and Pamuła, G. (2012). Multifractal background noise of monofractal signals. *Acta Phys. Pol. A* 121:PB-34-B-39. doi: 10.12693/APhysPolA.121.B-34

He, B. J., Zempel, J. M., Snyder, A. Z., and Raichle, M. E. (2010). The temporal structures and functional significance of scale-free brain activity. *Neuron* 66, 353–369. doi: 10.1016/j.neuron.2010.04.020

Hesse, J., and Gross, T. (2014). Self-organized criticality as a fundamental property of neural systems. *Front. Syst. Neurosci.* 8:166. doi: 10.3389/fnsys.2014.00166

Hutchison, R. M., Womelsdorf, T., Gati, J. S., Everling, S., and Menon, R. S. (2013). Resting-state networks show dynamic functional connectivity in awake humans and anesthetized macaques. *Hum. Brain Mapp.* 34, 2154–2177. doi: 10.1002/hbm.22058

Ivanov, P. C., Amaral, L. A. N., Goldberger, A. L., Havlin, S., Rosenblum, M. G., Struzik, Z. R., et al. (1999). Multifractality in human heartbeat dynamics. *Nature* 399, 461–465. doi: 10.1038/20924

Ivanov, P. C., Amaral, L. A. N., Goldberger, A. L., and Stanley, H. E. (1998). Stochastic feedback and the regulation of biological rhythms. *Europhys. Lett.* 43, 363–368. doi: 10.1209/epl/i1998-00366-363

Ivanov, P. C., and Bartsch, R. P. (2014). "Network physiology: mapping interactions between networks of physiologic networks," in *Networks of Networks: the Last Frontier of Complexity. Understanding Complex Systems*, eds G. D'Agostino and A. Scala (Cham: Springer), 203–222. doi: 10.1007/978-3-319-03518-5_10

Ivanov, P. C., Chen, Z., Hu, K., and Eugene Stanley, H. (2004). Multiscale aspects of cardiac control. *Phys. A Stat. Mech. its Appl.* 344, 685–704. doi: 10.1016/j.physa.2004.08.016

Ivanov, P. C., Ma, Q. D. Y., Bartsch, R. P., Hausdorff, J. M., Nunes Amaral, L. A., Schulte-Frohlinde, V., et al. (2009). Levels of complexity in scale-invariant neural signals. *Phys. Rev. E - Stat. Nonlinear Soft Matter Phys.* 79:041920. doi: 10.1103/PhysRevE.79.041920

Ivanov, P. C. H., Liu, K. K. L., and Bartsch, R. P. (2016). Focus on the emerging new fields of network physiology and network medicine Focus on the emerging new fi elds of network physiology and network medicine. *New. J. Phys.* 18:100201. doi: 10.1088/1367-2630/18/10/100201

Jaffard, S., Seuret, S., Wendt, H., Leonarduzzi, R., and Abry, P. (2019a). Multifractal formalisms for multivariate analysis. *Proc. R. Soc. A Math. Phys. Eng. Sci.* 475:20190150. doi: 10.1098/rspa.2019.0150

Jaffard, S., Seuret, S., Wendt, H., Leonarduzzi, R., Roux, S., and Abry, P. (2019b). Multivariate multifractal analysis. *Appl. Comput. Harmon. Anal.* 46, 653–663. doi: 10.1016/j.acha.2018.01.004

Jalili, M. (2016). Functional brain networks: does the choice of dependency estimator and binarization method matter? *Sci. Rep.* 6:29780. doi: 10.1038/srep29780

Kantelhardt, J. W., Zschiegner, S. A., Koscielny-Bunde, E., Havlin, S., Bunde, A., and Stanley, H. E. (2002). Multifractal detrended fluctuation analysis of nonstationary time series. *Phys. A Stat. Mech. its Appl.* 316, 87–114. doi: 10.1016/S0378-4371(02)01383-1383

Kristoufek, L. (2011). Multifractal height cross-correlation analysis: a new method for analyzing long-range cross-correlations. *EPL (Europhysics Letters)* 95:68001. doi: 10.1209/0295-5075/95/68001

Kristoufek, L. (2014). Spectrum-based estimators of the bivariate Hurst exponent. *Phys. Rev. E* 90:062802. doi: 10.1103/PhysRevE.90.062802

Kwapień, J., Oświęcimka, P., and Drożdż, S. (2015). Detrended fluctuation analysis made flexible to detect range of cross-correlated fluctuations. *Phys. Rev. E* 92:052815. doi: 10.1103/PhysRevE.92.052815

Kwapień, J., Oświęcimka, P., and Drożdż, S. (2005). Components of multifractality in high-frequency stock returns. *Phys. A Stat. Mech. Appl.* 350, 466–474. doi: 10.1016/j.physa.2004.11.019

La Rocca, D., Herwig, W., van Wassenhove, V., Philippe, C., and Patrice, A. (2021). Revisiting functional connectivity for infraslow scale-free brain dynamics using complex wavelets. *Front. Physiol.* 11:1651. doi: 10.3389/fphys.2020.578537

Lavancier, F., Philippe, A., and Surgailis, D. (2009). Covariance function of vector self-similar processes. *Stat. Probab. Lett.* 79:24152421. doi: 10.1016/j.spl.2009.08.015

Levin, A. R., Méndez Leal, A. S., Gabard-Durnam, L. J., and O'Leary, H. M. (2018). BEAPP: the batch electroencephalography automated processing platform. *Front. Neurosci.* 12:513. doi: 10.3389/fnins.2018.00513

Lin, A., Liu, K. K. L., Bartsch, R. P., and Ivanov, P. C. (2020). Dynamic network interactions among distinct brain rhythms as a hallmark of physiologic state and function. *Commun. Biol.* 3:197. doi: 10.1038/s42003-020-0878-874

Louis, S., Borgelt, C., and Grün, S. (2010). "Generation and selection of surrogate methods for correlation analysis," in *Analysis of Parallel Spike Trains*, eds S. Grün and S. Rotter (Boston, MA: Springer), 359–382. doi: 10.1007/978-1-4419-5675-0_17

Lowe, M. J., Sakaie, K. E., Beall, E. B., Calhoun, V. D., Bridwell, D. A., Rubinov, M., et al. (2016). Modern methods for interrogating the human connectome. *J. Int. Neuropsychol. Soc.* 22, 105–119. doi: 10.1017/S1355617716000060

DOI:10.14753/SE.2022.2667

Lutzenberger, W., Elbert, T., Birbaumer, N., Ray, W. J., and Schupp, H. (1992). The scalp distribution of the fractal dimension of the EEG and its variation with mental tasks. *Brain Topogr.* 5, 27–34. doi: 10.1007/BF01129967

Michel, C. M., and Brunet, D. (2019). EEG source imaging: a practical review of the analysis steps. *Front. Neurol.* 10:325. doi: 10.3389/fneur.2019.00325

Mukli, P., Nagy, Z., and Eke, A. (2015). Multifractal formalism by enforcing the universal behavior of scaling functions. *Phys. A Stat. Mech. its Appl.* 417, 150–167. doi: 10.1016/j.physa.2014.09.002

Mukli, P., Nagy, Z., Racz, F. S., Herman, P., and Eke, A. (2018). Impact of healthy aging on multifractal hemodynamic fluctuations in the human prefrontal cortex. *Front. Physiol.* 9:1072. doi: 10.3389/fphys.2018.01072

Murphy, A. C., Bertolero, M. A., Papadopoulos, L., Lydon-Staley, D. M., and Bassett, D. S. (2020). Multimodal network dynamics underpinning working memory. *Nat. Commun.* 11:3035. doi: 10.1038/s41467-020-15541-15540

Nagy, Z., Mukli, P., Herman, P., and Eke, A. (2017). Decomposing multifractal crossovers. *Front. Physiol.* 8:533. doi: 10.3389/fphys.2017.00533

Nunes Amaral, L., Ivanov, P., Aoyagi, N., Hidaka, I., Tomono, S., Goldberger, A., et al. (2001). Behavioral-Independent features of complex heartbeat dynamics. *Phys. Rev. Lett.* 86, 6026–6029. doi: 10.1103/PhysRevLett.86.6026

Oświęcimka, P., Drożdż, S., Forczek, M., Jadach, S., and Kwapień, J. (2014). Detrended cross-correlation analysis consistently extended to multifractality. *Phys. Rev. E* 89:023305. doi: 10.1103/PhysRevE.89.023305

Pal, M., Madhusudana Rao, P., and Manimaran, P. (2014). Multifractal detrended cross-correlation analysis on gold, crude oil and foreign exchange rate time series. *Phys. A Stat. Mech. its Appl.* 416, 452–460. doi: 10.1016/j.physa.2014.09.004

Penny, W., Friston, K., Ashburner, J., Kiebel, S., and Nichols, T. (2007). *Statistical Parametric Mapping*, 1st Edn. Amsterdam: Elsevier, doi: 10.1016/B978-0-12-372560-8.X5000-1

Podobnik, B., Jiang, Z.-Q., Zhou, W.-X., and Stanley, H. E. (2011). Statistical tests for power-law cross-correlated processes. *Phys. Rev. E* 84:066118. doi: 10.1103/PhysRevE.84.066118

Podobnik, B., and Stanley, H. E. (2008). Detrended cross-correlation analysis: a new method for analyzing two nonstationary time series. *Phys. Rev. Lett.* 100:084102. doi: 10.1103/PhysRevLett.100.084102

Poil, S.-S., Hardstone, R., Mansvelder, H. D., and Linkenkaer-Hansen, K. (2012). Critical-State dynamics of avalanches and oscillations jointly emerge from balanced excitation/inhibition in neuronal networks. *J. Neurosci.* 32, 9817–9823. doi: 10.1523/JNEUROSCI.5990-11.2012

Preißl, H., Lutzenberger, W., Pulvermüller, F., and Birbaumer, N. (1997). Fractal dimensions of short EEG time series in humans. *Neurosci. Lett.* 225, 77–80. doi: 10.1016/S0304-3940(97)00192-194

Prentki, M., Corkey, B. E., and Madiraju, S. R. M. (2020). Lipid-associated metabolic signalling networks in pancreatic beta cell function. *Diabetologia* 63, 10–20. doi: 10.1007/s00125-019-04976-w

Preti, M. G., Bolton, T. A., and Van De Ville, D. (2017). The dynamic functional connectome: state-of-the-art and perspectives. *Neuroimage* 160, 41–54. doi: 10.1016/j.neuroimage.2016.12.061

Prichard, D., and Theiler, J. (1994). Generating surrogate data for time series with several simultaneously measured variables. *Phys. Rev. Lett.* 73, 951–954. doi: 10.1103/PhysRevLett.73.951

Racz, F. S., Mukli, P., Nagy, Z., and Eke, A. (2018a). Multifractal dynamics of resting-state functional connectivity in the prefrontal cortex. *Physiol. Meas.* 39:024003. doi: 10.1088/1361-6579/aaa916

Racz, F. S., Stylianou, O., Mukli, P., and Eke, A. (2018b). Multifractal dynamic functional connectivity in the resting-state brain. *Front. Physiol.* 9:1704. doi: 10.3389/fphys.2018.01704

Racz, F. S., Stylianou, O., Mukli, P., and Eke, A. (2019). Multifractal and entropy analysis of resting-state electroencephalography reveals spatial organization in local dynamic functional connectivity. *Sci. Rep.* 9:13474. doi: 10.1038/s41598-019-49726-49725

Racz, F. S., Stylianou, O., Mukli, P., and Eke, A. (2020). Multifractal and entropy-based analysis of delta band neural activity reveals altered functional connectivity dynamics in schizophrenia. *Front. Syst. Neurosci.* 14:49. doi: 10.3389/fnsys.2020.00049

Rak, R., and Grech, D. (2018). Quantitative approach to multifractality induced by correlations and broad distribution of data. *Phys. A Stat. Mech. its Appl.* 508, 48–66. doi: 10.1016/j.physa.2018.05.059

Roux, S. G., Venugopal, V., Fienberg, K., Arneodo, A., and Foufoula-Georgiou, E. (2009). Evidence for inherent nonlinearity in temporal rainfall. *Adv. Water Resour.* 32, 41–48. doi: 10.1016/j.advwatres.2008.09.007

Rubinov, M., and Sporns, O. (2010). Complex network measures of brain connectivity: uses and interpretations. *Neuroimage* 52, 1059–1069. doi: 10.1016/j.neuroimage.2009.10.003

Santuz, A., and Akay, T. (2020). Fractal analysis of muscle activity patterns during locomotion: pitfalls and how to avoid them. *J. Neurophysiol.* 124, 1083–1091. doi: 10.1152/jn.00360.2020

Saupe, D. (1988). "Algorithms for random fractals," in *The Science of Fractal Images*, eds H. O. Peitgen and D. Saupe (New York, NY: Springer), 71–136. doi: 10.1007/978-1-4612-3784-6_2

Schulz, S., Adochiei, F.-C., Edu, I.-R., Schroeder, R., Costin, H., Bär, K.-J., et al. (2013). Cardiovascular and cardiorespiratory coupling analyses: a review. *Philos. Trans. R. Soc. A Math. Phys. Eng. Sci.* 371:20120191. doi: 10.1098/rsta.2012.0191

Schumann, A. Y., and Kantelhardt, J. W. (2011). Multifractal moving average analysis and test of multifractal model with tuned correlations. *Phys. A Stat. Mech. its Appl.* 390, 2637–2654. doi: 10.1016/j.physa.2011.03.002

Sockeel, S., Schwartz, D., Pélégrini-Issac, M., and Benali, H. (2016). Large-Scale functional networks identified from resting-state EEG using spatial ICA. *PLoS One* 11:e0146845. doi: 10.1371/journal.pone.0146845

Sporns, O. (2011). The human connectome: a complex network. *Ann. N. Y. Acad. Sci.* 1224, 109–125. doi: 10.1111/j.1749-6632.2010.05888.x

Stam, C. J. (2014). Modern network science of neurological disorders. *Nat. Rev. Neurosci.* 15, 683–695. doi: 10.1038/nrn3801

Stam, C. J., and de Bruin, E. A. (2004). Scale-free dynamics of global functional connectivity in the human brain. *Hum. Brain Mapp.* 22, 97–109. doi: 10.1002/hbm.20016

Tagliazucchi, E., von Wegner, F., Morzelewski, A., Brodbeck, V., and Laufs, H. (2012). Dynamic BOLD functional connectivity in humans and its electrophysiological correlates. *Front. Hum. Neurosci.* 6:339. doi: 10.3389/fnhum.2012.00339

Thomas Yeo, B. T., Krienen, F. M., Sepulcre, J., Sabuncu, M. R., Lashkari, D., Hollinshead, M., et al. (2011). The organization of the human cerebral cortex estimated by intrinsic functional connectivity. *J. Neurophysiol.* 106, 1125–1165. doi: 10.1152/jn.00338.2011

Topol, E. J. (2019). High-performance medicine: the convergence of human and artificial intelligence. *Nat. Med.* 25, 44–56. doi: 10.1038/s41591-018-0300-7

van den Heuvel, M. P., de Lange, S. C., Zalesky, A., Seguin, C., Yeo, B. T. T., and Schmidt, R. (2017). Proportional thresholding in resting-state fMRI functional connectivity networks and consequences for patient-control connectome studies: issues and recommendations. *Neuroimage* 152, 437–449. doi: 10.1016/j.neuroimage.2017.02.005

van den Heuvel, M. P., and Fornito, A. (2014). Brain networks in schizophrenia. *Neuropsychol. Rev.* 24, 32–48. doi: 10.1007/s11065-014-9248-9247

van den Heuvel, M. P., Hulshoff Pol, H. E., Heuvel, M. P., Van Den, and Pol, H. E. H. (2010). Exploring the brain network: a review on resting-state fMRI functional connectivity. *Eur. Neuropsychopharmacol.* 20, 519–534. doi: 10.1016/j.euroneuro.2010.03.008

Vossel, S., Geng, J. J., and Fink, G. R. (2014). Dorsal and ventral attention systems. *Neurosci.* 20, 150–159. doi: 10.1177/1073858413494269

Wang, J., Shang, P., and Ge, W. (2012). Multifractal cross-correlation analysis based on statistical moments. *Fractals* 20, 271–279. doi: 10.1142/S0218348X12500259

Wang, J., and Zhao, D.-Q. (2012). Detrended cross-correlation analysis of electroencephalogram. *Chinese Phys. B* 21:028703. doi: 10.1088/1674-1056/21/2/028703

Weil, K. G. (1994). *F. Cramer: Chaos and Order. The Complex Structure of Living Systems*. Foreword by I. Prigogine, translated by D. I. Loewus (New York, NY: VCH Verlagsgesellschaft Weinheim), 1211–1211. doi: 10.1002/bbpc.19940980939.

Weissman, A., and Binah, O. (2014). The fractal nature of blood glucose fluctuations. *J. Diabetes Compl.* 28, 646–651. doi: 10.1016/j.jdiacomp.2014.05.009

Wendt, H., Scherrer, A., Abry, P., and Achard, S. (2009). "Testing fractal connectivity in multivariate long memory processes," in *Proceedings of the*

DOI:10.14753/SE.2022.2667

2009 IEEE International Conference on Acoustics, Speech and Signal Processing (IEEE), (New York, NY: IEEE), 2913–2916. doi: 10.1109/ICASSP.2009.4960233

Werner, G. (2010). Fractals in the nervous system: conceptual implications for theoretical neuroscience. *Front. Physiol.* 1:15. doi: 10.3389/fphys.2010.00015

Winkler, I., Brandl, S., Horn, F., Waldburger, E., Allefeld, C., and Tangermann, M. (2014). Robust artifactual independent component classification for BCI practitioners. *J. Neural Eng.* 11:035013. doi: 10.1088/1741-2560/11/3/035013

Winkler, I., Haufe, S., and Tangermann, M. (2011). Automatic classification of artifactual ICA-Components for artifact removal in EEG signals. *Behav. Brain Funct.* 7:30. doi: 10.1186/1744-9081-7-30

Xia, M., Wang, J., and He, Y. (2013). BrainNet viewer: a network visualization tool for human brain connectomics. *PLoS One* 8:e68910. doi: 10.1371/journal.pone.0068910

Yekutieli, D., and Benjamini, Y. (2001). under dependency. *Ann. Stat.* 29, 1165–1188. doi: 10.1214/aos/1013699998

Yu, Q., Erhardt, E. B., Sui, J., Du, Y., He, H., Hjelm, D., et al. (2015). Assessing dynamic brain graphs of time-varying connectivity in fMRI data: application to healthy controls and patients with schizophrenia. *Neuroimage* 107, 345–355. doi: 10.1016/j.neuroimage.2014.12.020

Conflict of Interest: The authors declare that the research was conducted in the absence of any commercial or financial relationships that could be construed as a potential conflict of interest.

frontiers in Human Neuroscience

DOI:10.14753/SE.2022.2667

ORIGINAL RESEARCH
published: 18 October 2021
doi: 10.3389/fnhum.2021.740225

Multifractal Functional Connectivity Analysis of Electroencephalogram Reveals Reorganization of Brain Networks in a Visual Pattern Recognition Paradigm

Orestis Stylianou[1,2], Frigyes Samuel Racz[1], Keumbi Kim[1], Zalan Kaposzta[1], Akos Czoch[1], Andriy Yabluchanskiy[3,4,5], Andras Eke[1,6] and Peter Mukli[1,3]**

[1] Department of Physiology, Semmelweis University, Budapest, Hungary, [2] Institute of Translational Medicine, Semmelweis University, Budapest, Hungary, [3] Vascular Cognitive Impairment and Neurodegeneration Program, Department of Biochemistry and Molecular Biology, Oklahoma Center for Geroscience and Healthy Brain Aging, The University of Oklahoma Health Sciences Center, Oklahoma City, OK, United States, [4] The Peggy and Charles Stephenson Cancer Center, The University of Oklahoma Health Sciences Center, Oklahoma City, OK, United States, [5] Department of Health Promotion Sciences, College of Public Health, The University of Oklahoma Health Sciences Center, Oklahoma City, OK, United States, [6] Department of Radiology and Biomedical Imaging, Yale University School of Medicine, New Haven, CT, United States

OPEN ACCESS

Edited by:
Pedro Antonio Valdes-Sosa, University of Electronic Science and Technology of China, China

Reviewed by:
Olga Mikhailovna Bazanova, State Research Institute of Neuroscience and Medicine, Russia
Xi Zhu, Columbia University, United States

***Correspondence:**
Peter Mukli
mukli.peter@med.semmelweis-univ.hu
Andras Eke
eke.andras@med.semmelweis-univ.hu

Specialty section:
This article was submitted to Cognitive Neuroscience, a section of the journal Frontiers in Human Neuroscience

Received: *12 July 2021*
Accepted: *23 September 2021*
Published: *18 October 2021*

Citation:
Stylianou O, Racz FS, Kim K, Kaposzta Z, Czoch A, Yabluchanskiy A, Eke A and Mukli P (2021) Multifractal Functional Connectivity Analysis of Electroencephalogram Reveals Reorganization of Brain Networks in a Visual Pattern Recognition Paradigm. Front. Hum. Neurosci. 15:740225. doi: 10.3389/fnhum.2021.740225

The human brain consists of anatomically distant neuronal assemblies that are interconnected via a myriad of synapses. This anatomical network provides the neurophysiological wiring framework for functional connectivity (FC), which is essential for higher-order brain functions. While several studies have explored the scale-specific FC, the scale-free (i.e., multifractal) aspect of brain connectivity remains largely neglected. Here we examined the brain reorganization during a visual pattern recognition paradigm, using bivariate focus-based multifractal (BFMF) analysis. For this study, 58 young, healthy volunteers were recruited. Before the task, 3-3 min of resting EEG was recorded in eyes-closed (EC) and eyes-open (EO) states, respectively. The subsequent part of the measurement protocol consisted of 30 visual pattern recognition trials of 3 difficulty levels graded as Easy, Medium, and Hard. Multifractal FC was estimated with BFMF analysis of preprocessed EEG signals yielding two generalized Hurst exponent-based multifractal connectivity endpoint parameters, $H(2)$ and ΔH_{15}; with the former indicating the long-term cross-correlation between two brain regions, while the latter captures the degree of multifractality of their functional coupling. Accordingly, $H(2)$ and ΔH_{15} networks were constructed for every participant and state, and they were characterized by their weighted local and global node degrees. Then, we investigated the between- and within-state variability of multifractal FC, as well as the relationship between global node degree and task performance captured in average success rate and reaction time. Multifractal FC increased when visual pattern recognition was administered with no differences regarding difficulty level. The observed regional heterogeneity was greater for ΔH_{15} networks compared to $H(2)$ networks. These results show that reorganization of scale-free coupled dynamics takes place during visual pattern recognition independent of difficulty level. Additionally, the observed regional

DOI:10.14753/SE.2022.2667

variability illustrates that multifractal FC is region-specific both during rest and task. Our findings indicate that investigating multifractal FC under various conditions – such as mental workload in healthy and potentially in diseased populations – is a promising direction for future research.

Keywords: multifractal, functional connectivity, brain networks, electroencephalography, visual pattern recognition

INTRODUCTION

The human brain is a complex system encompassing spatially distinct neuronal populations interconnected via an intricate axonal grid. Functional brain networks emerge within this anatomical circuitry, which provides the neurophysiological basis for higher-order brain functions (Van Hoesen, 1993). For instance, visual pattern recognition requires coordinated interactions among disparate brain regions such as the visual cortex, where primary processing, and the association areas in the parietal and frontal cortices, where high-level cognitive evaluation takes place (Van Hoesen, 1993; Kandel et al., 2012). Based on the hypothesis that regions that exhibit statistically similar dynamics are functionally coupled, functional neuroimaging methods allowed the reconstruction of functional connectivity (FC) in the brain under cognitive (Friston et al., 1993) and motor (Biswal et al., 1995) tasks. A paradigm shift regarding resting-state studies occurred after discovering that even in the absence of external stimuli the brain is organized in resting-state networks (RSNs) (Raichle et al., 2001). This resting-state neural architecture is altered during task through a series of activations and deactivations of brain regions (Fox et al., 2005). Accordingly, we believe that studying the brain under mental workload could reveal valuable information.

Due to its high spatial resolution, functional magnetic resonance imaging (fMRI) has been commonly favored as the gold standard imaging technique for detecting task-related changes of FC (Fox et al., 2005; Krienen et al., 2014; Di et al., 2015; Elton and Gao, 2015; Kaufmann et al., 2017). Nevertheless, the low sampling frequency and the physical constraints of the fMRI systems present themselves as limitations when more elaborate experimental paradigms are designed. Albeit at the cost of a lower anatomical resolution, these limitations can be overcome using electroencephalography (EEG) owing to its high sampling rate and easy-to-use instrumentation. This led to numerous task-related EEG studies, ranging from traditional tasks like n-back (Hou et al., 2018; Kaposzta et al., 2021) and face perception (Yang et al., 2015) to more complex designs like urban navigation (Skroumpelou et al., 2015). By using a visual pattern recognition paradigm, Racz et al. demonstrated an increase in scale-specific FC during task (Racz et al., 2017); though, in that study the scale-free aspect of the connections was not taken into consideration.

Various statistical approaches have been applied and/or developed for characterizing the linear and nonlinear aspects of the coupled neural activities (Bastos and Schoffelen, 2016). A common limitation of these methods is that they capture interdependence on a single scale, despite the fact that the scale-free (or fractal) nature of the connections has already been demonstrated in various modalities such as EEG (Wang and Zhao, 2012; Stylianou et al., 2021), fMRI (Ciuciu et al., 2014) and magnetoencephalography (Achard et al., 2008). The univariate scale-free behavior of neural dynamics has already been shown both regionally (Popivanov et al., 2006) and globally (Stam and de Bruin, 2004). While estimating FC at a given time scale reflect the coupling between oscillatory (narrowband) components at specific cross-spectrum frequencies, our current approach assumes a significant scale-free (broadband) component of the cross-spectrum; a signature of statistical dependency spanning a broad range of frequencies (scales). Moreover, the true multifractal nature of coupled dynamics was recently validated in resting-state EEG (Stylianou et al., 2021). Scale-free FC estimators allow for capturing how the long-term memory and multifractality of the coupled dynamics are spatially distributed across brain networks; topological aspects that otherwise would remain obscured. Visual pattern recognition requires sustained interaction between brain regions involved in the processing of the visual information, which can be captured as increased cross-correlations (long-term memory) in the functional connections. Furthermore, cognitive stimulation implies a shift in FC that is typically governed by complex nonlinear dynamics (Rabinovich and Muezzinoglu, 2010; Werner, 2010), which might alter the multifractal profile of FC. To the best of our knowledge, this is the first study investigating the task-related network reorganization using multifractal connectivity analysis.

In the current study, we examined the task-related reorganization of FC by applying a bivariate, focus-based adaptation of multifractal analysis on EEG records. The task of choice was a complex pattern recognition paradigm, which has previously shown its utility in increasing FC in the prefrontal cortex (Racz et al., 2017). Our primary objectives were: (i) to test the hypothesis that shifts in scale-free coupled dynamics would occur during the transition from rest to task; and (ii) to examine the localization of multifractal FC within each mental state. Our secondary aim was to assess the relationship between cognitive performance and brain network measures reconstructed from scale-free FC estimators.

MATERIALS AND METHODS

Participants

Fifty-eight young, healthy volunteers (24.2 ± 3.4 years of age, 28 females, 9 left-handed) with no history of psychiatric/neurological illness were recruited for the study. Participants were instructed to have a good night's sleep before the day of the experiment. All subjects provided written informed consent prior to the measurement. The study was designed and carried out in accordance with the Declaration of Helsinki and

DOI:10.14753/SE.2022.2667

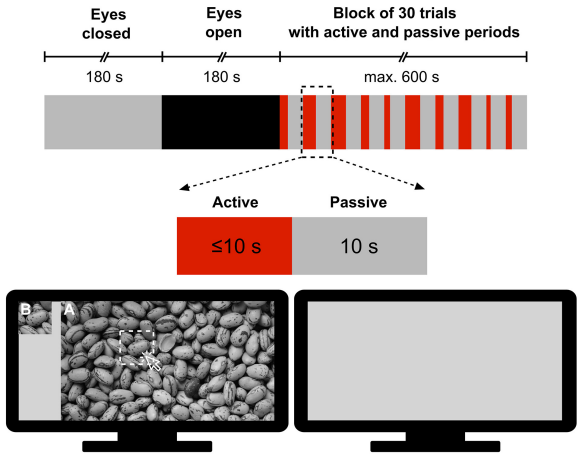

FIGURE 1 | Measurement protocol for obtaining electroencephalography records during resting states and subsequent visual pattern recognition. First, resting-state recordings were made in 180 s periods with eyes closed and eyes open, respectively. Then, the subject performed a pattern recognition task in a block of 30 trials, each consisting of a 10 s or less of active period and a 10 s passive period. In the active period, participants were presented a large-size image **(A)** and its cropped sub-region **(B)** and were required to click on **(A)** at the position of **(B)** if found *(The picture of* **Figure 1** *was taken from https://alphacoders.com/users/profile/97828)*.

was approved by the Regional and Institutional Committee of Science and Research Ethics of Semmelweis University (approval number: 2020/6).

Measurement Protocol

All measurements took place in the Department of Physiology at Semmelweis University in a quiet room under subdued ambient illumination. During the measurement, participants were seated comfortably in a chair in front of a computer monitor at an approximate distance of 0.8 m from the screen and were instructed to refrain from moving and facial expressions as much as possible. The measurement protocol was designed and implemented in MATLAB (version 2012, Mathworks, Natick, MA, United States) according to a pattern recognition paradigm modified after Racz et al. (2017). The session started with a 3-min eyes-closed (EC) period serving as a baseline, followed by a 3-min eyes-open (EO) resting-state period, as a control for the task state. Then, participants were engaged in a visual pattern recognition paradigm consisting of a block of 30 trials with active and passive periods (**Figure 1**). Specifically, in the active period of a trial, the subject was allowed a maximum of 10 s to identify a sub-region of a grayscale image by clicking on its assumed location; at that point, the active period was terminated. The active period was immediately followed by a passive (task-free) period, during which a gray background was displayed for 10 s. In this stimulation paradigm, a pool of 6 different grayscale images was permutated. Each of them was shown 5 times in total – with a different sub-region to be identified in each case – thus yielding a total of $6 \times 5 = 30$ trials. To investigate the impact of difficulty level, images were sorted into Easy, Medium and Hard categories with 2 images in each. Their classification was based on their complexity, defined as the file size ratio of compressed/uncompressed images [cf. Equation 1 in Yu and Winkler (2013)]. The order of the 30 trials was randomized with a different permutation sequence for each participant. The following metrics characterized the performance during pattern recognition: (i) reaction time, defined as the time between the beginning of the image presentation and response (left mouse click on the image) and (ii) success, defined as 1 if the participant correctly identified the sub-region's location and 0 otherwise. When the subject did not respond, the trial was considered a failure (success = 0) and the reaction time was set to 10 s.

Data Acquisition

EEG signals were recorded by a wireless Emotive Epoc+ device and its corresponding EmotivPRO software (Emotiv Systems Inc., San Francisco, CA, United States). After ensuring low electrical impedance (<20 kΩ), EEG signals from 14 brain regions (10–20 standard montage locations: AF3, AF4, F3, F4, F7, F8, FC5, FC6, T7, T8, P7, P8, O1, and O2) were recorded, at a 128 Hz sampling rate[1]. CMS and DRL electrodes at left and right mastoid processes were used as reference.

Preprocessing

The EEG device applied built-in band-pass (0.2–45 Hz, digital 5th order Sinc) and notch (50 and 60 Hz) filters to the raw data. To maximize the artifact-detection capacity of independent component analysis (ICA), first we performed wavelet-enhanced ICA (wICA) (Rong-Yi and Zhong, 2005; Gabard-Durnam et al., 2018). The purpose of wICA was to exclude wavelet components with coefficients higher than a certain threshold, resulting in the removal of high amplitude spikes. Subsequently, we manually excluded non-brain components, as ICA isolated them. wICA was performed in an automated manner, while the EEGLAB toolbox (Delorme and Makeig, 2004) was used for manual ICA.

Estimation of Multifractal Functional Connectivity

The scale-free coupled dynamics were estimated with bivariate focus-based multifractal analysis (BFMF), introduced by Mukli and colleagues (Mukli et al., 2018). The applicability of BFMF for multifractal FC estimation was demonstrated previously (Stylianou et al., 2021). Here we only provide a summary of the method, while further details are found in the references mentioned above. The scaling function S_{XY} (**Figure 2**) of two EEG time series (X and Y) of length L datapoints can be calculated as:

$$S_{XY}(q,s) = \left(\frac{1}{N_s} \sum_{v=1}^{N_s} |cov_{XY}(v,s)|^q \right)^{1/q}, \quad (1)$$

where N_s denotes the number of bridge-detrended, non-overlapping windows of size s ($s = 2^n$ with n being integers ranging from 2 to 8) indexed by v. The statistical moment order

[1] 18 recordings were carried out at 256 Hz sampling rate which were downsampled to 128 Hz prior to further preprocessing.

DOI:10.14753/SE.2022.2667

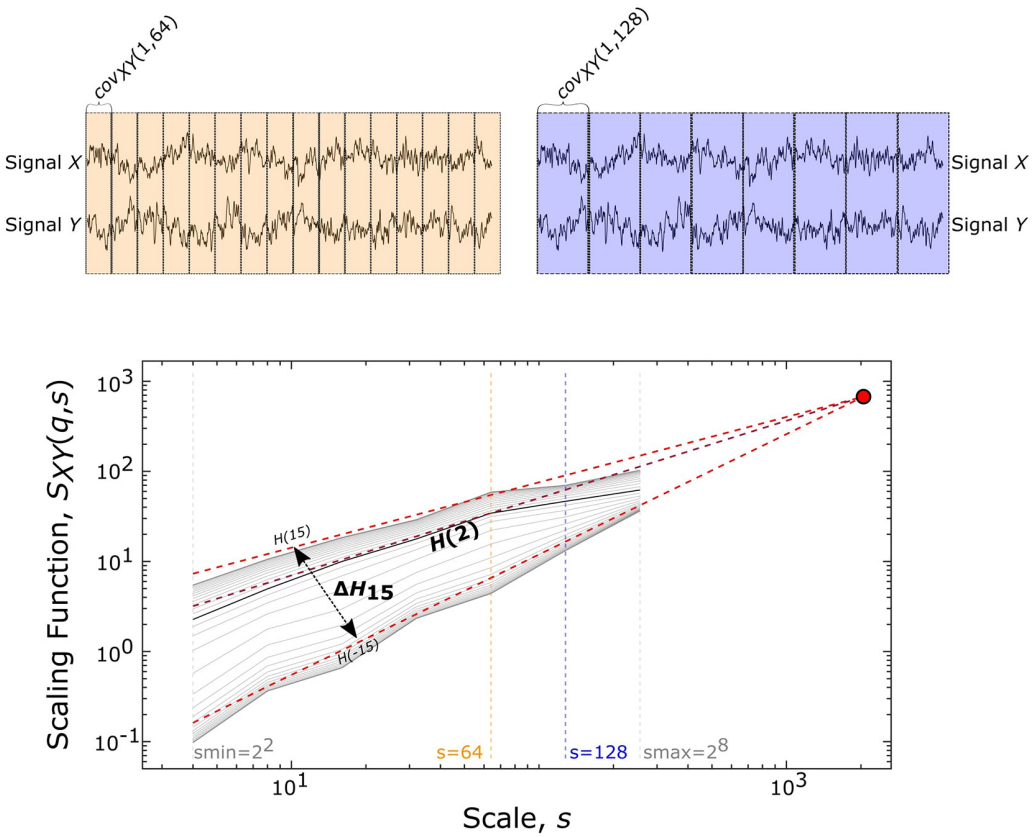

FIGURE 2 | Multifractal time series analysis and its endpoint parameters. On the upper panels, a representative pair of 2048 datapoint-long EEG segments (from Subject01) is displayed along with the windowing scheme for a smaller (s = 64, shown in yellow) and larger (s = 128, shown in purple) scale, which illustrates the calculation of covariance scaling function [$S_{XY}(q,s)$ displayed in the lower panel] according to Eq. 1. The *Focus* (red disk) is used as a reference point when simultaneously fitting linear models in the log-log transform of the $S_{XY}(q,s)$ vs s, the essential step of BFMF. The slope of each linear regression line represents the generalized Hurst exponent [$H(q)$] (shown for q = −15, +2, +15). $H(2)$ describes the long-term cross-correlation between the signals X and Y, while the degree of multifractality (ΔH_{15}) is captured in the difference between $H(q)$ values at the extreme [i.e., minimal (–15) and maximal (15)] statistical moments.

(q) ranges from −15 to 15 with increments of 1 and the window-wise covariance between simultaneous s-size segments of X and Y is denoted by $cov_{XY}(v, s)$. When q = 0, the scaling function takes the form:

$$S_{XY}(0, s) = e^{\left[\frac{1}{2N_s}\sum_{v=1}^{N_s}\ln\left(\left|cov_{XY}(v,s)\right|\right)\right]} \quad (2)$$

In the special case when the whole segment is used for obtaining the scaling function [$S_{XY}(q,L)$], the sum in Eq. 1 becomes independent of q and thus, the scaling function values of all moments converge to a so-called *Focus*. This *Focus* serves as a reference point when regressing for the log[$S_{XY}(q,s)$] vs log[s] relationship for every q simultaneously. In contrast with the standard approach where separate q-wise assessments of the power-law relationship are applied, fitting all statistical moments simultaneously results in a more robust analysis (Mukli et al., 2015). This is achieved by enforcing the monotonous decay of regression slopes, which represent the generalized, q-dependent bivariate Hurst-exponent function $H(q)$. The special case of $H(2)$ depicts the global long-term cross-correlation in the coupled dynamics underlying the functional connection. If this bivariate $H(2)$ is greater than 0.5, then there is functional coupling exhibiting long-term memory. $H(2)$ = 0.5 indicates uncorrelated, uncoupled dynamics, while $H(2)$ < 0.5 demonstrates anticorrelated coupling (Eke et al., 2002; Kristoufek, 2014). ΔH_{15}, calculated as $H(-15)$-$H(15)$, captures the degree of multifractality, an indicator of the q-wise dependence of the scaling function on large and small covariances. The whole segment of each trial (active section + 10 s of passive period) was analyzed with BFMF. As for the resting-state conditions, 9 non-overlapping segments of 20 s for each of the EC and EO states were analyzed. To remove the effect of different time lengths due to various response times, we also performed analyses adjusted to the length of time series (see **Supplementary Material**).

Assessing Multifractality

A series of statistical tests evaluated the true scale-free nature of the connections. In short, the purpose of these tests was to: (i) validate the power-law relationship of the connection both in the frequency and time domains (spectral slope and detrended cross-correlation coefficient tests, respectively),

DOI:10.14753/SE.2022.2667

(ii) distinguish true from spurious multifractality (phase randomization and shuffling tests), and (iii) determine if the emerging coupling between the two processes is genuine or only reflects a mere autocorrelation within each EEG signal (bivariate-univariate Hurst comparison). This series of tests reveal the qualitative nature of bivariate multifractality, which is assessed independently from its quantitative changes in this study. The complete account of the testing procedure followed in this study was reported elsewhere (Stylianou et al., 2021). We expanded the test yielding a distinction between extrinsic and intrinsic multifractality referred to as bivariate-univariate Hurst comparison. In our previous paper, only the inequality between the bivariate Hurst exponent and the mean of the univariate Hurst exponents comprising the connection was tested (Stylianou et al., 2021). In the present study, we considered a bivariate-univariate Hurst comparison test successful only when the bivariate $H(2)$ was lower than the mean of its univariate $H(2)$. This choice was made based on the fact that bivariate $H(2)$ can exceed the mean of univariate $H(2)$ only due to the finite length or non-normal distribution of the time series (Kristoufek, 2015a, 2016).

Brain Network Construction

We then proceeded with reconstructing functional networks and analyzing their architecture. For each subject, we isolated 48 different EEG segments (9 EC, 9 EO, 10 Easy, 10 Medium and 10 Hard). For each connection, the $H(2)$ and ΔH_{15} values obtained in the 5 different states were averaged, resulting in 5 different values per subject. Altogether, 5-5 (i.e., fully connected) networks (EC, EO, Easy, Medium, Hard) were reconstructed for every subject, based on either their $H(2)$ or ΔH_{15} values. In these analyses, we used untresholded networks as we did in our previous studies of EEG-based functional connectivity (Racz et al., 2018, 2019, 2020; Kaposzta et al., 2021). We characterized network topology via the local (D) and global ($\overline{D}$) weighted node degrees from the $H(2)$ and ΔH_{15} values of each connection, since earlier we found that in small networks, clustering coefficient and efficiency were highly correlated with node degree (Kaposzta et al., 2021). D represents the total connection strength of a node, while $\overline{D}$ (the average of all D) is an indicator of the network's interconnectivity[2]. The calculations of D and $\overline{D}$ were carried out using functions of the Brain Connectivity Toolbox (Rubinov and Sporns, 2010).

Statistical Evaluation

We evaluated between-states (e.g., Hard vs EC) and within-states (e.g., O1 vs O2 in EO) differences for both $H(2)$ and ΔH_{15} networks. To rule out that the observed differences could be attributed to opening of the eyes, we included both resting-state periods in the statistical evaluation. Therefore, the between-states comparisons consisted of global $\overline{D}$ and local D comparisons of the 5 different states (EC, EO, Easy, Medium, Hard). Since the normality assumption (Lilliefors test) was not satisfied for all distributions, we used the non-parametric Friedman test. Subsequently, paired comparisons were used to identify specific pairwise differences. If any of the two populations under investigation were non-normally distributed, Wilcoxon signed-rank test was carried out. If both distributions were normal, a paired sample t-test was used. Benjamini-Hochberg (BH) correction (with $\alpha = 0.05$) (Benjamini and Hochberg, 1995) was used to adjust for multiple testing. Then, we investigated the regional differences within every state's local D (i.e., 91 comparisons for each of the 5 states). The same statistical tests as in the between-states comparisons were utilized. Moreover, we estimated Kendall's coefficient of concordance (W) of D for both $H(2)$ and ΔH_{15} networks for each state.

We also contrasted the average success rate (SR) and average reaction time (RT) between the 3 difficulty levels, applying the same statistical pipeline as described above. Then we investigated the plausible relationships between performance metrics and network architecture since scale-free FC and behavioral variables have already been shown to correlate (Ciuciu et al., 2014). In that, we examined the effect of FC on task performance by calculating the Spearman's rank correlation (r) between SR-$\overline{D}$ and RT-$\overline{D}$ for each difficulty level. Every step of our analytical pipeline was implemented in MATLAB (version 2012, Mathworks, Natick, MA, United States).

RESULTS

Qualitative Assessment of Bivariate Multifractal Character

Table 1 summarizes the percentage of connections passing each multifractal test. The 5 different states showed similar success rates in the spectral slope, phase randomization and ΔH_{15} part of shuffling tests (the latter comparing the original ΔH_{15} with that of shuffled surrogates). On the other hand, the rest states exhibited higher success rates in the bivariate-univariate Hurst comparison test and passed the detrended cross-correlation coefficient tests more frequently. Finally, comparing the original $H(2)$ with that of shuffled surrogates had a higher success rate in the task states. As a result, more connections showed scale-free characteristics in the rest states (**Table 2**).

TABLE 1 | Success rate of multifractality tests at the subject level (mean ± standard deviation).

	Tests					
	PL	**PR**	**SΔH_{15}**	**S-$H(2)$**	**DCCC**	**Biv-Univ**
EC	92 ± 7%	96 ± 4%	99 ± 2%	70 ± 18%	93 ± 4%	85 ± 18%
EO	94 ± 3%	96 ± 6%	98 ± 4%	76 ± 16%	93 ± 4%	86 ± 15%
Easy	93 ± 2%	97 ± 4%	99 ± 2%	90 ± 8%	64 ± 19%	65 ± 17%
Medium	94 ± 2%	97 ± 4%	99 ± 2%	90 ± 9%	65 ± 16%	68 ± 18%
Hard	94 ± 2%	97 ± 3%	99 ± 2%	89 ± 9%	62 ± 17%	73 ± 16%

PL, power-law test; PR, phase randomization test; S-ΔH_{15}, ΔH_{15} part of the shuffling test; S-H(2), H(2) part of the shuffling test; DCCC, detrended cross-correlation coefficient test; Biv-Univ, bivariate-univariate Hurst comparison.

[2] D $\sum_{i=1}^{n} c_i$ where n represents all possible edges of a node, while c_i is the strength [either $H(2)$ or ΔH_{15}] of the ith connection. $\overline{D} = \frac{\sum_{j=1}^{N} D_j}{N}$ where N represents all nodes of the network, while ${D_j}^W$ is the weighted degree of the jth node.

TABLE 2 | Percentage of connections, at the subject level (mean ± standard deviation), that passed all multifractality assessment tests.

	State				
	EC	**EO**	**Easy**	**Medium**	**Hard**
***H*(2)**	48 ± 13%	55 ± 12%	31 ± 10%	34 ± 10%	35 ± 9%
ΔH_{15}	46 ± 13%	53 ± 12%	30 ± 10 %	33 ± 10%	34 ± 9%

Effect of Brain State on Multifractal Connectivity

The Friedman tests indicated a significant effect of state ($p < 0.01$), and post hoc pairwise comparisons revealed that the rest states (EC, EO) were characterized by lower $\overline{D}$ compared to the task states (Easy, Medium, Hard) (**Figures 3**, **4**). Additionally, we found higher $\overline{D}$ during EO compared to EC, for both $H(2)$ and ΔH_{15} networks. A similar motif emerged in the local level comparisons, with the D of several nodes being significantly different between the rest and task states, as well as between EC and EO for both networks (**Figure 5**).

As seen in **Figure 3**, the $H(2)$ networks had higher FC in the frontal regions, while higher values of ΔH_{15} were observed in the occipital cortex. This regional variability was statistically validated by the within-state comparisons, which showed significant differences within all 5 tasks, for both $H(2)$ and ΔH_{15} networks. We also observed that if the D of two nodes in the ΔH_{15} network were statistically different, there was a high chance of the equivalent nodes being statistically different in the $H(2)$ network as well, while the opposite did not occur. This can be easily visualized by the abundance of blue [both $H(2)$ and ΔH_{15} significant] and orange (only ΔH_{15} significant), in contrast to the sparse red [only $H(2)$ significant] boxes in **Figure 6**. Moreover, small subject concordance appeared only in the ΔH_{15} networks; on the contrary, no subject agreement was found in the $H(2)$ networks (**Table 3**).

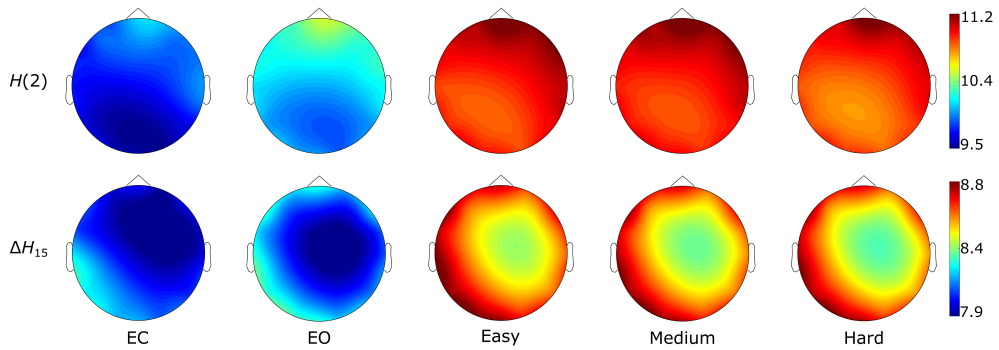

FIGURE 3 | State-dependent weighted node degree topology of $H(2)$ and ΔH_{15} brain networks. The color bars represent the values of the local node degrees.

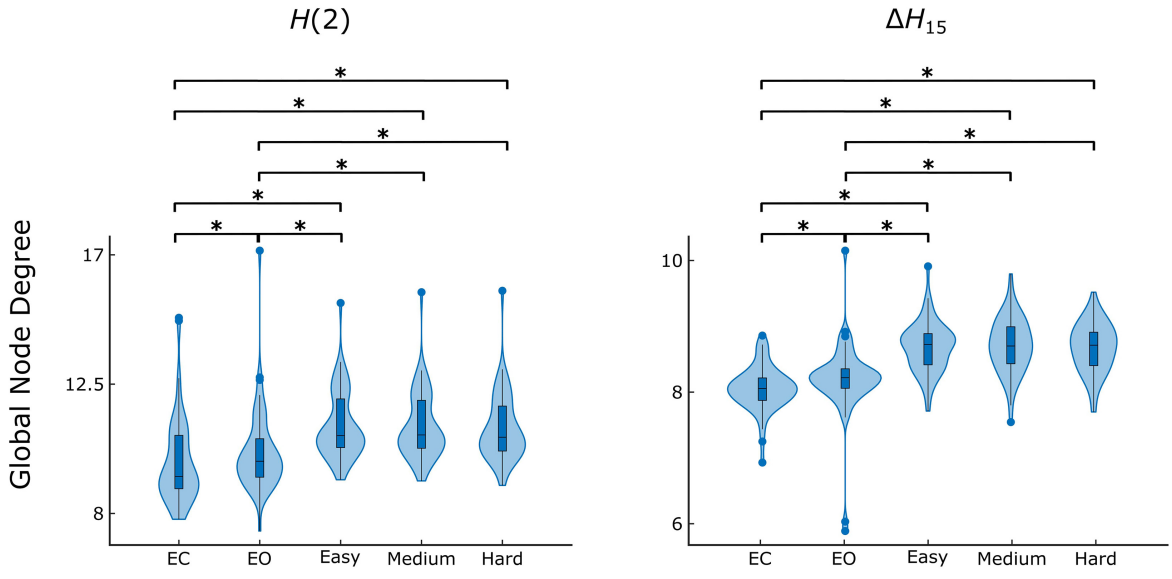

FIGURE 4 | State-dependent weighted global node degree distribution of $H(2)$ and ΔH_{15} brain networks. Significance marked by asterisk (*). Figure was created using Gramm (Morel, 2018).

DOI:10.14753/SE.2022.2667

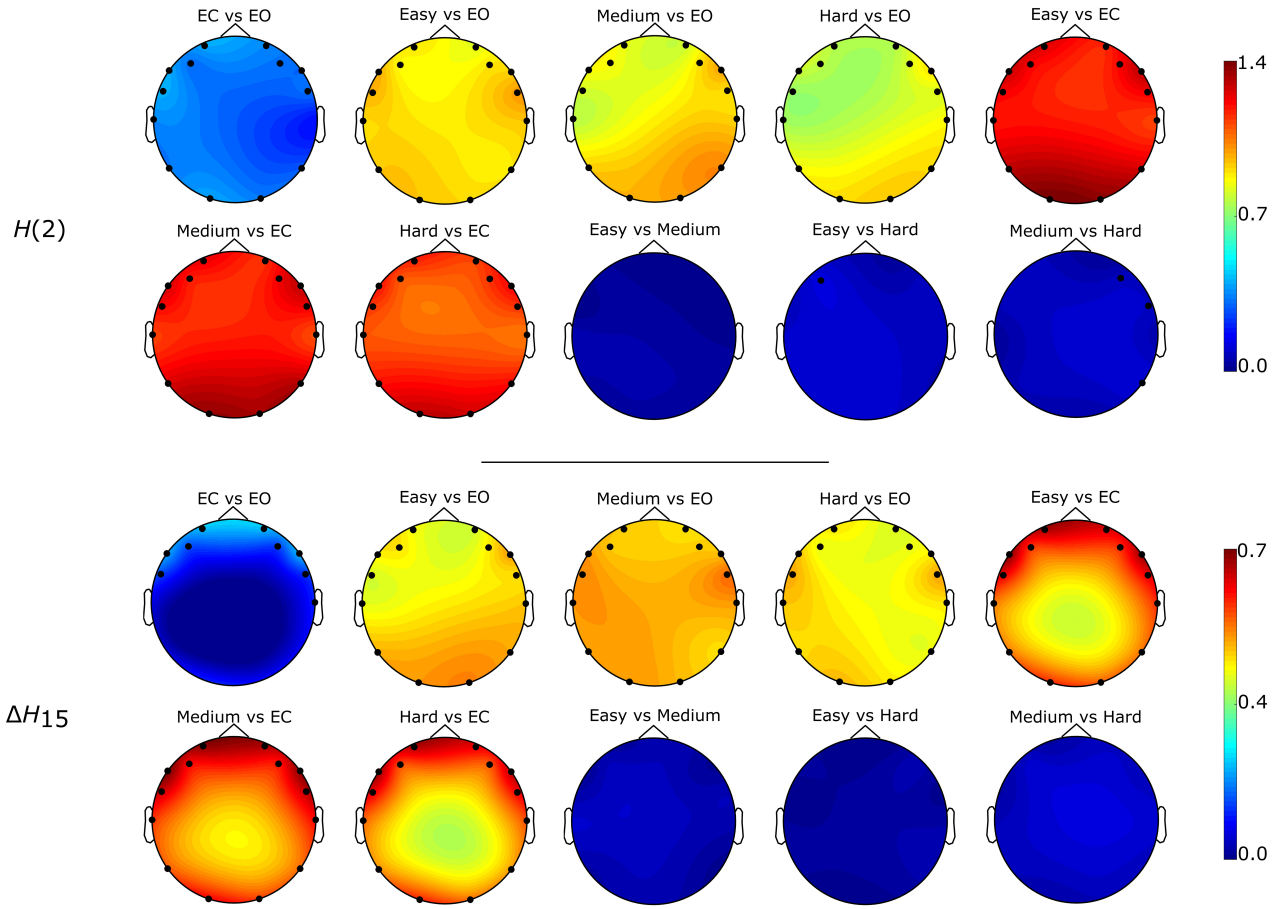

FIGURE 5 | Localization of significantly different weighted node degrees for every between state comparison of the $H(2)$ and ΔH_{15} brain networks. The colormap is based on the absolute difference of the node degrees of the states under investigation (e.g., $|D_{O2,EC} - D_{O2,EO}|$). Only the significantly different nodes are shown.

Cognitive Performance and Its Correlates With Functional Connectivity

The comparison of difficulty levels indicated a significant decrease of SR in the Hard state. RT was also statistically different between the 3 difficulty levels, with Easy having the fastest response and Hard having the slowest (**Figure 7**). Furthermore, significant ($p < 0.05$) positive correlations were found between RT and $\overline{D}$ of the ΔH_{15} networks during Easy and Hard (**Figure 8**). After BH correction, these correlations were rendered not significant.

DISCUSSION

This study investigated the scale-free coupled dynamics of brain activity in resting state and during a visual pattern recognition task of various difficulty levels. We employed two FC estimators derived from bivariate focused-based multifractal analysis, namely $H(2)$ and ΔH_{15}. They were used for constructing brain networks based on their multifractal connectivity for both rest and task conditions. Our findings show that: (i) the local and global functional connectivity measures increased during task when compared to resting conditions, indicating a reorganization of brain networks, and (ii) there was a substantial regional variability within the 5 different states. However, significant correlations were found only between the global node degree and average reaction time during Easy and Hard tasks in the ΔH_{15}-networks.

After acquiring the BFMF measures, $H(2)$ and ΔH_{15}, it was essential to perform an array of multifractality assessment tests since by default not all functional connections – or in general, not all dynamic processes – can be assumed to have multifractal character. Our tests showed that a considerable fraction of the connections had true multifractal characteristics (**Table 1**). Similar success rates have been found in the resting state previously (Stylianou et al., 2021). Despite the different channel density of the EEG devices and the different sampling populations, similar results were obtained in these studies, concluding that coupled dynamics between cortical regions are indeed multifractal during rest. The extent of multifractality decreased during task, as indicated by the lower number of connections passing our multifractality assessment tests (**Table 2**). To the best of our knowledge, this is the first study demonstrating the true multifractal nature of coupled dynamics

DOI:10.14753/SE.2022.2667

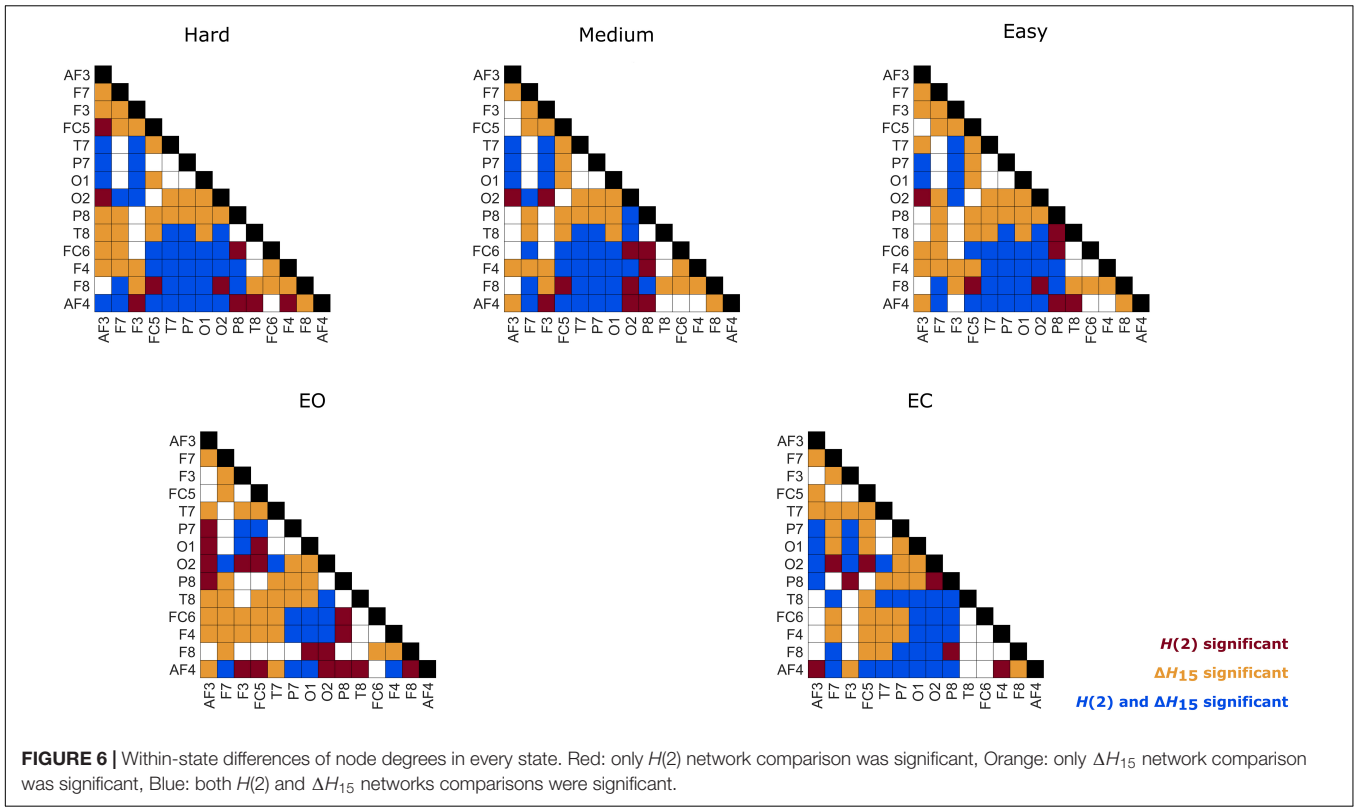

FIGURE 6 | Within-state differences of node degrees in every state. Red: only $H(2)$ network comparison was significant, Orange: only ΔH_{15} network comparison was significant, Blue: both $H(2)$ and ΔH_{15} networks comparisons were significant.

TABLE 3 | State-dependent subject concordance, as captured by Kendall's W.

	State				
	EC	**EO**	**Easy**	**Medium**	**Hard**
$H(2)$	0.10	0.09	0.09	0.12	0.11
ΔH_{15}	0.24	0.15	0.25	0.24	0.26

during complex mental tasks. This provides an opportunity to reveal novel aspects of rest and task states using BFMF by obtaining information that would have remained hidden otherwise [for a demonstration, see the **Supplementary Material** in Stylianou et al. (2021)].

The higher node degree in the fully connected (i.e., unthresholded) $H(2)$ and ΔH_{15} networks during task corresponds to increased $H(2)$ and ΔH_{15} values of the connections. The high values of $H(2)$ indicate a relative shift of the coupled dynamics toward lower frequency components. This greater long-term memory reflects a stronger coupling between the probed regions of the brain cortex. Conversely, Ciuciu and colleagues found a shift of scale-free coupled fluctuations in fMRI-BOLD signals toward the higher frequencies (i.e., decreasing Hurst-exponent), accompanied by a decrease in connectivity between resting-state networks during a motor task (Ciuciu et al., 2014). While the signs of changes were opposite, both studies showed a positive association between $H(2)$ and FC change during task. This difference could possibly be attributed to the differences in imaging modality and stimulation paradigm, which should be further investigated in future studies. Moreover, based on the elevated ΔH_{15} values of the connections, we can conclude that the coupling between recorded EEG signals transitioned into a state with increased multifractal strength suggesting increased nonlinearity (Ashkenazy et al., 2003). Multifractal dynamics are characterized by increased dependency between different time scales. As time scale relates to frequency, one such model is formulated by assuming a relationship between the phase of lower frequencies and the amplitude of higher frequencies (He et al., 2010). In that, a stronger phase-amplitude coupling is associated with higher nonlinearity as captured by increased ΔH_{15} (Ashkenazy et al., 2003). Taken together, BFMF reveals that task induces a redistribution of the long-term cross-correlation in coupled dynamics as indicated by higher Hurst exponent and renders them more interdependent across different time scales as manifested by increased ΔH_{15}. The more pronounced multifractal character of the connections can possibly be attributed to the recruitment of excitatory/inhibitory feedback loops (Poil et al., 2012) during task, whose transient is typically characterized by nonlinear dynamics (Rabinovich and Muezzinoglu, 2010). The elevated coupling [increased $H(2)$] and feedback loops (increased ΔH_{15}) that take place in this visual pattern recognition paradigm can be ascribed to the enhanced cooperation of distant brain areas involved in various aspects of visual processing, such as recalling short-term memory and making visual comparisons.

Both $H(2)$ and ΔH_{15} networks showed a significantly increased connectivity in task states compared to EO and EC, captured in their global and local weighted node degrees

DOI:10.14753/SE.2022.2667

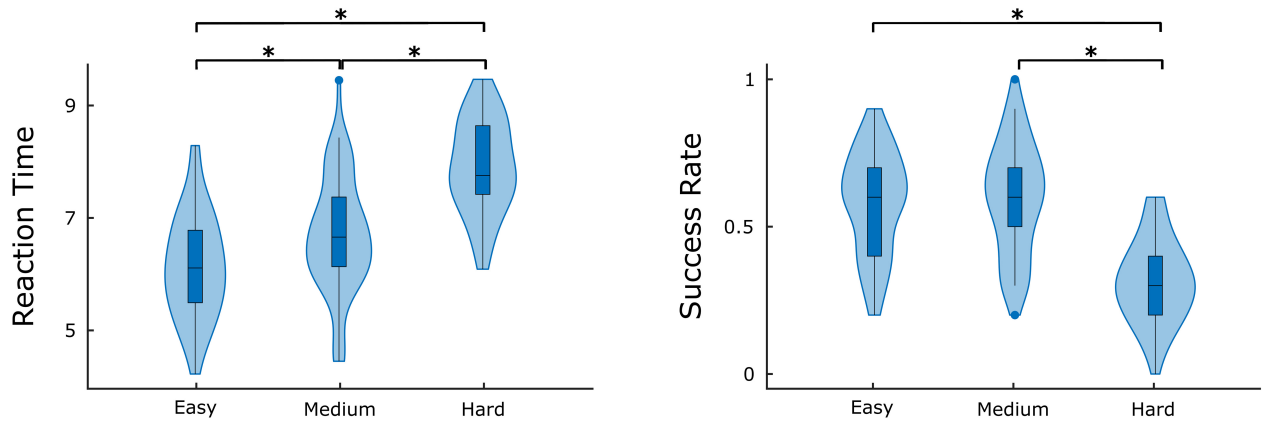

FIGURE 7 | Average success rate and reaction time for different difficulty levels. Significant differences are marked by asterisk (*). Figure was created using Gramm (Morel, 2018).

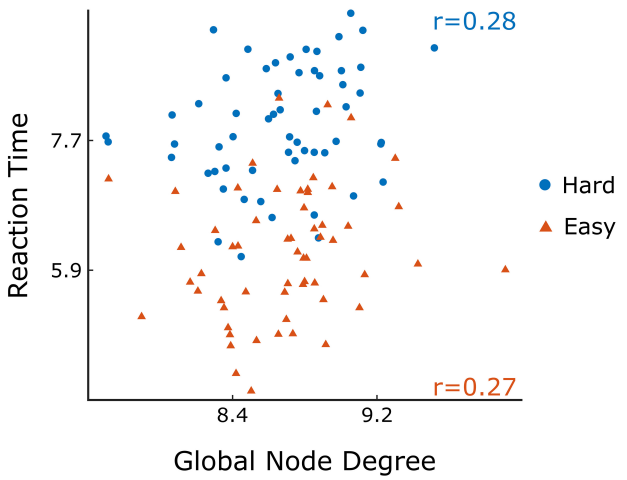

FIGURE 8 | Scatter plots of the reaction time vs global node degree for Easy (orange) and Hard (blue) task in ΔH_{15} networks and their Spearman's correlation (r). Figure was created using Gramm (Morel, 2018).

(**Figures 3–5**). Our results agree with the findings of a previous functional near-infrared spectroscopy study using a very similar cognitive paradigm. Racz et al. found global weighted node degree increased in the prefrontal cortex during task (Racz et al., 2017), using the scale-specific Pearson's correlation as FC estimator. Based on these two studies, it appears that both the scale-free and scale-specific connectivity of the brain increases during visual pattern recognition. This indicates that a significant reorganization of functional brain networks takes place in response to increased mental workload. Nevertheless, definite conclusions cannot be drawn due to the different modalities (EEG vs functional near-infrared spectroscopy). It is also noteworthy that FC increased during the transition from EC to EO. Since considerable brain capacity is devoted to visual processing, opening the eyes should substantially increase brain network activity. Thus, the observed higher node degrees during EO are consistent with the manifestation of increased mental workload. It should be recalled that a shift to higher frequencies characterizes cortical desynchronization during EO, contrasting with the earlier interpretation of increased $H(2)$ (i.e., shift to lower frequencies). We speculate that scale-free and oscillatory components of coupled electrophysiological activity have different origins and could be affected by the opening of the eyes differently. Previously, we have demonstrated that the global multifractal dynamics of FC are affected by the EC-EO transition (Racz et al., 2018), our present study extends these findings by revealing the local alterations in scale-free coupled dynamics (**Figure 5**). Still, the mental workload of EO was not as substantial as that of the pattern recognition task, since the node degrees of the EO networks differed significantly from those of the task states. On the other hand, the 3 task states (Easy, Medium and Hard) had statistically similar node degrees (**Figures 3–5**), even though the cognitive stimulation paradigm showed a lower success rate for more complex images (**Figure 7**). Similar results were found in an n-back EEG study (Kaposzta et al., 2021), in which there was no significant difference in the density, clustering coefficient and efficiency of the 2-back and 3-back brain networks. In this n-back study, the network measures decreased during task, which is in contrast with the current findings of increased FC. This apparent controversy in FC alterations between tasks has already been noticed, with n-back being the most different from the rest of the studied task conditions (Krienen et al., 2014). The use of different FC estimators could have impacted the reported results as well. Moreover, for both BFMF measures, the within-state comparisons showed apparent regional variability (**Figure 6**), similarly to our previous results (Stylianou et al., 2021). In that, we saw that the degree of multifractality (ΔH_{15}) varied more than the long-term cross-correlation [$H(2)$] across the brain, in all states. Additionally, significant differences in the long-term cross-correlation were accompanied by changes in the degree of multifractality, in most cases. A possible explanation could be that multifractality results from more complex dynamics

DOI:10.14753/SE.2022.2667

(Tel, 1988) which tend to vary more from region to region. On the other hand, this contradicts the findings of our previous resting-state study, where $H(2)$ values varied the most [cf. Table 2 in Stylianou et al. (2021)]. The different electrode densities of the EEG system used in these two studies (62 vs 14 channels) could well account for the observed differences. Nonetheless, these two studies indicate that scale-free coupled dynamics do not emerge homogenously in the brain, neither in rest nor in task states, which is a motivation for further studying the multifractal properties of FC at higher spatial resolution. Furthermore, small subject concordance within the different states was observed only for the ΔH_{15} network (**Table 3**). This agrees with a previous study (Mueller et al., 2013), which found inter-subject FC variation localized mainly in the high-order association cortices in the frontal and parietal lobes, i.e., regions strongly overlapping with those we recorded EEG from.

As to the performance metrics, the Easy state was associated with faster RT than the Medium and Hard states, while significant differences in the SR were observed only between Easy-Hard and Medium-Hard (**Figure 7**). Even though no significant differences in the SR were observed between Easy-Medium, the RT during the Medium task was longer. We believe that a significant difference in the SR between Easy-Medium could be found by including a larger or more diverse population sample in future studies. Furthermore, no significant associations were found between the global node degrees and performance metrics (SR and RT), with the exception of positive correlations between RT and $\overline{D}$ in the Easy and Hard states of the ΔH_{15} networks. Similarly, in another EEG n-back study, network measures were found significantly correlated only with RT, and not with SR (Dai et al., 2017). This suggests that lower multifractality corresponds to faster pattern recognition, while the subject's SR remains independent of scale-free coupled dynamics. These correlations did not remain significant after BH correction, suggesting that a larger, more representative sample of the population could potentially reveal significant correlations even after BH correction.

Our results derived from the main analytical pipeline are supported by further analysis accounting for the slightly different length of analyzed signals from the task states (**Supplementary Material**). Because the multifractal profile of a time series is influenced by its length (Grech and Pamuła, 2012; Rak and Grech, 2018), we anticipated a similar effect on our bivariate multifractal analysis (Kristoufek, 2015b); thus, we re-analyzed our dataset in a pipeline adjusted to the different lengths of analyzed pair of time series based on the different response times. The results agree with our primary analysis, indicating that the slightly varying signal length had no effect on the observed patterns. We also compared the $\overline{D}$ of every state after excluding connections that did not pass our multifractality assessment tests. While significant differences were found between rest and task states, they were of the opposite direction, i.e., $\overline{D}$ decreased during task (**Supplementary Figure 1**), which can be explained by the larger number of connections that passed our tests during rest (**Table 2**). However, there was great inconsistency among the multifractality assessment tests for every connection and task (e.g., out of the 10 Hard segments, the connection AF4-AF3 might have passed the test in only 4 of them). In order to avoid any bias, our main analysis focused on unthresholded networks. Additionally, the thresholded analysis showed significant positive correlations between $\overline{D}$-RT in the Easy and Medium states for both $H(2)$ and ΔH_{15} networks, warranting further investigation in future studies (**Supplementary Figure 2**). While a growing number of publications investigates the FC-related differences between the two sexes (Zhang et al., 2018; Ýçer et al., 2020), we found no significant sex-related differences in network architecture. Since the studies mentioned above had higher spatial resolution (higher density EEG or fMRI recordings), we believe that future experiments with higher number of EEG channels might be able to reveal such differences. As to the effect of handedness, no significant differences in $\overline{D}$ were identified between the left- and right-handed participants in any state (EC, EO, Easy, Medium, Hard) or network [$H(2)$ and ΔH_{15}]. To assess the test-retest reliability, 5 of our subjects repeated the same experiment a few months later. No significant differences were found in the SR and RT between the two sessions, suggesting that our experimental paradigm can be used in further reproducibility studies. Finally, we found a moderate concordance between $H(2)$ and ΔH_{15} values for every subject (**Supplementary Table 1**), indicating a relatively constant multifractal character of the connections. Further details of these analyses can be found in the **Supplementary Material**.

Future developments based on this study should consider the following shortcomings. Despite its sample size, the subject cohort of our study might not have been representative of the general population, thus limiting us in drawing more general conclusions. All participants were young, healthy and educated, university students or graduates. Differences observed in the multifractal FC during task could be augmented or attenuated if a larger cohort of volunteers participated. The recorded EEG signals might be affected by scalp muscle contraction (especially at the frontal and temporal sites), as shown previously (Goncharova et al., 2003). Since the spectral characteristics of electromyographic signals considerably overlap with EEG, part of the results could be attributed to activity of motor units rather than changes in local field potentials in the brain cortex. Nonetheless, independent component analysis can remove a significant part of these electromyographic contaminations (Yilmaz et al., 2019). Additionally, task-related EEG changes are not greatly affected by muscle contractions (Boytsova et al., 2016). Because during diverse tasks different brain network architectures emerge (Krienen et al., 2014), the construction of more extensive cognitive stimuli with several different paradigms should be considered. Studies found that FC changed as subjects repeated and thus learned a task (Lewis et al., 2009; Bassett et al., 2011), which warrants that our future experiments investigate the effect of learning. Additionally, the bimodality phenomenon observed in univariate focus-based multifractal analysis (Nagy et al., 2017) can be extended to the multifractal covariance scaling function with multiple scaling ranges.

DOI:10.14753/SE.2022.2667

As to future perspectives, it will be interesting to see the discriminatory power of multifractal FC between rest and task states at the individual level, which was beyond the scope of this study. In future studies, we intend to investigate the rest-state classification performance of BFMF compared to other measures of brain network dynamics (Racz et al., 2020). To reveal mechanistic background of scale-free coupled dynamics, further clinical trials and animal models are needed using anesthetics, antipsychotics, antiparkinsonian and other medications (Nasrallah et al., 2017). On a final note, a promising field where such visual pattern recognition task could be advantageous is in attention deficit hyperactivity disorder (ADHD) research, where brain network alterations during spatial working memory tasks have already been revealed (Jang et al., 2020).

CONCLUSION

In the present study, we reconstructed brain networks from measures of scale-free coupled dynamics in resting states and during a visual pattern recognition task estimated by our novel bivariate multifractal analytical algorithm. Initially, we showed that our method could capture true multifractal coupled dynamics that varied across different brain regions. Additionally, we saw an increase in functional connectivity during the transition from rest (EC and EO) to task states, which was however, independent of task difficulty. We also found higher functional connectivity when the participants transitioned from EC to EO. These findings could well facilitate future research of scale-free functional connectivity studies with complex experimental designs in healthy and diseased populations.

DATA AVAILABILITY STATEMENT

The raw data supporting the conclusions of this article will be made available by the authors, without undue reservation.

ETHICS STATEMENT

The studies involving human participants were reviewed and approved by Regional and Institutional Committee of Science and Research 111 Ethics of Semmelweis University (approval number: 2020/6). The patients/participants provided their written informed consent to participate in this study.

AUTHOR CONTRIBUTIONS

OS implemented the analytical framework, contributed to experiment design, performed experiments, data analysis and interpretation, and wrote the first draft of the manuscript. FR performed experiments and contributed to experiment design, data analysis, and manuscript development. KK, ZK, and AC performed experiments and contributed to data analysis. AY contributed to manuscript development. AE provided conceptual guidance and supervision throughout the study. PM developed the code for BFMF, specified the concept and aims of the study and contributed to experiment design. All authors contributed to reviewing the manuscript and approved its final version.

FUNDING

FR and PM acknowledge financial support from the "Development of Scientific Workshops for Medical, Health Sciences and Pharmaceutical Training" Project (EFOP-3.6.3-VEKOP-16-2017-00009). AY and PM acknowledge financial support from the "the Cellular and Molecular GeroScience CoBRE (P20GM125528, sub#5337)".

SUPPLEMENTARY MATERIAL

The Supplementary Material for this article can be found online at: https://www.frontiersin.org/articles/10.3389/fnhum.2021.740225/full#supplementary-material

REFERENCES

Achard, S., Bassett, D. S., Meyer-lindenberg, A., and Bullmore, E. (2008). Fractal connectivity of long-memory networks. *Phys. Rev. E Stat. Nonlin. Soft Matter Phys.* 77(3 Pt 2):036104. doi: 10.1103/PhysRevE.77.036104

Ashkenazy, Y., Havlin, S., Ivanov, P. C., Peng, C.-K., Schulte-Frohlinde, V., and Stanley, H. E. (2003). Magnitude and sign scaling in power-law correlated time series. *Physica A* 323, 19–41. doi: 10.1016/S0378-4371(03)00008-6

Bassett, D. S., Wymbs, N. F., Porter, M. A., Mucha, P. J., Carlson, J. M., and Grafton, S. T. (2011). Dynamic reconfiguration of human brain networks during learning. *Proc. Natl. Acad. Sci. U. S. A.* 108, 7641–7646. doi: 10.1073/pnas.1018985108

Bastos, A. M., and Schoffelen, J. M. (2016). A tutorial review of functional connectivity analysis methods and their interpretational pitfalls. *Front. Syst. Neurosci.* 9:175. doi: 10.3389/fnsys.2015.00175

Benjamini, Y., and Hochberg, Y. (1995). Controlling the false discovery rate: a practical and powerful approach to multiple testing. *J. R. Stat. Soc. Ser. B (Methodol.).* 57, 289–300. doi: 10.1111/j.2517-6161.1995.tb02031.x

Biswal, B., Zerrin Yetkin, F., Haughton, V. M., and Hyde, J. S. (1995). Functional connectivity in the motor cortex of resting human brain using echo-planar mri. *Magn. Reson. Med.* 34, 537–541. doi: 10.1002/mrm.1910340409

Boytsova, J. A., Danko, S. G., and Medvedev, S. V. (2016). When EMG contamination does not necessarily hide high-frequency EEG: scalp electrical recordings before and after Dysport injections. *Exp. Brain Res.* 234, 3091–3106. doi: 10.1007/s00221-016-4708-3

Ciuciu, P., Abry, P., and He, B. J. (2014). Interplay between functional connectivity and scale-free dynamics in intrinsic fMRI networks. *Neuroimage* 95, 248–263. doi: 10.1016/j.neuroimage.2014.03.047

Dai, Z., de Souza, J., Lim, J., Ho, P. M., Chen, Y., Li, J., et al. (2017). EEG cortical connectivity analysis of working memory reveals topological reorganization in theta and alpha bands. *Front. Hum. Neurosci.* 11:237. doi: 10.3389/fnhum.2017.00237

Delorme, A., and Makeig, S. (2004). EEGLAB: an open source toolbox for analysis of single-trial EEG dynamics including independent component analysis. *J. Neurosci. Methods* 134, 9–21. doi: 10.1016/j.jneumeth.2003.10.009

DOI:10.14753/SE.2022.2667

Di, X., Fu, Z., Chan, S. C., Hung, Y. S., Biswal, B. B., and Zhang, Z. (2015). Task-related functional connectivity dynamics in a block-designed visual experiment. *Front. Hum. Neurosci.* 9:543. doi: 10.3389/fnhum.2015.00543

Eke, A., Herman, P., Kocsis, L., and Kozak, L. R. (2002). Fractal characterization of complexity in temporal physiological signals. *Physiol. Meas.* 23, R1–R38. doi: 10.1088/0967-3334/23/1/201

Elton, A., and Gao, W. (2015). Task-related modulation of functional connectivity variability and its behavioral correlations. *Hum. Brain Mapp.* 36, 3260–3272. doi: 10.1002/hbm.22847

Fox, M. D., Snyder, A. Z., Vincent, J. L., Corbetta, M., Van Essen, D. C., and Raichle, M. E. (2005). The human brain is intrinsically organized into dynamic, anticorrelated functional networks. *Proc. Natl. Acad. Sci. U. S. A.* 102, 9673–9678. doi: 10.1073/pnas.0504136102

Friston, K. J., Frith, C. D., Liddle, P. F., and Frackowiak, R. S. J. (1993). Functional connectivity: the principal-component analysis of large (PET) data sets. *J. Cereb. Blood Flow Metab.* 13, 5–14. doi: 10.1038/jcbfm.1993.4

Gabard-Durnam, L. J., Mendez Leal, A. S., Wilkinson, C. L., and Levin, A. R. (2018). The harvard automated processing pipeline for electroencephalography (HAPPE): standardized processing software for developmental and high-artifact data. *Front. Neurosci.* 12:97. doi: 10.3389/fnins.2018.00097

Goncharova, I. I., McFarland, D. J., Vaughan, T. M., and Wolpaw, J. R. (2003). EMG contamination of EEG: spectral and topographical characteristics. *Clin. Neurophysiol.* 114, 1580–1593. doi: 10.1016/S1388-2457(03)00093-2

Grech, D., and Pamuła, G. (2012). Multifractal background noise of monofractal signals. *Acta Phys. Pol. A* 121, B–34–B–39. doi: 10.12693/APhysPolA.121.B-34

He, B. J., Zempel, J. M., Snyder, A. Z., and Raichle, M. E. (2010). The temporal structures and functional significance of scale-free brain activity. *Neuron* 66, 353–369. doi: 10.1016/j.neuron.2010.04.020

Hou, F., Liu, C., Yu, Z., Xu, X., Zhang, J., Peng, C.-K., et al. (2018). Age-related alterations in electroencephalography connectivity and network topology during n-back working memory task. *Front. Hum. Neurosci.* 12:484. doi: 10.3389/fnhum.2018.00484

Ýçer, S., Acer, Ý, and Baş, A. (2020). Gender-based functional connectivity differences in brain networks in childhood. *Comput. Methods Programs Biomed.* 192:105444. doi: 10.1016/j.cmpb.2020.105444

Jang, K.-M., Kim, M.-S., and Kim, D.-W. (2020). The dynamic properties of a brain network during spatial working memory tasks in college students with ADHD traits. *Front. Hum. Neurosci.* 14:580813. doi: 10.3389/fnhum.2020.580813

Kandel, E. R., Schwartz, J. H., and Jessell, T. M. (2012). *Principles of Neural Science*. New York, NY: McGraw-Hill Professional Pub.

Kaposzta, Z., Stylianou, O., Mukli, P., Eke, A., and Racz, F. S. (2021). Decreased connection density and modularity of functional brain networks during n-back working memory paradigm. *Brain Behav.* 11:116. doi: 10.1002/brb3.1932

Kaufmann, T., Alnæs, D., Brandt, C. L., Doan, N. T., Kauppi, K., Bettella, F., et al. (2017). Task modulations and clinical manifestations in the brain functional connectome in 1615 fMRI datasets. *Neuroimage* 147, 243–252. doi: 10.1016/j.neuroimage.2016.11.073

Krienen, F. M., Thomas Yeo, B. T., and Buckner, R. L. (2014). Reconfigurable task-dependent functional coupling modes cluster around a core functional architecture. *Philos. Trans. R. Soc. B Biol. Sci.* 369:20130526. doi: 10.1098/rstb.2013.0526

Kristoufek, L. (2014). Spectrum-based estimators of the bivariate hurst exponent. *Phys. Rev. E* 90:062802. doi: 10.1103/PhysRevE.90.062802

Kristoufek, L. (2015a). Can the bivariate hurst exponent be higher than an average of the separate hurst exponents? *Physica A* 431, 124–127. doi: 10.1016/j.physa.2015.02.086

Kristoufek, L. (2015b). Finite sample properties of power-law cross-correlations estimators. *Physica A* 419, 513–525. doi: 10.1016/j.physa.2014.10.068

Kristoufek, L. (2016). Power-law cross-correlations estimation under heavy tails. *Commun. Nonlinear Sci. Numer. Simul.* 40, 163–172. doi: 10.1016/j.cnsns.2016.04.010

Lewis, C. M., Baldassarre, A., Committeri, G., Romani, G. L., and Corbetta, M. (2009). Learning sculpts the spontaneous activity of the resting human brain. *Proc. Natl. Acad. Sci.* 106, 17558–17563. doi: 10.1073/pnas.0902455106

Morel, P. (2018). Gramm: grammar of graphics plotting in Matlab. *J. Open Source Softw.* 3:568. doi: 10.21105/joss.00568

Mueller, S., Wang, D., Fox, M. D., Yeo, B. T. T., Sepulcre, J., Sabuncu, M. R., et al. (2013). Individual variability in functional connectivity architecture of the human brain. *Neuron* 77, 586–595. doi: 10.1016/j.neuron.2012.12.028

Mukli, P., Nagy, Z., and Eke, A. (2015). Multifractal formalism by enforcing the universal behavior of scaling functions. *Physica A* 417, 150–167. doi: 10.1016/j.physa.2014.09.002

Mukli, P., Nagy, Z., Racz, F. S., Herman, P., and Eke, A. (2018). Impact of healthy aging on multifractal hemodynamic fluctuations in the human prefrontal cortex. *Front. Physiol.* 9:1072. doi: 10.3389/fphys.2018.01072

Nagy, Z., Mukli, P., Herman, P., and Eke, A. (2017). Decomposing multifractal crossovers. *Front. Physiol.* 8, 533. doi: 10.3389/fphys.2017.00533

Nasrallah, F. A., Singh, K. K. D. R., Yeow, L. Y., and Chuang, K.-H. (2017). GABAergic effect on resting-state functional connectivity: dynamics under pharmacological antagonism. *Neuroimage* 149, 53–62. doi: 10.1016/j.neuroimage.2017.01.040

Poil, S.-S., Hardstone, R., Mansvelder, H. D., and Linkenkaer-Hansen, K. (2012). Critical-state dynamics of avalanches and oscillations jointly emerge from balanced excitation/inhibition in neuronal networks. *J. Neurosci.* 32, 9817–9823. doi: 10.1523/JNEUROSCI.5990-11.2012

Popivanov, D., Stomonyakov, V., Minchev, Z., Jivkova, S., Dojnov, P., Jivkov, S., et al. (2006). Multifractality of decomposed EEG during imaginary and real visual-motor tracking. *Biol. Cybern.* 94, 149–156. doi: 10.1007/s00422-005-0037-5

Rabinovich, M. I., and Muezzinoglu, M. K. (2010). Nonlinear dynamics of the brain: emotion and cognition. *Phys. Uspekhi* 53, 357–372. doi: 10.3367/UFNe.0180.201004b.0371

Racz, F. S., Mukli, P., Nagy, Z., and Eke, A. (2017). Increased prefrontal cortex connectivity during cognitive challenge assessed by fNIRS imaging. *Biomed. Opt. Express* 8:3842. doi: 10.1364/BOE.8.003842

Racz, F. S., Stylianou, O., Mukli, P., and Eke, A. (2018). Multifractal dynamic functional connectivity in the resting-state brain. *Front. Physiol.* 9:1704. doi: 10.3389/fphys.2018.01704

Racz, F. S., Stylianou, O., Mukli, P., and Eke, A. (2019). Multifractal and entropy analysis of resting-state electroencephalography reveals spatial organization in local dynamic functional connectivity. *Sci. Rep.* 9:13474. doi: 10.1038/s41598-019-49726-5

Racz, F. S., Stylianou, O., Mukli, P., and Eke, A. (2020). Multifractal and entropy-based analysis of delta band neural activity reveals altered functional connectivity dynamics in schizophrenia. *Front. Syst. Neurosci.* 14:49. doi: 10.3389/fnsys.2020.00049

Raichle, M. E., MacLeod, A. M., Snyder, A. Z., Powers, W. J., Gusnard, D. A., and Shulman, G. L. (2001). A default mode of brain function. *Proc. Natl. Acad. Sci. U. S. A.* 98, 676–682. doi: 10.1073/pnas.98.2.676

Rak, R., and Grech, D. (2018). Quantitative approach to multifractality induced by correlations and broad distribution of data. *Physica A* 508, 48–66. doi: 10.1016/j.physa.2018.05.059

Rong-Yi, Y., and Zhong, C. (2005). Blind source separation of multichannel electroencephalogram based on wavelet transform and ICA. *Chin. Phys.* 14, 2176–2180. doi: 10.1088/1009-1963/14/11/006

Rubinov, M., and Sporns, O. (2010). Complex network measures of brain connectivity: uses and interpretations. *Neuroimage* 52, 1059–1069. doi: 10.1016/j.neuroimage.2009.10.003

Skroumpelou, K., Mavros, P., and Smith, A. H. (2015). Are we there yet? Exploring distance perception in urban environments with mobile electroencephalography. *GIS Res.*

Stam, C. J., and de Bruin, E. A. (2004). Scale-free dynamics of global functional connectivity in the human brain. *Hum. Brain Mapp.* 22, 97–109. doi: 10.1002/hbm.20016

Stylianou, O., Racz, F. S., Eke, A., and Mukli, P. (2021). Scale-free coupled dynamics in brain networks captured by bivariate focus-based multifractal analysis. *Front. Physiol.* 11:615961. doi: 10.3389/fphys.2020.615961

Tel, T. (1988). Fractals, multifractals, and thermodynamics. *Z. Für Nat. A* 1174, 1154–1174. doi: 10.1515/zna-1988-1221

Van Hoesen, G. W. (1993). The modern concept of association cortex. *Curr. Opin. Neurobiol.* 3, 150–154. doi: 10.1016/0959-4388(93)90202-A

Wang, J., and Zhao, D.-Q. (2012). Detrended cross-correlation analysis of electroencephalogram. *Chin. Phys. B* 21:028703. doi: 10.1088/1674-1056/21/2/028703

DOI:10.14753/SE.2022.2667

Werner, G. (2010). Fractals in the nervous system: conceptual implications for theoretical neuroscience. *Front. Physiol.* 1:15. doi: 10.3389/fphys.2010.00015

Yang, Y., Qiu, Y., and Schouten, A. C. (2015). Dynamic Functional brain connectivity for face perception. *Front. Hum. Neurosci.* 9:662. doi: 10.3389/fnhum.2015.00662

Yilmaz, G., Budan, A. S., Ungan, P., Topkara, B., and Türker, K. S. (2019). Facial muscle activity contaminates EEG signal at rest: evidence from frontalis and temporalis motor units. *J. Neural Eng.* 16:066029. doi: 10.1088/1741-2552/ab3235

Yu, H., and Winkler, S. (2013). "Image complexity and spatial information," in *Proceedings of the In 2013 5th International Workshop on Quality of Multimedia Experience (QoMEX)* (Klagenfurt: IEEE), 12–17. doi: 10.1109/QoMEX.2013.6603194

Zhang, C., Dougherty, C. C., Baum, S. A., White, T., and Michael, A. M. (2018). Functional connectivity predicts gender: evidence for gender differences in resting brain connectivity. *Hum. Brain Mapp.* 39, 1765–1776. doi: 10.1002/hbm.23950

Conflict of Interest: The authors declare that the research was conducted in the absence of any commercial or financial relationships that could be construed as a potential conflict of interest.

Publisher's Note: All claims expressed in this article are solely those of the authors and do not necessarily represent those of their affiliated organizations, or those of the publisher, the editors and the reviewers. Any product that may be evaluated in this article, or claim that may be made by its manufacturer, is not guaranteed or endorsed by the publisher.